Stellingen behorende bij het proefschrift

Crack growth in polyethylene

1 Als de platte beeldbuis normaal was geweest dan zou nu koortsachtig worden gewerkt aan de ontwikkeling van een gekromde beeldbuis.

2 In de winter is binnenshuis de kaars (of gaslamp) uit vroegere tijden nog steeds de meest efficiënte manier van verlichting. Licht en warmte worden direct gecombineerd zonder omzetting van de brandstof in beweging en electriciteit.

3 Het TV programma Klokhuis heeft mij bewezen dat een mens nooit te oud is om te leren. Studio Sport bewijst dat veel mensen geen zin hebben om te leren.

4 Het sportieve karakter van de Europeaan ten opzichte van de Amerikaan blijkt uit het verschil in gemiddeld lichaamsgewicht en het feit dat Europa in de auto nog steeds "sportief" schakelt.

5 Sociale uitkeringen kunnen deels worden gezien als het afkopen van sociale onvrede met netto een positief resultaat.

6 Het uitzenden van troepen in een vredesmacht confronteert nieuwe generaties aan den lijve met de gruwelen van een oorlog en vormt hiermee een krachtige basis om oorlog in eigen land te voorkomen.

7 Het boek over een reis naar de maan van Jules Verne was in 1865 minder geloofwaardig dan de film "Jurrassic Park" nu is.

8 Computers zijn redelijk bestand tegen hydraulische olie maar gaan verloren bij brand.

9 Het idee dat bij barre weersomstandigheden de thermostaat hoger gezet moet worden duidt op weinig begrip van meet- en regeltechniek.

10 Naast de gebruikelijke blaastest bij alcoholcontrole zou een *blow*test ingevoerd moeten worden om rijden onder invloed van hasj te controleren.

11 Binnen een religie is moderniseren van geloofsopvattingen moeilijk te combineren met de aanname van één absolute waarheid.

12 Het aloude spreekwoord "Wat Gij niet wilt dat U geschied, doe dat ook een ander niet" zou kunnen dienen als universeel kapstok artikel voor wetgeving en moraal.

Ton Riemslag
april 1997

Crack growth in polyethylene

Cover:

A SEM image of a craze, visible as the bright region with a triangular geometry situated just ahead of the crack tip. A craze is the area in which the material is subject to intense loading, resulting in failure. Failure of the material within the craze is the basic mechanism of crack growth.

Crack growth in polyethylene

PROEFSCHRIFT

ter verkrijging van de graad van doctor
aan de Technische Universiteit Delft,
op gezag van de Rector Magnificus Prof.dr.ir. J. Blaauwendraad,
in het openbaar te verdedigen ten overstaan van een commissie,
door het College van Dekanen aangewezen,
op maandag 2 juni 1997 te 13.30 uur

door

Anton Cornelis RIEMSLAG
werktuigkundig ingenieur
geboren te Amsterdam

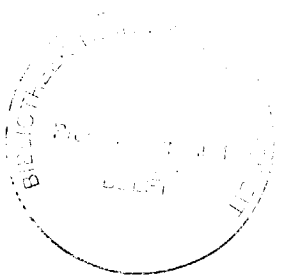

Dit proefschrift is goedgekeurd door de promotor:
Prof. dr. ir. A. Bakker

Samenstelling promotiecommissie:

Rector Magnificus	Technische Universiteit Delft, voorzitter
Prof.dr.ir. A. Bakker	Technische Universiteit Delft, promotor
Dr.ir. J. Zuidema	Technische Universiteit Delft, toegevoegd promotor
Prof.dr.ir. R. Marissen	Technische Universiteit Delft
Prof.dr.ir. A. Posthuma de Boer	Technische Universiteit Delft
Prof.dr. P.C. Powell	Universiteit Twente
Prof.ir. J.L. Spoormaker	Technische Universiteit Delft
Prof.ir. L.B. Vogelesang	Technische Universiteit Delft

This work was sponsored by **GASTEC**, the Dutch Center of Gas Technology, Apeldoorn, The Netherlands.

Published and distributed by Delft University Press, Mekelweg 4, 2628 CD Delft, The Netherlands.
Telephone: 31(0)15 278 3254
Telefax: 31(0)15 278 1661

CIP-DATA KONINKLIJKE BIBLIOTHEEK, DEN HAAG

Riemslag, T

Crack growth in polyethylene / T. Riemslag. - Delft : Delft University Press.-Illustrations.
Thesis Delft University of Technology.- With ref. - With summary in Dutch.
ISBN 90-407-1453-3
NUGI 813
Subject headings: polyethylene, fatigue, creep crack growth, brittle failure

To the memory of my mother

Contents

Nomenclature

a	crack length
a_{cr}	critical crack length
a_{st}	start crack length
b	exponent of "Paris law" for creep crack growth.
B	thickness
C	constant
C_{ccg}	constant in the "Paris law" for creep crack growth
C'_{ccg}	constant
C_{pent}	correction factor
$CTOD_{bulk}$	crack tip opening displacement of bulk material
$CTOD_{craze}$	craze-inherent crack tip opening displacement
$CTOD_{Dugdale}$	crack tip opening displacement according to the Dugdale model
$CTOD_{total}$	total amount of crack tip opening displacement = $CTOD_{bulk}$ + $CTOD_{craze}$
da/dN	fatigue crack growth rate, crack length increase per cycle
da/dt	crack growth rate in the time domain, crack length increase per unit of time
$(da/dt)_{im.}$	extrapolated value of the crack growth rate
E	elastic modulus
f	frequency of cyclic fatigue load
K	stress intensity factor
K_I	mode I stress intensity factor
K_{max}	maximum value of the stress intensity factor
K_{min}	minimum value of the stress intensity factor
k	Boltzmann's constant
L	length of CCT-type fatigue specimen
L_c	length of a craze
$L_{c,Dugdale}$	length of a craze predicted by the Dugdale model
$L_{c,meas.}$	length of a craze actually measured
m	exponent of the Paris fatigue crack growth law
N	number of fatigue cycles
n	constant
N_s	number of data points in the moving average procedure of the fatigue crack growth rate calculation

R	load ratio of the fatigue load = (K_{min}/K_{max})
r	radius in polar coordinates
R_f	reduction factor
T	temperature, periodic time
t_{delay}	duration of crack arrest
T_f	failure time
T_g	glass transition temperature
t_{hold}	duration of constant load level
T_m	melt temperature
t_s	time interval
$t_{surplus}$	characteristic time interval
W	width of CCT-type fatigue specimen
x	result of a measurement
x_{true}	the true value of the variable measured
Δa_{meas}	crack length interval
ΔK	range in stress intensity = K_{max} - K_{min}
ΔU	potential barrier (Arrhenius equation)
ε	strain
ν	frequency of chain segments
ν_0	natural frequency (Arrhenius equation)
θ	angle in polar coordinates
ρ	radius of a blunted crack tip
σ	stress
σ_x	stress in x direction
σ_y	stress in y direction, yield stress.
$\sigma_{y,inf.}$	inferred yield stress
τ_{xy}	shear stress in the xy plane

Summary: Crack growth in polyethylene

The significance of this work is related to the use of polyethylene as a structural material for gas distribution pipes. In this specific application the constant gas pressure in the pipe can induce a failure mechanism called "creep crack growth", potentially leading to the dangerous situation of gas leakage. The mechanism of creep crack growth is a very slow process taking many years before gas leakage occurs. For obvious reasons it is essential to have a knowledge of the long-term failure process before installing a complete gas pipe network.
The initial purpose of this thesis was to evaluate a new test method in which cyclic loading (i.e. fatigue) is used in order to accelerate crack growth. New kinds of short-term test methods were required, as traditional test methods could not discriminate between recently developed types of polyethylene.
Apart from evaluating fatigue as a means of achieving improved prediction of creep crack growth, a more general understanding of crack growth in polyethylene is obtained. Crack growth under cyclic and constant load conditions is evaluated and compared.

The crack growth behaviour of polyethylene was tested for three particular types of polyethylene gas pipe materials, in order to distinguish between general crack growth behaviour and such effects which might only occur for one specific type of material. In fact, this approach proved to be essential, since contradictory behaviour on the part of the materials tested was indeed encountered on a regular basis.

The test programme involved direct measurements of macroscopic crack growth rates as well as a more fundamental approach, studying micromechanisms at crack tip level.
In fatigue, crack growth rates were obtained by the introduction of a new method for measuring crack lengths in polymers, based on the technique of digital image processing.
The study of micromechanisms resulted in the recognition of the crack tip in polyethylene as a two-phase system, consisting of highly drawn material within the actual craze and bulk material at the craze boundaries.

In both fatigue crack growth and creep crack growth the mechanism of blunting, induced by creep, was found to play a key role. The total amount of blunting is determined by deformations of the craze itself and the surrounding bulk material. The crack growth behaviour therefore depends on the mechanical behaviour of highly stretched material in combination with the response of bulk material. The relatively high crack growth rate in fatigue is found to be caused by embrittlement of the highly drawn material within the craze, induced by an apparently cyclic damaging mechanism. The embrittlement effectively reduces the extent of blunting, with a consequent increase in crack growth rate.

With regard to the suitability of fatigue as a tool to predict creep crack growth, it was found that one individual fatigue test definitely cannot consistently predict creep crack growth behaviour. However, a series of fatigue tests was introduced in which a fatigue load is gradually transformed into a constant load situation. In this way the fatigue behaviour can be extrapolated to the constant load response. For two of the three materials tested this test procedure worked well.

Samenvatting: Scheurgroei in polyetheen

Dit onderzoek is gerelateerd aan de toepassing van polyetheen als basismateriaal voor gasbuizen. In die specifieke toepassing kan de constante gasdruk in de pijp een falen door kruipscheurgroei veroorzaken, waardoor uiteindelijk een gevaarlijk gaslek kan ontstaan. Kruipscheurgroei is een heel langzaam proces waarbij het jaren kan duren voordat uiteindelijk een gaslek ontstaat. Vanzelfsprekend is het essentieel om het langeduur faalgedrag te kennen voordat een compleet ondergronds netwerk van gaspijpen wordt geïnstalleerd.
De oorspronkelijke opzet van het onderzoek was om een nieuwe test te beoordelen, waarbij cyclische belasting (d.w.z. vermoeiing) wordt gebruikt om scheurgroei te versnellen. Nieuwe snelle typen beproevingen zijn nodig gebleken, omdat traditionele testmethoden, bij recent ontwikkelde materialen, geen kwaliteitsverschil meer kunnen onderscheiden.
Naast het onderzoek of vermoeiing voldoet als methode voor een betere voorspelling van kruipscheurgroei is ook een meer algemeen inzicht verkregen in scheurgroei van polyetheen. Scheurgroei bij cyclische en constante belasting is in beschouwing genomen en vergeleken.

Het scheurgroeigedrag van polyetheen is beproefd met drie verschillende typen polyetheen gasbuismateriaal, om onderscheid te kunnen maken tussen algemeen scheurgroeigedrag en gedrag dat karakteristiek is voor één type materiaal. Deze aanpak is essentieel gebleken, omdat tegenstrijdige effecten bij verschillende materialen ook daadwerkelijk en regelmatig zijn waargenomen. Beproevingen zijn deels uitgevoerd met directe meting van de macroscopische scheurlengte, terwijl ook micromechanismen op scheurtip niveau zijn bestudeerd, voor een meer fundamenteel inzicht. Bij vermoeiingsproeven zijn scheurgroeisnelheden gemeten door toepassing van een nieuwe methode om scheurlengtes in kunststoffen te meten. Deze nieuwe methode is gebaseerd op digitale beeldbewerking.
Het onderzoek van micromechanismen heeft geleid tot het inzicht dat de scheurtip in polyetheen een twee fasen systeem is, bestaande uit sterk verstrekt materiaal binnen de zogenaamde craze en bulkmateriaal rondom de grenzen van de craze.

In zowel vermoeiings- als kruipscheurgroei, blijkt door kruip veroorzaakte blunting een belangrijke rol te spelen. De totale hoeveelheid blunting bestaat uit vervormingen van de craze zelf met daarbij nog vervormingen van naburig bulkmateriaal. Het scheurgroeigedrag wordt dus bepaald door de combinatie in mechanisch gedrag van verstrekt en bulk materiaal.
De relatief hoge scheurgroeisnelheid bij vermoeiing houdt verband met verbrossing van het sterk verstrekte materiaal, klaarblijkelijk veroorzaakt door de wisselende belasting. De verbrossing van de craze beperkt de hoeveelheid blunting, met een hoge scheurgroeisnelheid als gevolg.

Één enkele vermoeiingsproef is niet geschikt gebleken om kruipscheurgroei eenduidig te voorspellen. Er is echter wel een serie vermoeiingsproeven geïntroduceerd waarbij de vermoeiingsbelasting geleidelijk in een constante belasting overgaat. Op die manier kan vermoeiingsgedrag worden geëxtrapoleerd naar het scheurgroeigedrag onder constante belasting. Deze methode bleek voor twee van de drie beproefde materialen goed te voldoen.

1. Introduction

1.1 Background and objective

This work is concerned with the service of the underground networks of polyethylene gas pipes currently used in the Netherlands and worldwide. The lifetime of polyethylene gas pipes in service is determined by a failure mechanism called "creep crack growth", which is a slow crack growth mechanism under a constant (i.e. non-cyclic) tensile load condition. In the literature creep crack growth is sometimes also referred to as "slow crack growth", "creep rupture" or "static fatigue". The constant load condition in a gas pipe is basically provided by the internal gas pressure, which results in a pipe wall hoop tensile stress (up to 4 MPa). However, stresses can become much higher locally due to improper embedding of the pipe in the trench (i.e. rock impingement) or incorrect processing conditions of the pipe. The latter aspect mostly concerns the presence of high tensile stresses on the inside of the pipe due to fast cooling down of the outside of the pipe during the extrusion process.

During service, at stress concentrations, a crack may initiate in the wall of the gas pipe and subsequently grow through the wall thickness, with gas leakage as a result. The whole process, from crack initiation to gas leakage, may take up to several years, demonstrating the long-term behaviour of creep crack growth.[1] For obvious reasons it is essential to have a knowledge of this long-term behaviour *before* installing a complete gas distribution network. Section 2.3.1 deals in detail with *short-term* test methods predicting *long-term* creep crack growth behaviour under service conditions.

In the literature, amongst other methods, fatigue loading is reported as a possible new method to predict long-term creep crack growth in a relatively short testing time (see also section 2.3.1). Primarily, the point of departure for this thesis was the important question of whether creep can *consistently* be predicted by means of fatigue tests. The scepticism regarding fatigue tests in relation to creep crack growth is evident from the fact that creep and fatigue mechanisms are generally not considered to be related. It is not an obvious step to link the nature of cyclic damage (fatigue) with mechanisms of viscoelastic creep (creep crack growth). However, a link between creep crack growth and fatigue crack growth becomes plausible when similarities in fracture surfaces are considered. Both macroscopic and microscopic features of fracture surfaces indicate corresponding micromechanisms.

In order to evaluate the potential of some form of fatigue tests for the prediction of creep crack growth, the main focus of the thesis is on the interaction of creep mechanisms during fatigue crack growth in polyethylene. In addition, creep crack growth is studied separately to find the factors that control it.

The literature shows a fair number of publications on the specific topic of slow crack growth in polyethylene. The work of the group led by Professor Brown at the University of Pennsylvania is particularly comprehensive and was used intensively during the project [1 to 19].

[1] This study does not focus on crack initiation. The main interest is the *growth* of a crack already initiated.

1.2 "Stress intensity (K)" versus "stress (σ)" as a fracture parameter

In general there are two ways of approaching crack growth whether fatigue or creep crack growth. The first and more traditional way is to consider average stress and observe the associated total period of time needed for a crack to initiate and grow until final fracture has occurred. Typically, high stress levels result in shorter failure times and in this respect a relation between stress level and crack growth is established. Relations measured between stress levels and failure times are valid only for the specific product (or specimen) geometry tested and cannot be applied to other geometries. However, testing failure times is easy to carry out and is useful as a quality control method.

The second and more advanced approach to crack growth involves the application of stress intensity factor K, as defined in the field of "fracture mechanics". The stress intensity factor K characterises the stress distribution at a crack tip and has proved to be an adequate crack growth parameter for many materials ([41]). In the theoretical case of an infinitely wide plate, K is a function of average tensile stress level (σ) and crack length (a) according to $K = \sigma\sqrt{\pi a}$. For practical geometries (i.e. finite dimensions) the formula is extended by a "correction factor" C.
Crack growth of a material, as a function of the K value, must be measured empirically. Normally this is done in a laboratory, using standard specimens. The behaviour of crack growth as a function of K can be used to study the fundamental mechanisms of crack growth. Moreover K also provides a practical advantage, in that K can be calculated for any geometry. Consequently, laboratory results can be applied to the crack growth behaviour of products. In other words: crack growth as a function of K can be considered a material property.
To calculate K, it is necessary to know the crack length (a) and this requires monitoring the crack during crack growth. In using K, the necessary crack length measurements complicate the experiments compared with the tests of the stress-lifetime approach.
The theory of K is based on pure linear elastic material behaviour and strictly spoken cannot be applied to many practical materials. Nevertheless, in a large number of materials, K as a crack growth parameter has been found to work adequately as long as plastic zone dimensions are limited. The use of K in practice is therefore restricted to relatively brittle materials or large specimens, and the application of K in ductile polyethylene would not appear to be appropriate. In spite of this impression, the use of K in polyethylene can be justified, as discussed in section 5.2 with respect to fatigue crack growth.

In this thesis different crack growth test methods are employed. Some tests use the concept of stress intensity, while for practical reasons other tests are based on the stress-lifetime approach. Fatigue tests are performed using crack length measurements (K approach, section 3.2). Creep crack growth is evaluated predominantly by the "stress-lifetime" procedure, which currently represents the customary approach to creep crack growth (PENT tests, section 3.3). However, some creep crack growth experiments using the K concept were also performed during the extrapolation load series (section 3.2, values at R = 1).

1.3 General approach

Three types of polyethylene are tested with respect to their crack growth behaviour. Crack growth under both cyclic and constant load conditions are studied and the results evaluated in relation to one other. The micromechanisms of failure at crack tip level are also considered.

Materials tested

Crack growth in polyethylene is tested for three distinct types of polyethylene gas pipe materials. By using several types of material, general crack growth behaviour can be distinguished from exceptional effects related to one specific type of material only. The understanding of general crack growth behaviour has more potential than knowledge of restricted effects. Section 2.1 contains general information about polyethylene, while section 3.1 provides detailed information about the materials tested.

Macroscopic crack growth behaviour

Crack growth behaviour is characterised by macroscopic measurement of crack growth rates as a function of several crack growth parameters. With crack growth a clear distinction between fatigue crack growth and creep crack growth must be made.

Fatigue crack growth = Crack growth under *cyclic* loading conditions.
Fatigue crack growth is evaluated with notched CCT specimens loaded in a servo-hydraulic test machine with automated crack length measurement. ΔK is considered to be the governing crack growth parameter, while variation of load ratio R and frequency f of the cyclic load applied are used to assess the role of creep mechanisms during fatigue. Furthermore the effects of temperature, waveform and specimen thickness are considered. Experimental details are given in section 3.2 and chapter 4. Fatigue crack growth results are discussed in section 5.2.

Creep crack growth = Crack growth under *constant* load conditions.
Creep crack tests are predominantly performed using a standard "PENT test" protocol. In this test method a constant load (using dead weights) is applied to notched SENT specimens. Basically the COD is measured automatically at several load levels, resulting in stress-lifetime data with optional assessment of crack growth rates. The PENT tests in the first place result in a ranking of the three types of materials used with regard to their creep crack growth properties. Experimental details of the PENT test are given in section 3.3, while test results are discussed in section 5.1.

The relation between creep crack growth and fatigue crack growth is evaluated quantitatively in a test series in which cyclic fatigue loads are gradually transformed into a constant load. This method of testing is designated "extrapolation" load series and is performed with CCT specimens loaded in a servo-hydraulic fatigue machine. Details of the extrapolation load series are given in section 3.2, while results are discussed in section 5.3.

Micromechanisms at crack tip level

Ultimately, crack growth is manifested by failure of material in the confined region of the crack tip. The microscopic failure process at the crack tip basically determines the macroscopic crack growth behaviour as measured. Evaluation of the micromechanisms leads to a more basic understanding of the macroscopic crack growth observed.

SEM observations:

To visualise the process at crack tip level, both fracture surfaces and side view images of the crack tip are observed in the Scanning Electron Microscope (SEM). Fracture surfaces reflect the situation after fracture. Degree of deformations, markings etc. provide information about the failure mechanism.

A side view of a crack tip is obtained by cutting out a small volume of material located around an existing crack tip, leaving the crack tip intact. Subsequently, the sample containing the crack tip is studied in the SEM, reflecting the situation as present during the process of crack growth. The geometry and configuration of the crack tip is essential in order to understand the micromechanisms of crack growth.

Details of procedures using the SEM are given in section 3.5, while results are discussed in section 6.2.

Mechanical properties:

The crack tip in polyethylene can be considered as a two-phase system consisting of a region of highly stretched material (the craze) surrounded by intensely loaded bulk material. Details of the configuration of the crack tip in polyethylene are given in section 2.2.

Tensile and creep properties are measured in order to evaluate whether macroscopic mechanical behaviour can be related to the micromechanism at crack tip level. Normal tensile specimens are used to reflect the behaviour of bulk material around the craze. In addition, specially shaped specimens are used to simulate the behaviour of highly stretched material within the craze

Experimental details are given in section 3.4 and results are discussed in section 6.1.

Overall, the combination of crack growth behaviour, tensile and creep response, together with the SEM observations, give a broad understanding of the factors controlling crack growth.

2. Crack growth in polyethylene and other thermoplastics

Crack growth in general is determined by the load level, external factors (temperature, chemical environment) and material properties (type of material, microstructure etc.).

2.1 Polyethylene; structure and mechanical behaviour

Polyethylene, a straightforward polymer, containing only C and H atoms, is produced by polymerisation of ethylene ($CH_2 = CH_2$), resulting in long regular chains. The regular structure makes it possible for the chains to be closely packed next to each other, which represents crystallisation. The regular chains are sometimes "disturbed" by side groups (or branches) with a length ranging from 2 to 10 C atoms. The occurrence of branching locally prevents crystallisation, resulting in volumes of randomly arranged molecules designated as amorphous regions. A high degree of branching results in polyethylene with low degree of crystallisation.

The density of a crystalline region is higher than the density of an amorphous region. Consequently, the degree of crystallinity affects the density of the semi-crystalline polyethylene. A crystalline volume percentage of 70-85% results in a density of polyethylene of approximately 950 kg/m^3. This type of polyethylene is indicated as High Density Polyethylene or HDPE. Likewise a crystalline volume percentage of 45-55% results in a density of polyethylene of approximately 920 kg/m^3 , which is indicated as Low Density Polyethylene or LDPE.

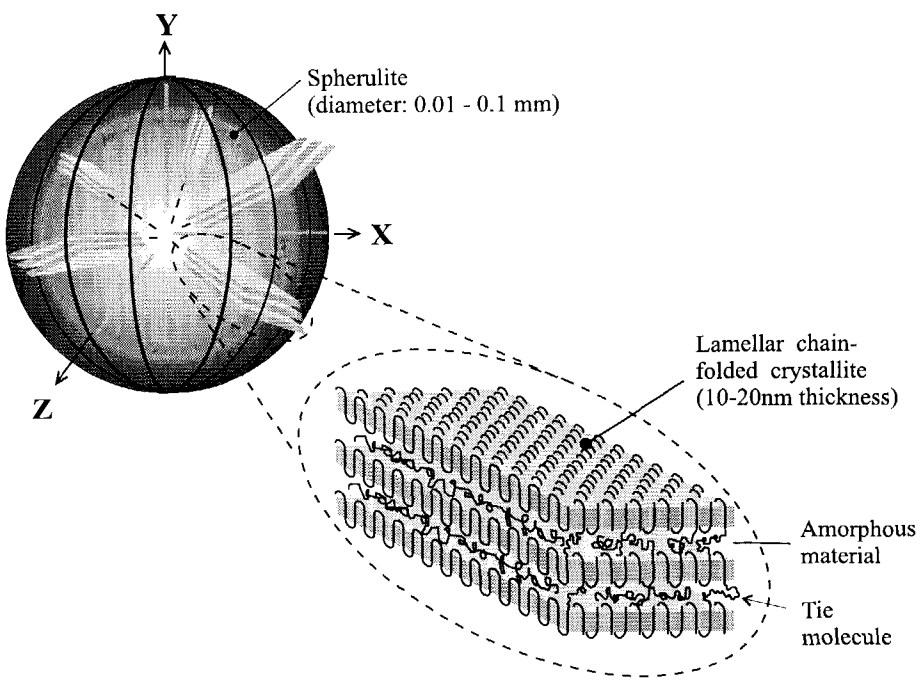

Figure 2-1 : Semi-crystalline structure of polyethylene with lamellar chain-folded crystallites and formation of spherulites.

For practical reasons, polyethylene is generally characterised by its density, as this is easy to measure and the density directly corresponds to the degree of crystallinity. The degree of crystallinity greatly affects the mechanical behaviour of polyethylene. At room temperature the crystalline regions give polyethylene its strength, while the amorphous regions are mainly responsible for its ductile, time-dependent behaviour. In this respect semi-crystalline polyethylene can considered to be a composite material with crystalline and amorphous regions as components.

The configuration of alternating crystalline and amorphous regions is given schematically in figure 2-1. According to [20], the crystalline regions consist of folded-chains, producing thin lamellae. The lamellae are also indicated as crystallites. Individual crystallites are separated by amorphous regions, constituting a layered structure of alternating crystalline and amorphous regions. Sometimes a single molecule interconnects the crystallites. Such interconnecting molecules are called tie-molecules.

An aggregate of lamellar crystallites can be further arranged in a spherical structure with a diameter of 0.01-0.1 mm. The spherical structure is indicated as a spherulite and is composed of many different lamellar crystallites and, in addition, some amorphous material.

Time-temperature equivalence

Relative movement between chain segments is controlled by the way in which the segments interact. It is customary to describe relative movement within a polymer chain as a process in which a potential barrier (ΔU) has to be overcome [21]. The driving force for chain movements is their thermal energy (kT). The Arrhenius equation describes the frequency (ν) of chain segments in order to overcome the potential barrier:

$$\nu = \nu_0 \cdot e^{\left(\frac{-\Delta U}{kT}\right)} \quad : \text{ Arrhenius equation} \qquad \{1\}$$

ν_0 = natural frequency
ΔU = potential barrier
kT = thermal energy
(where k is Boltzmann's constant and T the absolute temperature)

The frequency ν reflects the occurrence of chain movements. Clearly, with a rising temperature the value of ν increases along with the temperature. Therefore deformation is facilitated at a higher temperature.
Equation {1} can also be interpreted in the time domain. The frequency ν also determines the time scale (τ) in which deformations mainly occur. A high value of ν represents a short deformation time scale (i.e. $\tau \div 1/\nu$). A high temperature and high value of ν therefore is equivalent to a short time-scale of deformation. The relation between the time-scale of deformation and temperature, as given by equation {1}, basically represents the time-temperature equivalence of deformation in thermoplastic polymers. A rise in temperature is equivalent to a decrease in deformation time and vice versa (i.e. the influences of time and temperature are interchangeable).

Glass transition Tg in amorphous regions

A striking feature of the amorphous state is the transition in mechanical behaviour at a certain temperature T_g, the glass transition temperature. Below T_g the amorphous region is relatively stiff (*glassy* state), while above T_g the modulus is largely reduced (*rubbery* state), see figure 2-2.

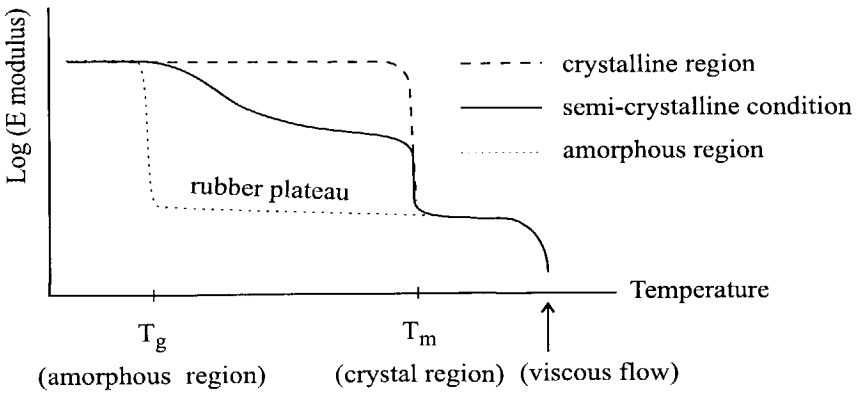

Figure 2-2: Temperature dependence of the modulus of a semi-crystalline polymer, showing the glass transition.

The occurrence of T_g is related to the relationships between chain flexibility, temperature and time, as discussed above. At T_g the vibration frequency of main chain segments becomes comparable with the time scale of deformations at which the E modulus is commonly measured, roughly in the order of 1 minute. In terms of energy, T_g can be interpreted as the starting point from which the thermal energy (kT in equation {1}) outbalances the potential energy barrier of main chain movement (ΔU in equation {1}) and facilitates relative motion between adjacent molecules in the amorphous network [22, 23]. Deformations in the rubbery state are limited fortunately, by the existence of physical crosslinks, the entanglements. The entanglements provide the plateau range of rubber-like behaviour and act in a similar way to the chemical crosslinks in vulcanised rubber. However, at high stresses (or long loading times) disentanglement will occur, representing irreversible creep or viscous flow. Other deformation-limiting mechanisms, such as constraint by crystalline regions and the existence of tie molecules, will be discussed later.

Viscoelastic behaviour in amorphous regions

The transition from the glassy to the rubbery state does not happen instantaneously but takes place gradually over a temperature range i.e. the glass transition region. Within this intermediate temperature range the material displays viscoelastic behaviour, i.e. a combination of elastic and viscous properties. The elastic behaviour can be linked to both the glassy and the rubbery state, in which the moduli are relatively constant and time-independent. The viscous behaviour is ascribed to friction between moving chains, comparable to shear processes in a viscous liquid. The viscous behaviour is reflected by the dependence of the modulus on temperature (and time), constituting *time-dependent* material behaviour. In practice, viscous properties are experienced as creep and recovery phenomena (i.e. time-dependent).

Viscoelastic material behaviour can be illustrated by a "Burgers" damper-spring model (see figure 2-3), comprising a combination of a Maxwell element (I) and a Voigt element (II) in series. The model is especially useful for visualising viscoelastic behaviour but it is inadequate for actual modelling purposes ([22]). In part I, the damper represents irreversible deformation (i.e. viscous flow), while the spring in part I allows instantaneous elastic deformations. The configuration of part II reflects delayed and reversible deformations.
Damper-spring elements can model only linear viscoelastic behaviour, i.e. a linear relation between the applied load and resulting deformation. In reality, however, most viscoelastic materials behave in a non-linear manner and other models have to be used [22].

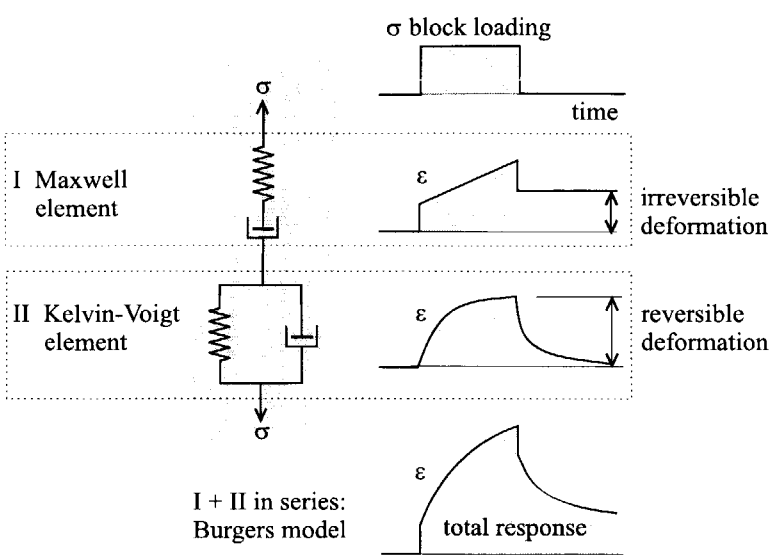

Figure 2-3 : Damper-spring configurations, visualising viscoelastic behaviour.

Mechanical interaction of amorphous and crystalline regions in semi-crystalline polyethylene

The glass transition temperature of pure amorphous polyethylene is approximately -120 °C. The crystal regions are stronger and stiffer than the amorphous regions and act as fillers which constrain deformation in adjacent amorphous regions and consequently raise T_g. Moreover, the constraint is not evenly distributed throughout an amorphous region but will be more pronounced at the crystalline-amorphous interface. Correspondingly, T_g is not raised evenly throughout the amorphous region, resulting in a broadening of glass transition when the overall material behaviour is considered [24, 22].

Apart from the presence of constraint and entanglements, existing "*tie molecules*" can also prevent large deformations in amorphous regions. A tie molecule interconnects two separate crystalline regions by having both ends in different crystalline regions while the middle section of the chain passes through an amorphous region (see also figure 2-1). Therefore tie molecules *directly* interconnect crystalline regions and can be regarded as intercrystalline chemical crosslinks.

Copolymers

The polyethylene gas pipe materials initially used were homopolymers with only ethylene as monomer in the polymerisation process. These homopolymers are sometimes referred to as first generation gas pipe materials.
Currently, gas pipe polyethylenes are produced by copolymerisation of ethylene and a small amount of another type of monomer, commonly butene or hexene. Officially, a copolymer of ethylene and butene should be referred to as an ethylene-butene copolymer. Usually, however, the material is simply called a polyethylene copolymer without specific reference to the type of comonomer. In relation to gas pipe applications, a polyethylene copolymer is usually referred to as a material of the second generation.

In a polyethylene copolymer, the small amount of comonomer provides the backbone chain of regularly distributed branches, with a typical number of 5-10 branches per 1000 C atoms. Moreover the branches are relatively long. The branches inhibit crystallisation and consequently reduce the density. The decrease in density is not, however, accompanied by an overall decrease in mechanical strength, as would be the trend in homopolymers when densities are lowered. In copolymer polyethylenes the preservation of strength is ascribed to an increased amount of tie molecules. The exact mechanism by which the tie molecules are formed is not fully understood yet. ([25])

The most recent distinction in polyethylene gas pipe materials concerns copolymer polyethylenes in which branching is controlled so as to be more pronounced in the longer molecules with respect to the current molecule length distribution. This type of polyethylene, in which the tie molecules are longer, with more capacity to bridge crystalline regions, is called third generation polyethylene.

Table 1-1 specifies some properties of the three types of polyethylene tested in this thesis, indicating the comonomer. Two of the materials are of the "second generation", while the third material belongs to the "third generation".

	Material code		
	O	**T**	**F**
Material origin	extruded plate	gas pipe	gas pipe
Density [kg/m^3]	0.958	0.958	0.948
Comonomer	butene	butene	hexene
Generation	second	third	second

Table : 1-1 : Properties of materials tested.

The black box approach with respect to molecular structure

Molecular structure cannot be characterised by one parameter but is a collection of properties which together control mechanical behaviour (including creep crack growth). In this study much attention is given to the evaluation of creep during crack growth. Since creep crack growth is basically localised creep, a relation between general creep properties and creep crack growth behaviour can be expected (section 2.3). Creep can be considered the phenomenon controlling creep crack growth, without actual knowledge of the mechanism on a molecular scale.

Thus, with respect to crack growth the materials tested are characterised not by their molecular structure but by their general creep behaviour. The connection between molecular structure and creep behaviour is not considered beyond the level of general backgrounds (section 2.1). Further information about the effect of physical and chemical properties on mechanical behaviour is given in [26, 27, 28 and 53].

2.2 The craze : the "plastic zone" of thermoplastic polymers

The term "craze" originates from the field of ceramics, where a pattern of fine, evenly distributed, surface cracks can sometimes be observed. For ceramics such a surface is referred to as a "crazed surface". In thermoplastic polymers, especially the clear transparent ones, a similar appearance of surface cracks is possible. By analogy with ceramics the terminology "crazed surface" has been maintained. However, it was found that cracks in polymers may differ from ordinary cracks, as the fracture may display an intermediate state in which the crack is partially filled with highly drawn material. The original term *craze* was again maintained, now in order to distinguish the "filled crack" state in polymers from a real crack. A craze still has a load-bearing capacity, as the surrounding bulk material is bridged by the contents of the craze. The highly drawn material in the craze is often in the form of many adjacently situated fibres called *fibrils*. A craze can be considered a mixture of fibrils and voids. The fibrils may finally break, turning the craze into a real crack. At the new crack tip, a craze can be formed again and the whole process repeated, constituting a discontinuous crack growth process (section 2.6.). As a rough indication, the craze can be interpreted as the equivalent of the plastic zone at the tip of cracks in metals.

The condition of many simultaneous crazes in a thermoplastic polymer is mentioned only in order to illustrate the origin of the term craze. In gas pipe service conditions, crack growth is

predominantly restricted to one location where an accidental stress concentration has lead to the initiation of one particular craze, with subsequent crack growth. During test conditions this situation can be simulated by use of notched specimens. A craze is forced to initiate at the tip of the notch. As a result, crack growth can be monitored by observation of this one well-defined craze.

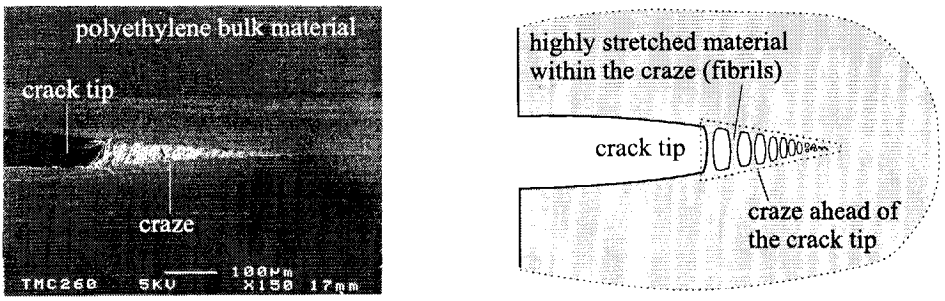

Figure 2-4 : Real craze ahead of a loaded crack tip in polyethylene (left) and its schematic representation (right).

Figure 2-4 represents a crack in polyethylene with a craze at the crack tip[1]. The craze normally has a wedge-shaped form which can be characterised by a height (at the base of the craze) and a length. An essential feature of a craze is its stability.

The stability of a craze is due to three factors: a) the uniaxial stress state in the craze fibrils, b) blunting at the crack tip and c) the mutually independent fibril structure.

a) Uniaxial stress state in the craze fibrils

The initiation of a craze is stimulated by the hydrostatic stress state at the crack tip. However, once a craze is formed the stress state in the craze is reduced to the stress state of each individual fibril. The fibrils are to a greater or lesser degree mechanically uncoupled in the plate thickness direction resulting in an uniaxial stress state in the fibrils. Hence, deformation of the fibrils is not constrained and the fibrils can become elongated to their maximum extent with corresponding ordering of molecules (i.e. crystallisation) and increasing fibril strength (strain hardening). Consequently, the craze as a whole behaves in accordance with strain hardening, which increases the stability of the craze.

[1] In reality the fibrils do not individually bridge the crack flanks. Instead, the craze material consists of a network of highly drawn material, resembling a cellular structure [29].

b) Blunting

Blunting reduces the extent of the high stresses and strains at the crack tip and is to be regarded as a major barrier for crack growth. The amount of blunting can be expressed as the distance between the crack flanks at the crack tip, which is also referred to as Crack Tip Opening Displacement or CTOD (see figure 2-5). From figure 2-4 it is obvious that the CTOD in the presence of a craze is equal to the height at the craze base, which in terms of blunting is extremely great. Therefore the craze in itself provides a considerable amount of crack tip blunting which stabilises the crack tip. It should be noted that various materials show some degree of "natural" blunting due to inevitable plastic deformations at the crack tip (i.e. the plastic zone)[30]. However, blunting caused by crazes is exceptional due to the unconstrained deformation potential of the fibrils. Blunting is described in more detail in section 2.5.

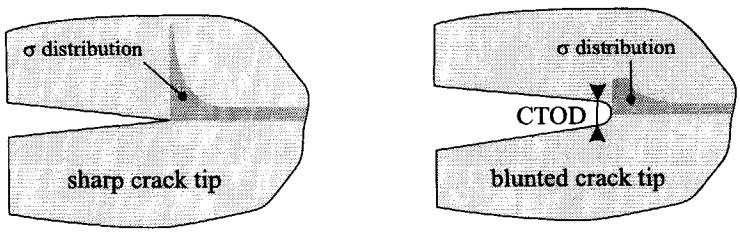

Figure 2-5: A sharp and a blunted crack tip.

c) Partially independent fibril structure

Another stabilising factor of crazes is the fact that mutual fibrils are, to some extent, mechanically uncoupled. In homogeneous materials a running crack constantly creates its own new crack tip. In a craze, the failure of one individual fibril does not necessarily result in *physical* damage to the other fibrils. Of course, indirectly the surrounding network of fibrils is affected, as it takes over the load that the broken fibril was previously carrying. Nevertheless, accidental failure of one fibril will not directly result in general craze breakdown, which is favourable for the stability of the craze.

The crack tip can be characterised by the craze and its surrounding bulk material. The fundamentally different structure and properties of a craze compared with the surrounding bulk material leads to the interpretation of the crack tip as a two-phase system, the two phases being homogeneous bulk material and highly drawn craze material. In [31,38] the crack tip is also specifically regarded as a two-phase system and the damaged material of the craze is indicated as "the crack layer".

2.2.1 Multiple and single crazing

At low load levels or low stress intensity the volume of the highly stressed area at the crack tip is small and comparable in size with the deformation grade of a craze itself. Therefore at low load levels a single craze can absorb most of the high stresses at the crack tip. Once the single craze has developed, stresses in the vicinity of the craze are relieved and development of more crazes is suppressed.
At high loads (or high stress intensity), the extended volume of the highly stressed area can only be reduced partially by one single craze. In that case other secondary crazes develop in the surrounding bulk material (of the initial single or primary craze). The existence of more crazes at the crack tip is referred to as "multiple crazing" and is illustrated for polyethylene in figure 2-6. Multiple crazing extends the volume of plastic deformation and also the amount of blunting is increased. Therefore multiple crazing acts as an additional stabilising mechanism if cracks are loaded more intensively.

The presence of single or multiple crazing is reflected by the appearance of the fracture surface. When a crack has proceeded through a single craze the fracture surface is smooth and is referred to as "mirror region". The crack path through a multiple craze can jump from one craze to another, resulting in a rough fracture surface referred to as "mist region" [32, 53].

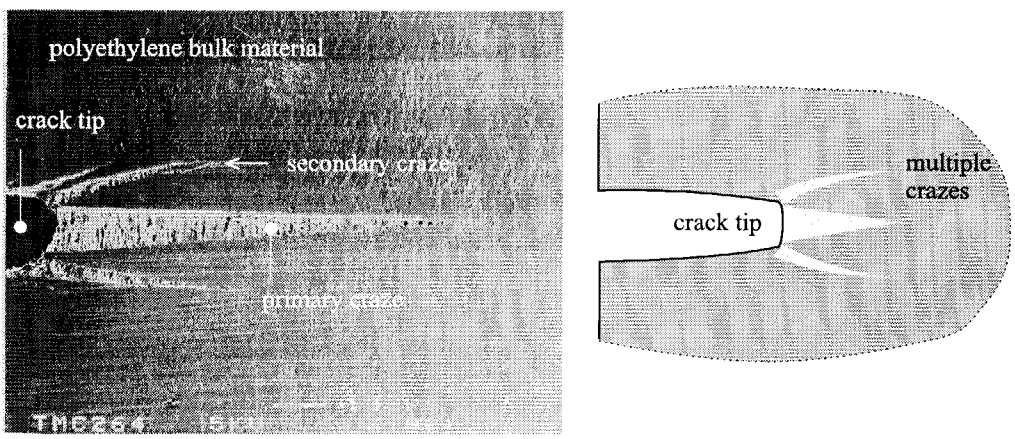

Figure 2-6 : Real multiple crazing at a loaded crack tip in polyethylene (left) and the schematic representation (right).

2.2.2 Application of the Dugdale model to predict the craze dimension

In 1960 Dugdale introduced a "strip-yield" model to characterise the plastic zone in metals. The model is based on ideal elastic-plastic stress-strain behaviour, in which above the yield stress no strain hardening occurs. The assumed stress-strain behaviour is an approximation of actual mechanical properties of strain hardening metals but the assumption was made to simplify the calculations. In figure 2-7, however, the stress-strain curve of polyethylene is given, which actually resembles ideal elastic-plastic behaviour. The plateau in the stress-strain curve of polyethylene is caused by necking (cold drawing), gradually extending over the length of the specimen. When necking has covered the whole length of the specimen, the original chain-folded crystallites break up into chains that are forced to align with strain hardening as a result.
In section 6.2.2 it will be shown that the Dugdale approach is suitable for calculations of craze dimensions.

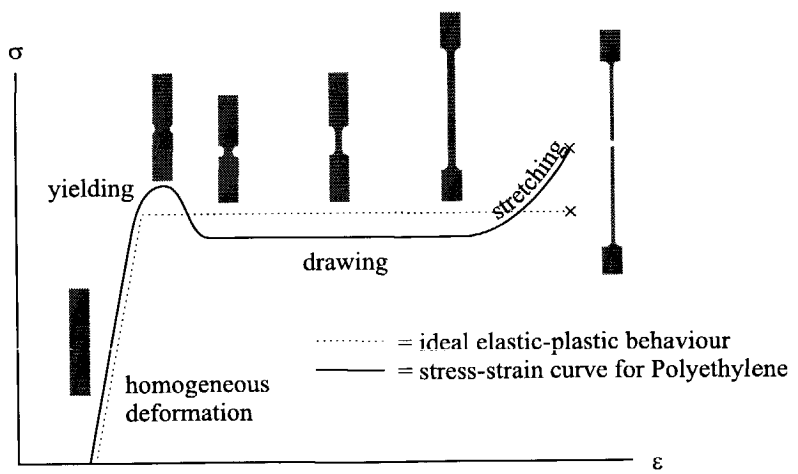

Figure 2-7 : The stress-strain curve for polyethylene, resembling ideal elastic-plastic behaviour.

2.3 Creep crack growth

When a polyethylene tensile specimen is loaded (with a constant load) it will creep, with deformations distributed uniformly over the length of the specimen. This type of creep can be indicated as "bulk creep". If the load is high enough the specimen will ultimately break somewhere along its length, due to advanced disentanglement in combination with physical fracture of chains (chain scission). This type of failure is ductile and is designated here as "bulk creep failure".
The fibrils of a craze at a crack tip in polyethylene can be regarded as a collection of microscopic tensile specimens that are highly loaded with corresponding features of necking and stretching (figure 2-6). Therefore, the fibrils can also fracture ultimately, as in bulk-creep failure in macroscopic tensile specimens. The failure of fibrils constitutes craze breakdown and the onset of creep crack growth. The fibrils fracture in a ductile way and consequently the mechanism of creep crack growth is in essence a ductile failure mechanism. However, since the ductile deformations are confined to the microscopic scale of the craze, the macroscopic appearance of creep crack growth is brittle and creep crack growth is usually classified as brittle failure. *To prevent confusion it should be kept in mind that the micromechanism of creep crack growth is very ductile but in contrast creep crack growth is classified as brittle failure in view of its macroscopic appearance.*

Note: Also brittle, but fundamentally different from creep crack growth, is the phenomenon of "rapid crack propagation". Rapid crack propagation may occur in polyethylene gas pipes during maintenance routines, for instance a sudden impact load applied accidentally by a shovel. Here, the short fracture time span causes brittle fracture, both on a macroscopic and on a microscopic scale.
A crack formed during a slow creep crack growth process constitutes a potential initiation notch for rapid crack growth to occur. In this respect rapid crack propagation depends on the slow crack growth properties of a material.

2.3.1 Overview of accelerated fracture tests predicting creep crack growth

Under gas pipe service conditions (i.e. ambient temperature and low stress levels) creep crack growth is a very slow mechanism. Accelerated fracture tests aim to predict creep crack growth behaviour within a reasonable testing time. For gas pipes a minimum lifetime of 50 years is commonly required. Creep crack growth is basically a localised creep phenomenon, which implies a promotion of creep crack growth by raising temperature and/or stress. A variety of tests have been developed using increased temperature or stress to accelerate creep crack growth. An overview of test methods is given here. Not all test methods mentioned were actually carried out for this thesis but they are discussed nevertheless in order to complete the historical background of creep crack growth testing.

The hydrostatic pressured pipe test and notch test are accepted by standardisation authorities (EuroNorm EN921 and EN33479 respectively). These two test methods were not actually used for this thesis, as the test equipment required was not available. The PENT test is a recently developed alternative for testing creep crack growth and was used for this thesis since the test is simple to perform. However, the PENT test is not yet widespread, as recognition as a standard test has been achieved only recently (ASTM F1473).

Application of fatigue to predict creep crack growth is a controversial technique and standardisation does not exist. Fatigue tests are specifically performed for the purposes of this thesis in order to evaluate the relation between fatigue and creep crack growth.
Apart from fatigue there are other test methods that can be classified as "alternative" with regard to their significance in predicting creep crack growth, for example, testing in a soap-water solution [4]. Only fatigue will be evaluated from among the various alternative test methods for predicting creep crack growth.

Original hydrostatic pressured pipe test; ductile and brittle failure (EN 921)

The hydrostatic pressured pipe test uses a complete piece of pipe of a certain length, which classifies the test as a "full-scale" testing method. The pipe is immersed in a water-filled container while the pipe is internally pressurised in combination with raised temperature. The time to failure (T_f) is measured at multiple combinations of pipe wall hoop stress and temperature. The results are commonly presented graphically with double logarithmic scaling, as illustrated in figure 2-8. Results tested at the same temperature can normally be fitted by two straight lines with different slopes. The two lines represent different failure mechanisms, ductile and brittle failure. Ductile failures appear at high stresses with short failure times and relate to bulk creep failure. Brittle failures constitute creep crack growth at low stress levels with long failure times. Only the brittle failures can be used to predict creep crack growth under service conditions. It should be noted that the total brittle failure time is composed of a craze initiation period and a subsequent crack growth interval.

As illustrated in figure 2-8, elevated temperatures cause brittle failure to occur at lower stress levels. However, more importantly the transition from ductile to brittle failure takes place at shorter failure times. *This means that brittle failure can be reached within shorter testing times at elevated temperatures.*

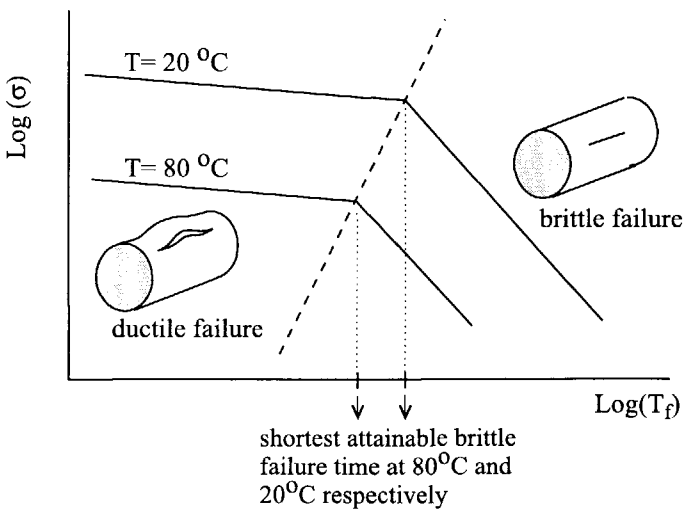

Figure 2-8 : Relation between stress level and time to failure in a hydrostatic pressured pipe test.

Alternative accelerated test methods: the notch test, the PENT test and fatigue testing

The hydrostatic pressured pipe test worked well for materials of the first generation (homopolymers) in which brittle failures were reached within weeks. The enhanced quality of current second and third generation materials (i.e. copolymers), however, requires prolonged testing times if brittle failure happens at all. An adjustment to the standard pressurised pipe test was found in notching the pipes in the lengthwise direction. In this way the initiation of a craze is accelerated with consequent reduction of total failure time. Frequently the test with a notched pipe is simply referred to as a "notch test", although it basically remains a "hydrostatic pressured pipe test". The notch in the pipe is machined by means of a cutter wheel. The notch test is standardised in EuroNorm EN33479.

Brown reduced the full scale notch test to a test using small specimens sampled from the pipe and subsequently notched with a razor blade (see figure 3-6) [5]. The test is known as the PENT test and is standardised in ASTM F1473. The PENT test was used for this thesis. Details can be found in section 3.3. Like pressured pipe tests, the PENT test comprises testing at several combinations of temperature and stress, while the resulting time to failure is recorded. The test results of the PENT test are also represented in accordance with figure 2-8. The PENT test produces shorter failure times than the notch test, due to a further reduced initiation time caused by the improved notching procedure with a razor blade. Apart from shorter failure times, the PENT test is easy to carry out and does not require extensive test equipment.

A potential new method to accelerate creep crack growth is the use of cyclic loading. Cyclic loading (i.e. fatigue) is found to produce brittle failures, whereas the fracture surface looks similar to that formed during creep crack growth. Hence a corresponding fracture micromechanism is likely. Comparison of fatigue properties with creep crack growth properties gave the same ranking of materials within a group of polyethylene materials of the same copolymer type [2]. This indicates at least the existence of a qualitative correlation between fatigue and creep crack growth.
Nevertheless, prediction of creep crack growth using fatigue is still a controversial technique, which is also reflected in the variety of fatigue testing procedures reported. The test methods range from full-scale *pulsation-pressured* pipe tests ([33]) to tests using tensile fatigue specimens ([2, 3, 6, 35, 36, 37, 38, 39, 40, 42]). In most reports failure times are measured as a function of fatigue load level and are compared with results of constant load tests. Obviously fatigue testing to predict creep crack growth is not yet standard.

The acceleration of fatigue is not confined to the initiation period but also applies to the crack growth stage. In this thesis the fatigue behaviour is mainly studied by measurement of the fatigue crack growth rate da/dN, giving more detailed information than the measuring time to failure only. Details of the fatigue tests performed are given in section 3.2.

2.4 Fatigue crack growth

Basics of fatigue, historically based on behaviour of metal alloys

Fatigue is the phenomenon of delayed failure of a material under prolonged *alternating* load conditions. Typically, the level of loading is moderate and would normally, during a single loading-unloading procedure, not cause failure.

Fatigue in metals has been experienced for over a hundred years and has been studied intensively. Fatigue is associated with the initiation and subsequent growth of a crack. Hence, fatigue is a localised damage mechanism. In metals the fundamental damaging mechanism of cyclic loading is identified as *cyclic* plastic deformation in a part of the plastic zone (at the crack tip). In general plastic deformation damages material. Repeated plastic deformation constitutes accumulation of damage and will finally result in fracture. Thus, during each fatigue load cycle some part of the cyclic plastic zone will fracture, establishing a crack extension Δa during each load cycle N. Considering the governing role of load cycles, fatigue crack growth rate is expressed as da/dN. For metals, the mechanism of crack growth per load cycle is confirmed by SEM observation, in which dimensions of markings (striations) can be matched with macroscopic calculated values of da/dN.

The amount of *cyclic* plastic deformation is determined by the *range* in loading or ΔK in terms of stress intensity, while the absolute level of loading is of less importance. Correspondingly, fatigue crack growth in metals is determined mainly by ΔK.

Fatigue in thermoplastic polymers

When polymers were introduced the applications were initially confined to non load-bearing products in which fatigue has no relevance. However, during the last two decades polymers have been used increasingly as load-bearing construction materials. These polymers are referred to as "engineering plastics". Naturally, along with load-bearing applications, fatigue failure was increasingly encountered in polymer products. The current knowledge of fatigue in metals was applied with reasonable success to fatigue in polymers. For polymers, the mechanism of fatigue as an initiation and subsequent crack growth mechanism, as well as the application of stress intensity as a fatigue parameter, was adopted successfully from the field of metal fatigue. However, differences in polymer fatigue behaviour are bound to occur, owing to the different nature of polymers with regard to viscoelastic behaviour and the occurrence of crazing. The configuration of a craze as a mixture of voids and fibrils is unlikely to produce a mechanism of cyclic plasticity identical to that in fatigue of metals. Instead, viscoelastic disentanglement, induced by cyclic stretching of the fibrils, is regarded as the basic damaging mechanism in polymer fatigue [53, 3]. The different nature of fatigue in polymers compared with metals is also reflected in differently acting crack growth mechanisms. Typically, discontinuous crack growth is observed in polymers, as discussed in section 2.6.

In spite of different damaging mechanisms, fatigue in metals and polymers are both governed by ΔK. Dependence of fatigue behaviour on temperature, frequency, waveform and average load level is ascribed to the viscoelastic nature of polymers.

The parameters of fatigue and the Paris fatigue crack growth model

A fatigue load is defined by the range of stress intensity (ΔK), load ratio R ($= K_{min}/K_{max}$), frequency of loading (f) and shape of the cyclic load. A typical fatigue load is illustrated in figure 2-9. ΔK is the governing parameter controlling fatigue crack growth, while other parameters are considered as secondary.

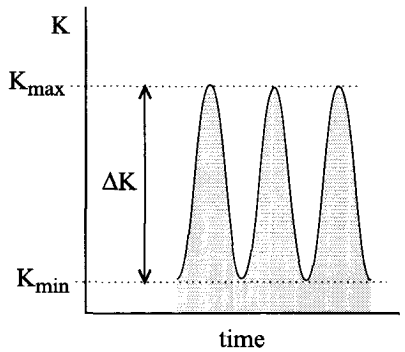

Fatigue load parameters are:

- ΔK
- $R = \frac{K_{min}}{K_{max}}$
- waveform and frequency of cyclic load

Figure 2-9 : The parameters characterising a fatigue load.

The dominant influence of ΔK is demonstrated by the frequent use of the Paris fatigue crack growth model. In this model only ΔK is used as an active parameter:

$da/dN = C\,(\Delta K)^m$: Paris crack growth law. {2}

Crack growth rates as a function of ΔK are conveniently represented graphically using double logarithmic scaling, as Paris behaviour in this way appears as a straight line (with slope m, see figure 2-10) The values of C and m are found by fitting procedures and comprise all secondary parameters. Although fatigue is very sensitive to ΔK, this is not the only reason why the Paris law has widespread application. The consistent trend in ΔK-dependence, among different materials under different conditions, also contributes to the popularity of the Paris law. The small range in values of the exponent "m" observed in the Paris law is illustrative. Most materials, including metals and polymers, have a value of "m" between 3 and 5.

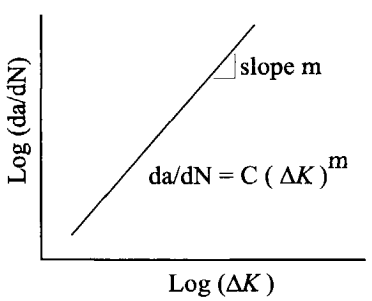

Figure 2-10: Representation of Paris fatigue crack growth behaviour.

Secondary parameters can also have a considerable effect on crack growth which would justify modification of the Paris law. In many cases, the influence of secondary parameters is, however, confined to one type of material and general validity is therefore not obtained. For example, in some polymers the effect of frequency is substantial while for other polymers no such effect is found. Consequently, a general effect of frequency cannot be modelled.

Creep contributions during fatigue crack growth in viscoelastic materials

Creep crack growth is controlled by creep mechanisms only. Fatigue crack growth, however, cannot be ascribed exclusively to cycle-induced damage mechanisms. Cyclic tensile fatigue loads always include the presence of an average tensile component. The tensile component can act in a similar way as the constant load during creep crack growth. Therefore, what is normally called fatigue crack growth, is in actual fact a combination of "pure fatigue" and creep crack growth. The designation "pure fatigue" is used here to indicate the exclusively cycle-related damage. The term "fatigue" alone is used here in the traditional way (i.e. the phenomenon of crack growth under cyclic loading conditions), although this may be accompanied by creep contributions.

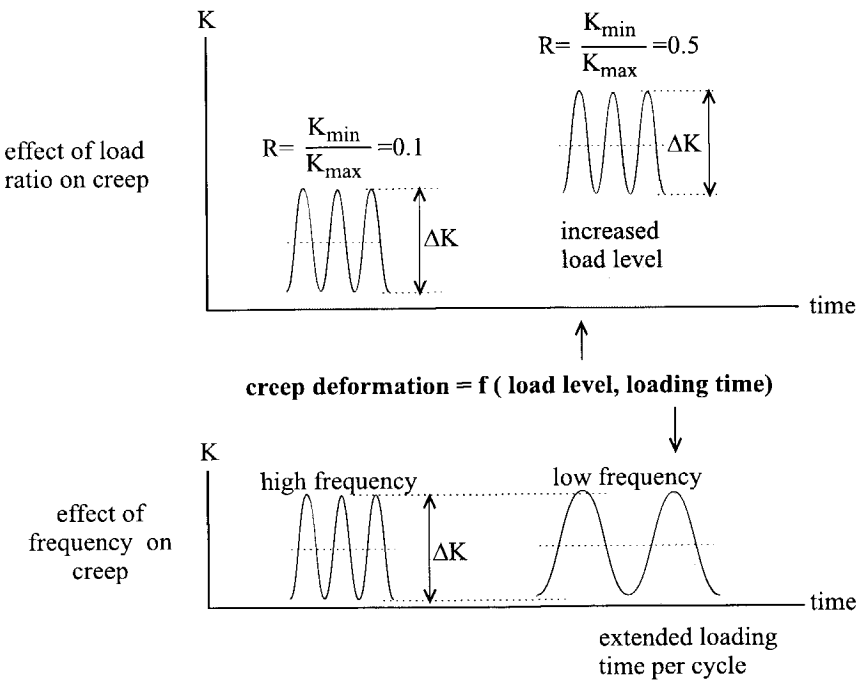

Figure 2-11 : The significance of load ratio and frequency on creep behaviour.

Understanding the contribution of creep mechanisms during fatigue may contribute to the question of whether or not fatigue can be used for the prediction of creep crack growth.
Effects of the secondary parameters of fatigue load, frequency (f) and load ratio (R), may be related to creep induced behaviour (see figure 2-11). In general, a creep deformation is determined by both level and duration of loading. Thus, creep is determined by aspects of time and load level.

At lower frequencies the time for each *individual load cycle* is extended and creep deformations per cycle are promoted by time-induced creep. In [53] the Frequency Sensitivity

Factor (FSF) is introduced as the factor by which *da/dN* increases per decade increase of periodic time. FSF is a convenient parameter to characterise frequency effects. A value of FSF = 1 is associated with "pure fatigue" i.e. a damage mechanism acting per load cycle and not affected by load frequency. A value of FSF = 10 corresponds to a constant crack growth rate per unit of time i.e. *da/dt* is constant, related exclusively to time-dependent creep mechanisms. Intermediate values of FSF (between 1 and 10) imply the coexistence of creep and fatigue mechanisms during crack growth under cyclic load conditions.

Apart from creep contributions, frequency effects are often claimed to originate from hysteretic crack tip heating. This issue is discussed in a later section.

The constant load amplitude test (*CA* fatigue test[1]) is the customary way to characterise *da/dN* over a broad range of ΔK. In a *CA* fatigue test, ΔK increases during crack growth while the load ratio R remains at a fixed value. The load ratio does not reflect absolute values of average load level. Instead, the load ratio R specifies the average load level in proportion to ΔK (see figure 2-11). A rise in load ratio R establishes an relative increase in the creep component of the cyclic fatigue load (load level induced creep). In [53] the effect of load ratio on *da/dN* is given for a number of polymers. As with frequency, the effect of load ratio is also not consistent when different polymers are considered. Depending on the polymer, an increase or decrease in *da/dN* is found at increasing values of load ratio. In section 5.2 the effect of load ratio R is discussed for the polyethylene materials tested.

In general, the load ratio may influence *da/dN* by the mechanism of crack closure. At lower load ratios, closure of the crack is obstructed by residual plastic deformations at the fracture surface, reducing the effective range in ΔK at the crack tip. In polyethylene crack closure is not likely to occur in the positive regime of R-values (see also section 5.2).

Frequency and load ratio do not consistently affect *da/dN* when fatigue behaviour of different polymers is compared. However, creep may still account for these apparently contradictory effects. As will be discussed in section 2.5, creep basically promotes creep crack growth but inherently constitutes blunting with corresponding attenuation of crack growth. The net result of the competitive effects of creep determines the final actual crack growth. In section 2.5 creep is discussed in the context of creep crack growth but the discussion can also be applied to the creep component of fatigue. In section 5.5 the consideration of creep contributions during fatigue is continued on the basis of results found in polyethylene materials tested.

[1] In the field of fatigue it is common to refer to Constant-load Amplitude tests simply as *CA* tests. This practice is adopted in the thesis.

2.5 Interaction of blunting and crack growth

In section 2.1 the significance of blunting as a barrier for crack growth has already been mentioned; the craze itself constitutes a self-contained blunting mechanism. The amount of this craze-inherent blunting is linked directly to the elongation of the fibrils (see figure 2-12). In its turn the elongation of the fibrils represents the extent of damage in the fibrils which is the fundamental cause of fibril breakdown in the first place. Therefore, the development of a craze (i.e. elongation of fibrils) is basically a damaging mechanism but in the process more blunting is produced, effectively reducing the stress level. The related phenomena of craze development and blunting determine the net resulting crack growth rate.

Blunting does not have to be restricted to the craze itself but may also extend to bulk material at the craze boundaries. This contribution to blunting is referred to as bulk blunting (figure 2-12). Bulk blunting forms a straightforward relief of the craze with resulting restraint in crack growth. Although bulk blunting also constitutes damage of bulk material, crack growth is not affected by failure of bulk material, since the fibrils in the craze are the weakest link determining crack growth behaviour. Hence, bulk blunting will always result in attenuation of crack growth.

The combined contributions of craze-inherent blunting and bulk blunting constitute the total amount of blunting. Usually the contribution of bulk blunting is small compared with the amount of craze blunting. Bulk blunting is constrained by the presence of a hydrostatic stress component in the bulk material at the crack tip.

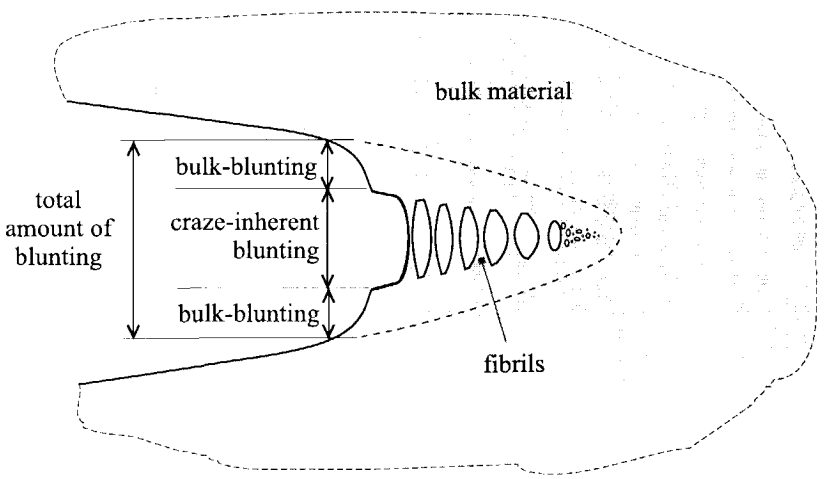

Figure 2-12 : Composition of blunting at the crack tip.

Effect of blunting on stresses at the crack tip area

Stresses are finite at a blunted crack tip. In [41] an elastic solution of stresses at a blunted crack tip is given by moving the origin of the polar coordinate system (of a sharp crack) an amount equal to one half the crack tip radius (figure 2-13,).

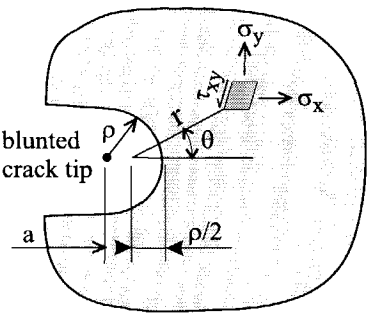

$$\sigma_x(r,\theta) = \frac{K_I}{\sqrt{2\pi r}}\cos\frac{\theta}{2}\left(1-\sin\frac{\theta}{2}\sin\frac{3\theta}{2}\right) - \frac{K_I}{\sqrt{2\pi r}}\left(\frac{\rho}{2r}\right)\cos\frac{3\theta}{2}$$

$$\sigma_y(r,\theta) = \frac{K_I}{\sqrt{2\pi r}}\cos\frac{\theta}{2}\left(1+\sin\frac{\theta}{2}\sin\frac{3\theta}{2}\right) + \frac{K_I}{\sqrt{2\pi r}}\left(\frac{\rho}{2r}\right)\cos\frac{3\theta}{2} \quad \{3\}$$

$$\tau_{xy}(r,\theta) = \frac{K_I}{\sqrt{2\pi r}}\sin\frac{\theta}{2}\cos\frac{\theta}{2}\cos\frac{3\theta}{2} - \frac{K_I}{\sqrt{2\pi r}}\left(\frac{\rho}{2r}\right)\sin\frac{3\theta}{2}$$

Figure 2-13 : Stress distribution around a blunted crack tip.

In all equations of figure 2-13 the stress intensity K_I is given by $K_I = \sigma\sqrt{\pi a}$. In the y-direction, for $\theta = 0$, equation {3} can be simplified to:

$$\sigma_y(r)_{\theta=0} = \frac{K_I}{\sqrt{2\pi r}}\left(1+\frac{\rho}{2r}\right) \quad \{3a\}$$

At the crack tip, $r = \rho/2$, this further yields:

$$\sigma_{y,\theta=0,\rho=\rho/2} = \frac{2K_I}{\sqrt{\pi\rho}} \quad \{3b\}$$

The recognition of blunting, with consequent reduction in stresses at the crack tip, does not reduce the significance of the stress intensity approach. In the blunted situation, according to equation {3a}, the stress distribution is still characterised mainly by the stress intensity K. With equation {3b}, the relative effect of blunting can be evaluated by comparing two cracks with crack tip radii ρ_1 and ρ_2 respectively. At the same value of K (i.e. the elastic solution) the ratio of stresses at both crack tips yields :

$$\frac{\sigma_{y,\rho_1}}{\sigma_{y,\rho_2}} = \sqrt{\frac{\rho_2}{\rho_1}} \quad \{4\}$$

For example: according to equation {4}, increasing the amount of blunting four times results in a factor two decrease in stress level at the crack tip. The ratio of stress levels according to equation {4} is not confined to the exact crack tip location but also extends to stress levels near the crack tip, reflecting a general change in stress intensity. In this respect the ratio of equation {4} can also be interpreted as a stress intensity correction factor in comparing two blunted crack tips.

Although blunting reduces stresses at the crack tip to a finite value, this value still exceeds the yield stress, as blunting was caused by plastic deformation in the first place. Therefore, both sharp cracks and blunted cracks may be associated with local high stress levels and plastic deformations at the crack tip. In this respect there is no fundamental difference between sharp and blunted cracks.

Interaction of blunting, creep and crack growth rate

In viscoelastic materials, the amount of blunting is initially governed by the load level. However, due to creep effects the amount of blunting will increase with time. The time-dependent part of blunting can be referred to as creep-induced blunting. At the crack tip, both creep in the actual craze as well as creep of surroundings of bulk material contribute to the total amount of blunting (see figure 2-12).
As discussed before, the development of blunting in time is obvious since creep deformation within the craze is the fundamental cause for creep crack growth in the first place.

During crack growth, the crack tip moves through the material. Material near the crack tip is loaded intensely as the crack tip passes by. Figure 2-14 shows the stress build-up in time as manifested in material through which the crack grows. Situations at a low and high crack growth rate are given. Clearly at a low crack growth rate, material near the crack tip is subjected to high stresses for a longer duration, promoting creep-induced blunting.

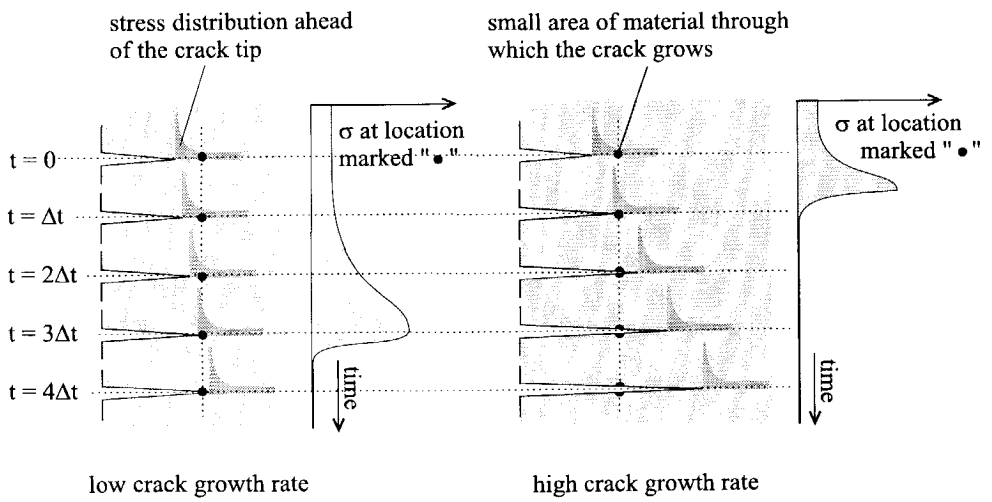

Figure 2-14 : The stress build-up in material near the crack tip as the crack is passing by.

The interrelation of crack growth rate and blunting can theoretically result in a downward spiral of decreasing crack growth and increasing creep blunting. A decrease in crack growth rate results in promotion of creep-induced blunting, which in its turn may decrease the crack growth rate even more etc. Finally this downwardly spiralling mechanism could lead to a

loading of the craze below the threshold value, with subsequent crack arrest. The interdependence of blunting and crack growth rate is shown in figure 2-15.

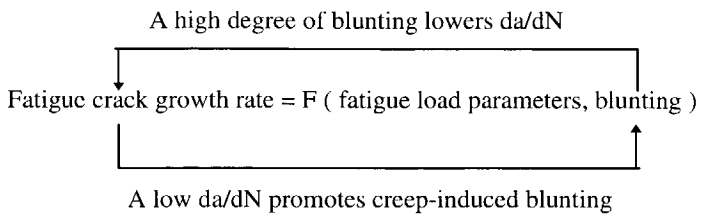

Figure 2-15 : The interdependence of blunting and the crack growth rate.

2.6 Discontinuous crack growth

A remarkable feature of both fatigue and creep crack growth in polyethylene is the occurrence of discontinuous crack growth, which is a process of chronological development, weakening and final breakdown of the craze. The mechanism of discontinuous crack growth is apparent from crack growth bands on the fracture surface (see figures 4-11). In the case of fatigue crack growth, each band is formed during many load cycles. The mechanism of discontinuous crack growth is a common feature of many polymers [53, 32] and is sometimes also referred to as "retarded" crack growth.

2.7 Hysteretic crack tip heating

A delicate topic in fatigue of polymers is the possibility of local hysteretic heating at the crack tip induced by cyclic loading. The effect of crack tip temperature on the crack growth rate is not all that obvious, since contradictory aspects are involved. At rising temperature polyethylene basically weakens, which favours crack growth. At the same time, however, both blunting and ductility are promoted, inhibiting crack growth ([53]).

Contradictory crack tip temperature measurements, in different polymers, have been reported and therefore local crack tip heating cannot be regarded as a universal phenomenon ([42],[43]). In [42] the temperature at the specimen surface, near the crack tip, was measured during a fatigue test in polyethylene, loaded with the relatively high frequency of 10 Hz. An infrared temperature device was used with a circular measurement spot of about 1 mm in diameter, of the same order of magnitude as crazes in polyethylene. With this test set-up no temperature rise could be measured compared with the ambient test temperature.

In section 5.2 the issue of hysteretic crack tip heating is further considered for the polyethylene materials tested.

3. Experimental procedures

Experimental procedures performed can be grouped into six categories. The categories are listed below and further information is given in table 3-1

1) Fatigue crack growth testing with crack length measurements.
2) Creep crack growth tests by the PENT test procedure.
3) Common tensile and creep tests.
4) Tensile, creep and fatigue testing using "fibril" tensile specimens.
5) Fractography of fracture surfaces.
6) Obtaining side views of crazes.

Field of interest (test methods)	**Apparatus**	**Specimens**	**Remarks**
Fatigue crack growth (cyclic loading)	Schenck servo-hydraulic test machine	CCT 270x100x10(19) mm (fig. 3-2)	Crack length measurement with digital image processing Testing temp. 20°C, 80°C
Creep crack growth (constant load)	Dead weight load facility.	SENT (70x25x10 mm) (fig.3-6)	COD measurement with clip gauges. Testing temp. 80°C.
General mech. Behaviour. (Tensile and creep tests)	Instron electro-mechanical test machine.	Standard round bar tensile spec. 80 x Ø8 mm (fig. 3-7)	Strain from grip displacement (tensile tests) or clip gauges (creep tests). Testing temp, 20°C, 80°C
Fibril simulation (tensile, creep and fatigue testing)	Instron electro-mechanical test machine.	Specially shaped specimen (fig. 3-8)	Strain from grip displacement. Testing temp.80 °C
Fractography (SEM observation)	JEOL JSM-6400F	Fracture surfaces	Surfaces sputtered with gold.
Side view of crazes (SEM observation)	JEOL JSM-6400F	Sliced samples cut from the crack tip area (figure 3-12)	During the SEM observation the crack tip was opened using a miniature tensile rig.

Table 3-1 : Quick reference of test procedures.

3.1 Origin of materials and specimens

The polyethylene materials are coded as **O**, **T** and **F**. An outline of the material properties is given in table 1-1 .

Materials **T** and **F** were only available in the shape of existing gas pipes. All specimens of materials **T** and **F** consequently had to be machined out of the walls of these gas pipes. In real failures of gas pipes the load direction (hoop stress) is orientated perpendicular to the direction of extrusion. However, this situation cannot be obtained for the relatively long specimen types (CCT and tensile types) which had to be cut out in the lengthwise direction of the pipe (= extrusion direction). To maintain consistency, all specimens were sampled in this direction. Thus in all cases the load direction is aligned with the direction of extrusion. Although this may conflict with the orientation of real pipe failures, the laboratory results obtained with specimens can still be used to rank material behaviour.

Material **O** was specifically processed for the purpose of the tests used for this thesis. The granulate was taken from one batch of resin material and extruded into plates 1000 mm wide with thicknesses of 10 and 19 mm. To minimise internal stresses, the extrusion speed was low and the plate was cooled slowly in stationary air. The extrusion procedure ensured a sufficient quantity of test material with uniform properties to favour the reproducibility of tests. Moreover the test specimens could easily be cut from the extruded plates. Corresponding with materials **T** and **F** the specimens of material **O** were also sampled in alignment with the direction of extrusion. For material **O** a fatigue test was performed using a specimen cut out perpendicular to the direction of extrusion. This was found to have no effect on the crack growth rate.

	Material code		
	O	**T**	**F**
Material origin	extruded plate	gas pipe	gas pipe
Density [kg/m^3]	0.958	0.958	0.948
Comonomer	butene	butene	hexene
Generation	second	third	second

Table 1-1 (repeated): Properties of materials tested.

3.2 Fatigue crack growth testing

The main objective of a fatigue crack growth test is to characterise the crack growth rate *da/dN* as a function of fatigue parameters applied. In a normal fatigue crack growth test a pre-notched specimen is loaded with a cyclic load, causing fatigue crack growth. During the test, crack length and the number of cycles elapsed are measured and recorded. After the test is completed the data stored is used to calculate the fatigue crack growth rate *da/dN*. In table 3-2 at the end of this section (page 34) all fatigue crack growth tests performed are listed with a short description. Interpretation of fatigue test results is discussed in section 5.2.

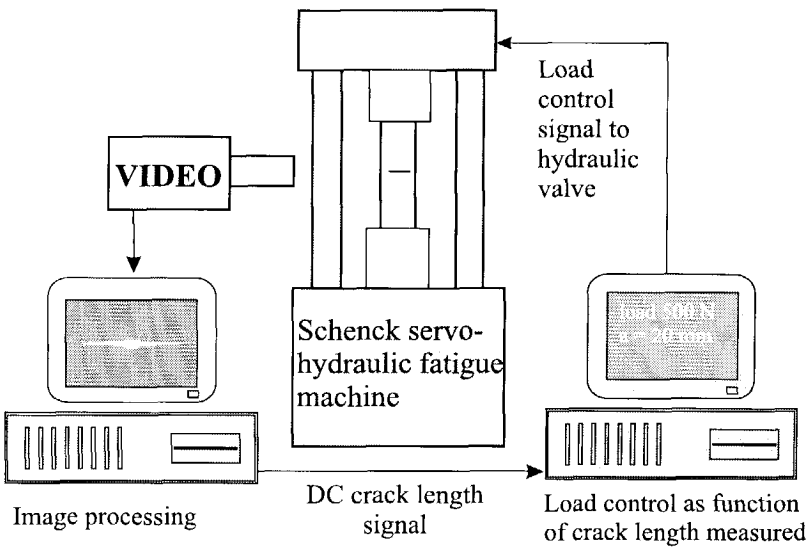

Figure 3-1: Set-up of the fatigue crack growth test facility.

Equipment and specimens used; experimental procedures

The fatigue tests were performed on a Schenck servo-hydraulic fatigue machine with a maximum load capacity of 25 kN. The fatigue machine was equipped with a temperature chamber enabling testing at elevated temperatures up to 80°C

Originally the controls of the servo-hydraulic fatigue machine could only be operated manually. At the start of the polymer testing programme the fatigue machine was extended by two major accessories in order to enable *automatic* controlled fatigue testing. First, load level controls were linked to a personal computer, enabling automatic monitoring and adjustment of load levels. Secondly, a new automatic crack length measuring system was introduced, based on digital image processing techniques.

Figure 3-1 shows the set-up of the fatigue facility. The crack length measured is transmitted to the control computer by means of a DC output voltage. In turn the control computer is provided with a flexible protocol to adjust the output load signal, depending on the crack length signal. Controlling the load level as a function of crack length can be used to achieve the desired level of stress intensity K (or ΔK) throughout the range of crack length tested. The

option of control by stress intensity can be applied to obtain a constant ΔK level independent of crack length. In this way small effects of secondary parameters can be measured over a wide range of crack lengths, without being obscured by the dominant influence in the case of a shifting ΔK level. The principle of fatigue testing under constant ΔK conditions is incorporated in the "extrapolation load series" and "interrupted fatigue tests", which are discussed separately in this section.

However, the majority of fatigue tests are *CA* fatigue tests in which the fatigue load levels are maintained at the same value throughout the test. Therefore, the level of stress intensity increases during crack growth ($K = C\sigma\sqrt{\pi a}$). A *CA* fatigue test is convenient for scanning the crack growth behaviour over a wide range of ΔK. The response of *da/dN* as a function of ΔK represents general fatigue behaviour and can usually be modelled by the Paris crack growth law: $da/dN = C\,(\Delta K)^m$.
Individual *CA* fatigue tests were performed at several values of load ratio R and frequency f to evaluate creep contributions during fatigue crack growth. The effect of test temperature and waveform was also established. Results are discussed in section 5.2.

The constant ΔK and *CA* fatigue tests, as discussed above, are fairly common test procedures, practised widely in the field of fatigue. In addition to these customary tests, two unusual methods of testing were used. The unusual test schedules are designated as "extrapolation load series" and "interrupted fatigue test". They will be discussed later in this section.

During all fatigue tests the crack length measured, together with the number of load cycles elapsed, was stored on a computer hard disk, producing an *"N-a"* data file. After the test was completed the *"N-a"* data file was used to calculate *da/dN*. Details of data processing are discussed in section 4.6.

The crack length measuring system used contains a number of components but as a whole is a stand-alone unit. The only physical interface with the fatigue testing machine is the DC output voltage, representing the crack length measured.
Image processing itself is a proved technique and use is widespread in the photographic publishing trade, where it is used to improve the appearance of pictures. Moreover, measuring size by image processing is not new. It is used, for example, to measure grain sizes in the field of metallography. However, the specific application of image processing to measure crack lengths in a growing crack is not yet an established procedure. Therefore special attention is given to this aspect of the experiments in a separate section (chapter 4).

The CCT-type specimen used is a standardised fatigue specimen according to ASTM E647-93 [44], with dimensions according to figure 3-2. The specimens were provided with side grooves to promote a situation of plane strain and to prevent crack tunnelling. Limiting the amount of crack tunnelling improves the accuracy of the crack length value measured, taking into consideration the image processing technique used (i.e. light shining through the opened crack). The CCT-type specimen is chosen for its well-defined Stress Intensity (K) over a large range of crack length. Compared with specimen geometries like Compact Tension and Bend specimens, the CCT specimen is relatively stiff, which is an advantage when low-stiffness polymers are being tested with equipment that is normally used for metals.

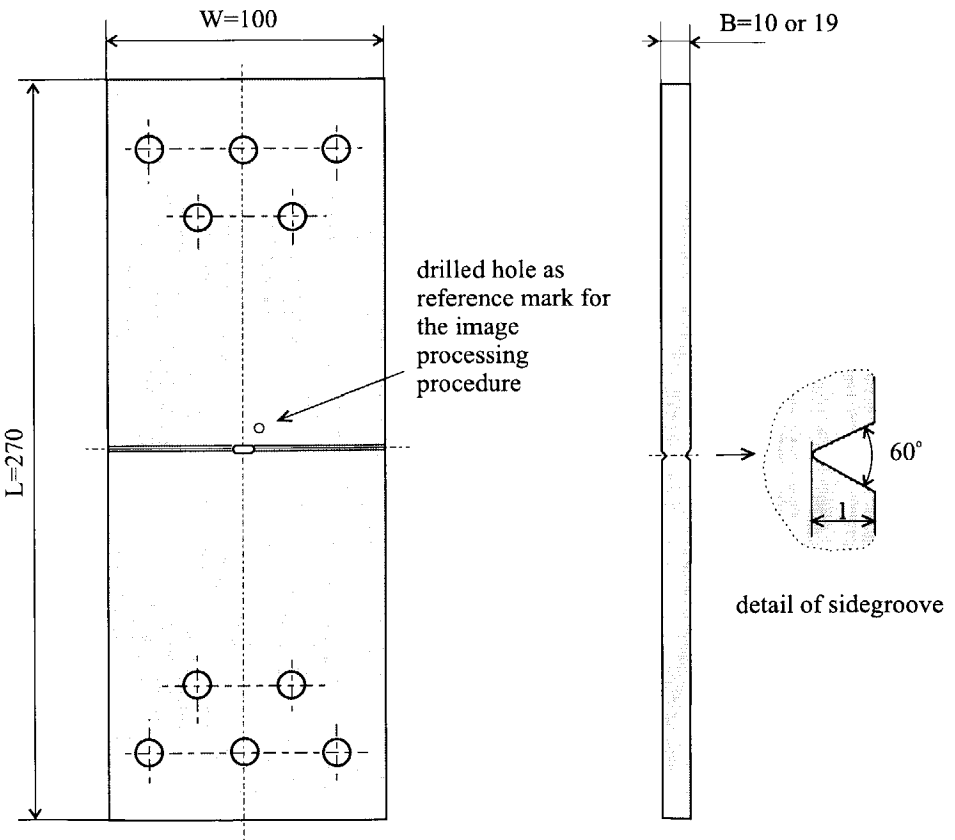

Figure 3-2 : Geometry of the CCT-type fatigue specimen.

The specimens were notched by slowly pressing a new razor blade into the machined centre hole of the specimen. The pre-cracking is performed in accordance with the recommendations of ASTM E647-93. A disadvantage of the CCT-type specimen is the possibility of asymmetrical crack growth. In this case the left and right crack originating from the centre of the CCT-type specimen have different crack lengths. It was found that polyethylene does not

show too much asymmetrical crack growth provided the notching procedure is performed accurately.

The "extrapolation load series"

The relation between fatigue crack growth and slow crack growth of polyethylene was evaluated with a loading schedule of different load ratios while K_{max} was kept constant. The load schedule is illustrated in figure 3-3. At increasing load ratios, the average load component of the fatigue load increases while the fatigue portion (ΔK) decreases i.e. *a typical fatigue load ($R = 0.1$) is gradually transformed into a constant load condition ($R = 1$).* The load schedule is designated as "extrapolation load series". The approach based on the extrapolation load series is intended to give a practical and quantitative view of relations between fatigue crack growth and creep crack growth. It is recognised that separate influences of ΔK and R cannot be assessed, since both parameters change simultaneously.

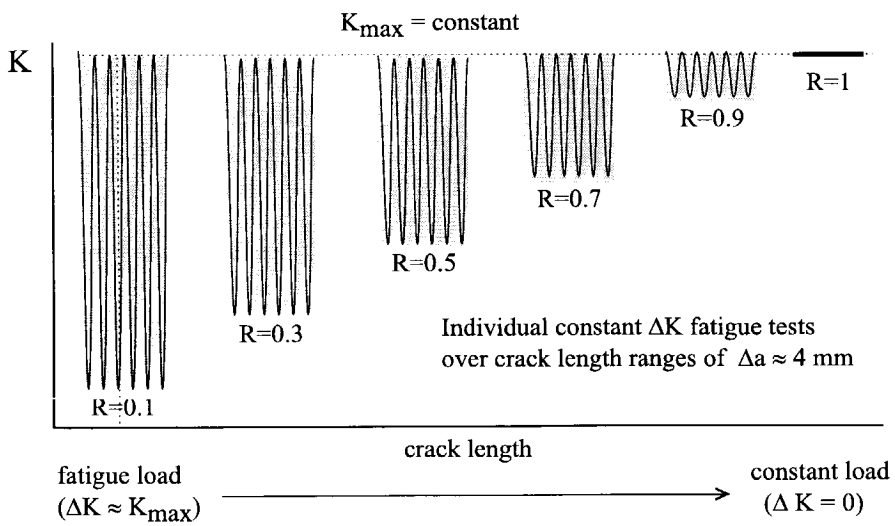

Figure 3-3 : Schematic load schedule of the "extrapolation load series".

The implementation of the extrapolation load schedule in an actual fatigue test requires some consideration. First of all, in the region of high R and low ΔK values, the crack growth rates will be small. Nevertheless, a certain amount of crack growth, Δa, is required to enable an accurate calculation of da/dN As a result, prolonged testing times are inevitable. Moreover, experience has shown that the complex equipment used in fatigue testing is sensitive to technical troubles. Unfortunately, during a long-duration test in fatigue, technical troubles are likely to happen occasionally.

Another practical problem was encountered with the automated crack length measurement. In the regime of creep-dominated crack growth (low ΔK, high R) the crack tip could not be distinguished as well as in the fatigue domain (high ΔK, low R). To compensate for increased

scatter in crack lengths measured, the value of *da/dN* must be averaged over an extended crack length range of at least 3 mm.

Taking into consideration the practical drawbacks of fatigue testing in the creep-dominant regime (at low ΔK and high R) the extrapolation load series was set up as a number of separate tests. Each individual test was performed under a specific *constant* ΔK condition (during at least 3 mm crack growth). Of course, in each test the same level of K_{max} was applied, as shown in figure 3-3. Therefore the idea of a gradually changing load is represented by a discrete number of separate constant ΔK tests.

Extrapolation load series were carried out at a temperature of 80°C. Lower temperature levels do not produce creep crack growth in a reasonable testing time. Materials **O** en **T** were tested only, since material **F** was found not to produce fatigue crack growth at 80°C.

Interrupted fatigue testing

An "interrupted fatigue test" is basically a constant ΔK test in which at subsequent crack growth intervals (≈ 4mm) the cyclic loading is stopped at a level corresponding to K_{max} of the cyclic loading (see figure 3-4). Thus, during the interruption time a high load level is maintained, promoting creep deformations at the crack tip. The crack tip geometry will become more blunted with retardation of crack growth as a result. After the interruption time the cyclic fatigue loading is resumed. The response of *da/dN* before and directly after the interruption time is observed in order to evaluate the significance of creep with respect to time-dependent blunting. The aim is to obtain an idea of the way in which creep mechanisms and blunting interact during a fatigue crack growth mechanism. Interrupted fatigue tests were performed with a range of interruption periods. Results are discussed in section 5.4.

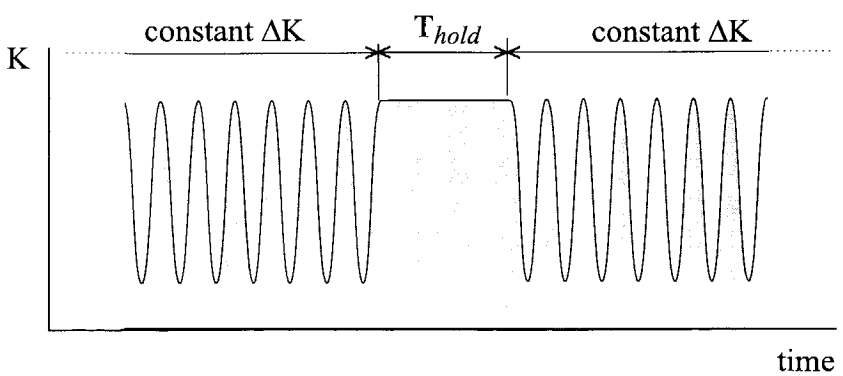

Figure 3-4: Detail of the load schedule in the interrupted fatigue tests.

Quick reference of fatigue crack growth tests

Table 3-2 contains a quick reference of all fatigue crack growth tests performed. For each type of test a short description is given.

Type of fatigue test performed	Short description
CA fatigue tests (in general)	Constant cyclic fatigue load, rising ΔK level during crack growth. Easy determination of general fatigue behaviour: da/dN as function of ΔK. Modelling according to the Paris crack growth law: $da/dN = C\ (\Delta K)^m$. Individual tests at different load ratios R, frequency f, temperature T and waveforms. Results are discussed in section 5.2.
Constant ΔK tests	Constant level of ΔK during crack growth. Evaluation of effects of secondary parameters without effects being obscured by the dominant influence in the case of a shifting ΔK level. Incorporated in "extrapolation load series" and "interrupted fatigue tests". Evaluating the validity of ΔK as governing crack growth parameter. Results are discussed in section 5.2.
Extrapolation load series	Individual constant ΔK tests reflecting the change from fatigue to creep crack growth. Results are discussed in section 5.3 "Extrapolation load series".
Interrupted fatigue tests	Constant level of ΔK during crack growth interrupted by periods with a constant load level. Comparison of da/dN before and after the interruption period reflects the effect of creep-induced blunting on fatigue. Results are discussed in section 5.4 "Results of interrupted fatigue ".

Table 3-2 : Quick reference of fatigue crack growth tests performed.

3.3 PENT test

The objective of a PENT test is to characterise the creep crack growth behaviour in terms of *time to failure* as a function of stress and temperature levels applied. During a PENT test a pre-notched specimen is loaded with a constant load, causing creep crack growth. The time to failure is recorded and related to the stress and temperature levels applied. Therefore the PENT test directly reflects the lifetime at a given stress level. PENT test results are discussed in section 5.1.

Equipment and specimens used; experimental procedures

PENT tests are carried out using a dead weight creep facility equipped with a large temperature room which allows testing of 10 specimens at the same time (i.e. 10 parallel load channels). The dead weights are located outside the temperature room and connected to the specimens by means of a tensile rod which is guided through the bottom wall of the temperature room (figure 3-5). Before loading a specimen is placed in the temperature room for at least one hour to acclimatise. Then the grips on the top of the specimen are moved slowly upwards by an electrically driven gearbox. As a result the weight is lifted in a controlled manner and the load is applied gently (without dynamic overshoot effects).

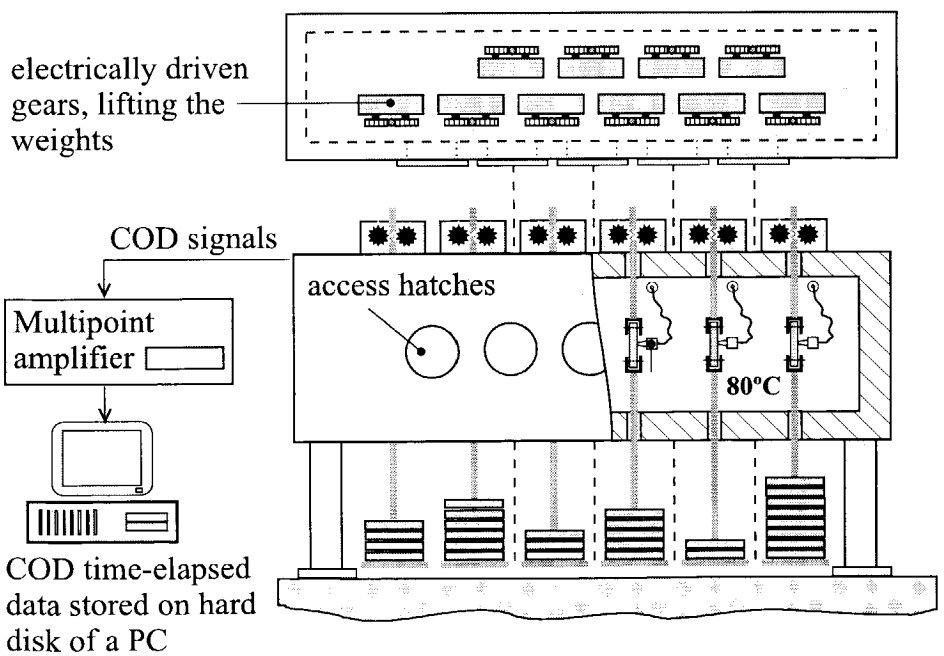

Figure 3-5 : The dead weight load facility used in the PENT test procedure.

In the PENT test a Single-Edge Notched Tension (SENT) specimen is used with dimensions according to figure 3-6. These dimensions are in accordance with recommendations of the PENT test standard ASTM F1473. The small size permits the sampling of these specimens out of the wall of a gas pipe. A delicate part of the PENT test is the procedure of pre-notching. In [5] it is reported that inaccurate performance of pre-notching leads to unacceptable scatter in test results (due to scatter in initiation time). The pre-notching procedure consists of pressing a new genuine razor blade 3.5 mm into the specimen, with a controlled slow speed of 0.2 mm/min at room temperature. Actual notching was performed using an Instron mechanical materials test machine. To verify if pre-notching was performed correctly the reproducibility of the PENT test was evaluated with 29 replicate measurements. Results are discussed in section 5.1.
Using the razor blade notching technique, the specimen was also provided with side grooves 1 mm deep. It was recognised that the side grooves do not need to be very sharp and the notching technique was only used because of its convenience.

During a PENT test the Crack Opening Displacement (COD) is measured with a clipgauge. The two knives of the clipgauge were mounted close to the pre-notch to favour a crack growth discriminating COD signal. Figure 3-6 shows the mounting of the clipgauge on the specimen. The signal from the clipgauge was processed in a "multi-channel" conditioner made by Hottinger. The output signal of the conditioner represents the COD value and was stored on a computer hard disk together with time elapsed. A typical response of COD as a function of loading time is given in figure 3-6. The initiation time of the first craze from the pre-notch is indicated. The subsequent steps in the COD signal correspond to the sudden breakdown of the craze and reflect the discontinuous creep crack growth mechanism. The COD approach does not directly measure the crack length. Absolute values of COD are not linked to absolute crack length values. However, the time interval of plateaus in the COD signal can be related to dimensions of crack growth bands on the fracture surface. In this way an average crack growth rate da/dt can be determined, present during one step of the discontinuous crack growth mechanism. The total time to failure can also easily be read from the COD curve.

PENT tests performed

The PENT test procedure was applied to materials **O**, **T** and **F**. The standard value for temperature was maintained (80°C) while stress levels ranged from 1.6-4.2 MPa. Results are discussed in section 5.1 "PENT test results".

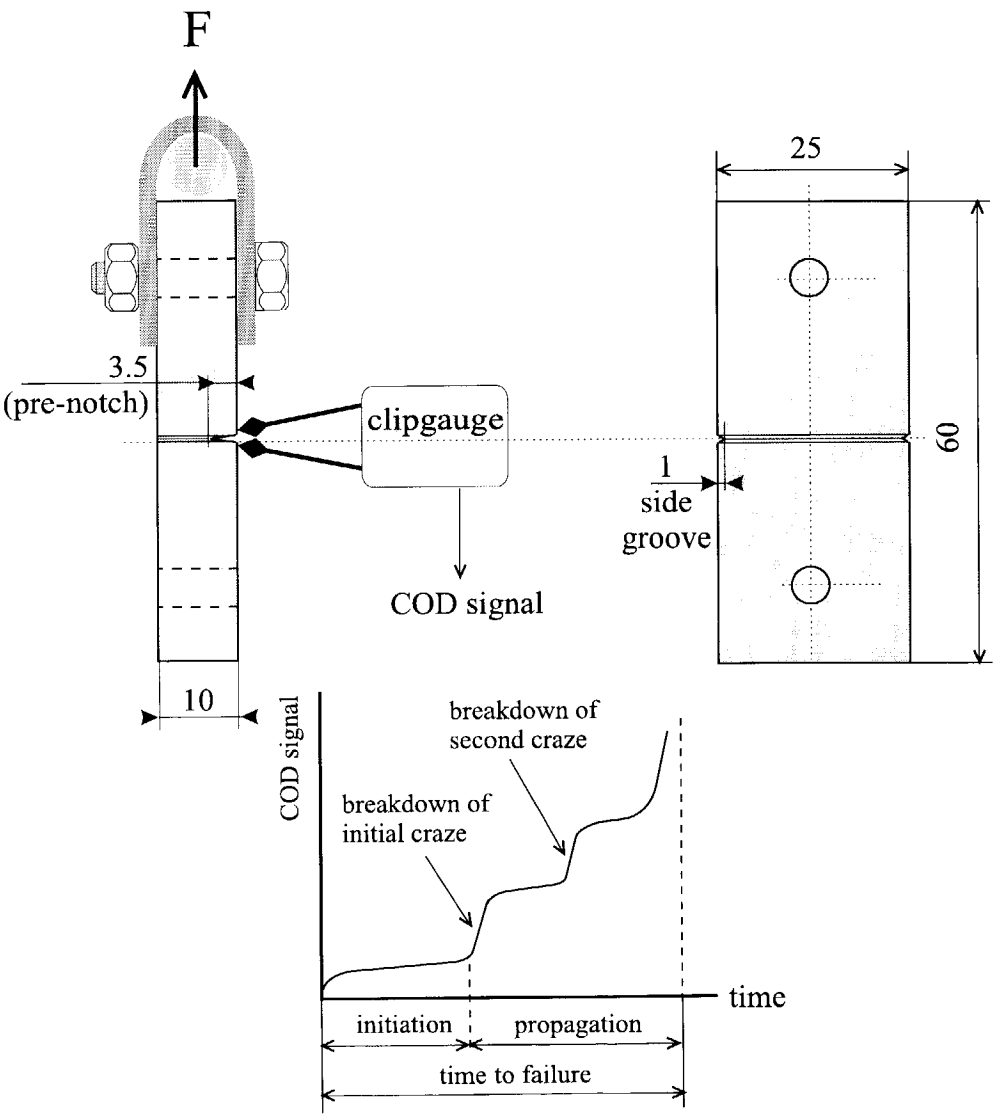

Figure 3-6 : Details of the SENT specimen and mounting of the clipgauge during a PENT test.

3.4 Tensile, creep and fatigue testing with tensile specimens

Two types of tensile specimens must be distinguished here, designated as "normal" and "fibril" tensile specimens. (figures 3-7 and 3-8 respectively). In both cases the specimens are used for both tensile testing and creep testing. Tensile tests determine general mechanical properties like yield stress, elongation at fracture, etc. Creep tests measure time-dependent deformations under a constant load condition (i.e. viscoelastic properties). In table 3-3 at the end of this section (page 42) all fatigue crack growth tests performed are listed with a short description.
The interpretation of test results with tensile specimens is discussed in section 6.1.

The "normal" specimens are tested in a traditional way and reflect the behaviour of bulk material.
The range of elongation is restricted when tensile tests are performed within the limited space of a temperature room. In this case high strain levels can still be obtained when the "fibril" specimen is used. Highly stretched fibril specimens are intended to simulate macroscopically the behaviour of actual craze fibrils. This kind of testing is also reported in the literature, for example [45].
The "fibril" tensile specimens are also subjected to a cyclic load procedure to evaluate the fatigue response of highly drawn material. The number of cycles to failure indicates the fatigue resistance of drawn material.

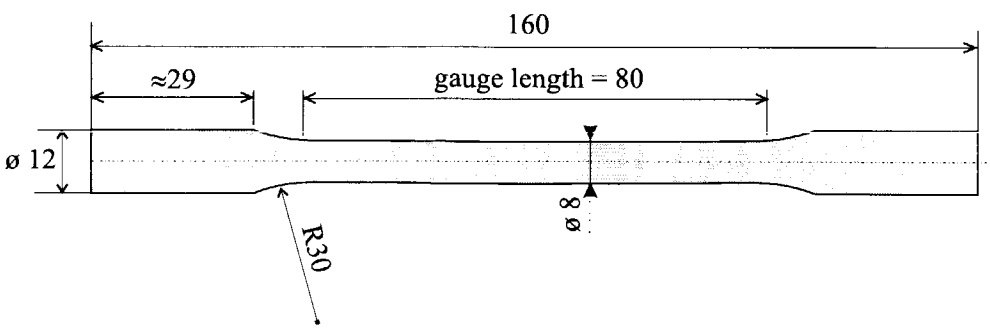

Figure 3-7 : Geometry of the standard tensile specimen.

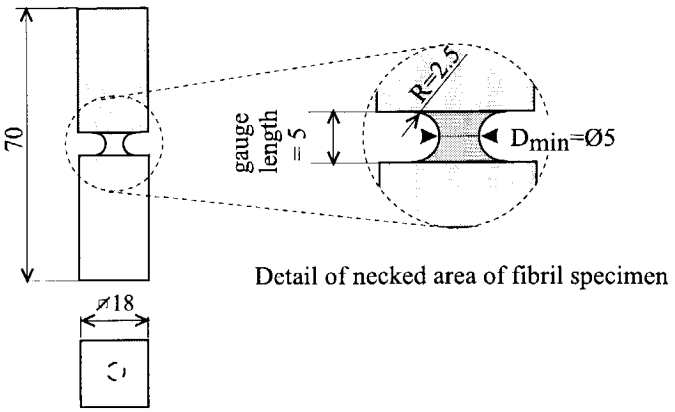

Figure 3-8 : Geometry of the "fibril" tensile specimen.

Equipment and specimens used; experimental procedures

The tensile and creep tests were predominantly[1] performed on an Instron electro-mechanical material testing machine, model 4505, with a maximum load capacity of 100 kN. Load cells with capacities of 1, 10 and 100 kN are available, of which only those of 1 en 10 kN were used. A temperature room can be fitted in the frame of the Instron to perform tests at a temperature of 80°C. All data measured were stored on a computer hard disk.

The tensile tests with "normal" tensile specimens were performed in the traditional way. A specimen is elongated by a fixed rate of grip displacement while the resulting load response is measured. Polyethylene is a very ductile material with strains that can reach levels up to 1000%. However, the displacement range of the testing machine is limited, especially when the temperature room is used. Therefore, at 80°C, tensile tests with "normal" tensile specimens were confined to a maximum strain level of about 100% and did not include final fracture. Moreover, owing to the high level of elongation, the strains were adequately determined by relating the displacement of the grips to the gauge length of the specimen.

For creep testing the "load control" feature of the Instron 4505 was used. A constant load was applied to the "normal" tensile specimen while the elongation was measured by mounted clipgauges. The clipgauges were used because in creep testing the level of strains are limited compared with levels in tensile testing.

Tensile testing with "fibril" specimens were performed in a similar manner to that of the "normal" tensile specimens. The pronounced necking in the "fibril" specimen concentrates deformation at the minimum diameter. The initial length between the fixation grips (i.e. gauge length) is small, and large strains can be achieved within a confined range of displacement. The actual process of drawing begins after yielding and strain softening have been completed. For the geometry used the process of drawing extends over a strain range of 700%, while

[1] Some of the long-term creep data were obtained with the dead weight load facility, as described in section 3.3

strain hardening is manifested by an increase in load level from 150N to 250N (the values given are approximate and an average for the materials tested). With "fibril" specimens the tensile test can be completed up to fracture. It is recognised that the diameter of the "fibril" specimen varies along its gauge length and therefore exact stress-strain behaviour is not obtained. The results of the "fibril" specimen can be considered indicative of high strain material response when comparing different materials (i.e. ranking material behaviour).

Creep testing of a "fibril" specimen was performed in a two-step procedure (see figure 3-9). Step one brings the material into a pre-drawn condition with an intermediate degree of drawing. In this way some drawing potential remains for subsequent creep testing. Step two constitutes the actual creep testing of pre-drawn material.

Step one is basically performed by a tensile test under displacement control, covering the processes of yielding, stress weakening and a small amount of stress hardening. When, during strain hardening, a load level of 200 N is reached the displacement control is switched to load level control, during which the load level of 200 N is maintained. The response of the elongation is measured subsequently by registration of the grip displacement, which constitutes actual creep testing (i.e. the second step).

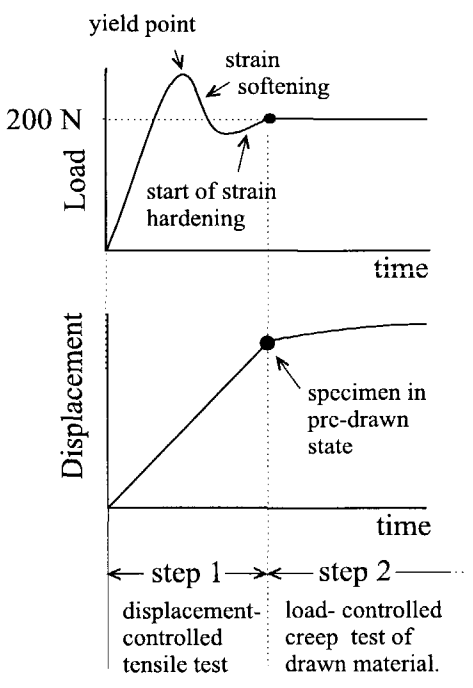

Figure 3-9 : two-step procedure in creep testing of "fibril" tensile specimens.

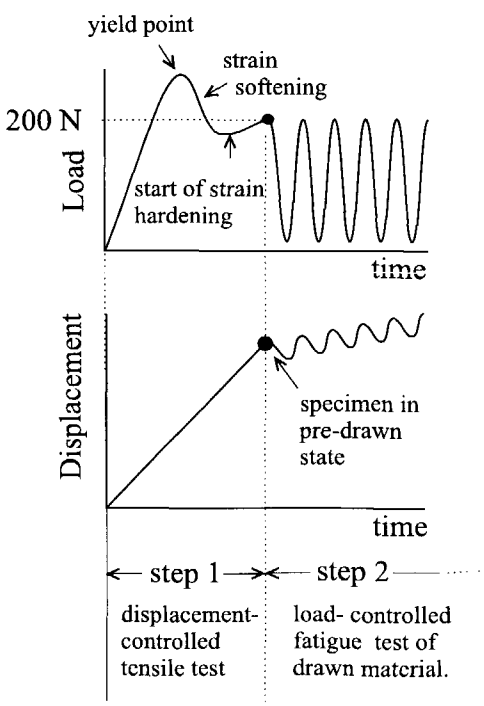

Figure 3-10: two-step procedure in fatigue testing of "fibril" tensile tests.

"Fibril" tensile specimens were also used to evaluate the fatigue resistance of material in a drawn condition. As in the creep test, a two-step test procedure was used (see figure 3-10). Actual fatigue loading (i.e. the second step) was performed by subjecting the specimens to a sinus cyclic loading with a frequency[1] of 0.3 Hz. In all individual tests the maximum load level was 200 N, while minimum load levels were set to a different value in each test. This loading pattern between individual tests is similar to the stress intensity load schedule of the extrapolation load series. It is an attempt to simulate the situation of real fibrils as present in crazes during crack growth in the extrapolation load series.

With a discrete sample rate, time elapsed and grip displacement (= elongation) can be stored on a computer hard disk during a fatigue test. The elongation, however, consists of a slowly changing creep component and a cyclic elastic component. The latter varies in accordance with cyclic loading. When the displacement is measured at a randomly chosen sample rate, the elastic component might appear as random scatter on the creep component. To avoid this, special attention is given to the time interval of the displacement measurements. The measurement interval is chosen as a fixed multiple of the load cycle periodic time to which a small time interval is added. In this way the displacement signal will show as a sinus of very low frequency. The maximum and minimum of the delayed sinus output signal gives an indication of elastic deformation levels caused by the cyclic load. The principle is shown in figure 3-11.

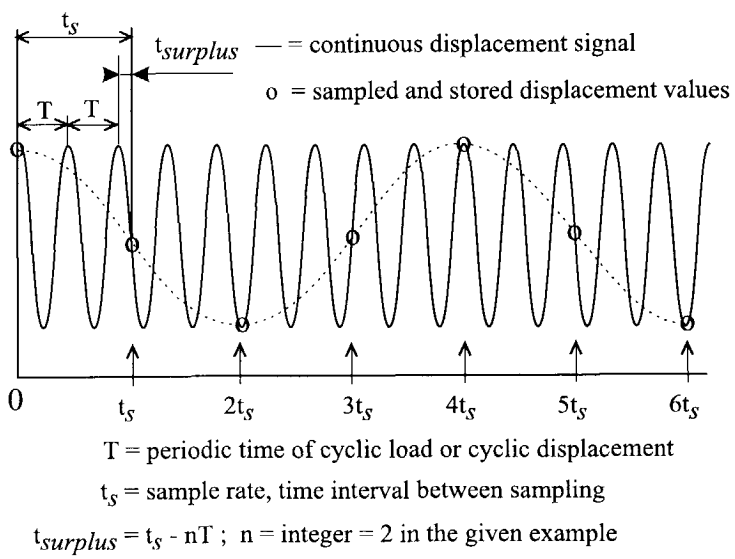

Figure 3-11 : Choosing the sample rate during fatigue tests with "fibril" tensile specimens.

[1] The Schenck hydraulic fatigue machine is not designed to test the fragile "fibril" tensile specimens. The Instron 4505 is equipped with a cyclic loading feature. However, due to the mechanical nature of the machine the attainable frequencies are limited.

Tests performed with "normal" and "fibril" tensile specimens

In table 3-3 a quick reference is given of all fatigue crack growth tests performed. A short description is given for each type of test.

spec. type	Type of testing	Short description
normal	Tensile	Stress-strain behaviour obtained by a displacement-controlled tensile test. Yield stresses reflect mechanical strength of bulk material. The mechanisms of yield, strain softening and drawing are covered. Strain hardening and final fracture cannot be experienced, due to the large elongations required.
	Creep	Strain response in time during a constant load condition. This creep behaviour is intended to characterise the amount of time-dependent blunting of bulk material in the vicinity of the crack tip. (i.e. growth-inhibiting)
fibril	Tensile	Load-strain behaviour obtained by a displacement-controlled tensile test. The mechanical response is intended to relate to real fibril behaviour within an actual craze. The mechanisms of yield, strain softening and strain hardening are covered.
	Creep	Strain response of a pre drawn specimen during a constant load condition. This creep behaviour is intended to characterise the amount of time-dependent deformation (and failure) of fibrils in an actual craze.
	Fatigue	Cycles to failure of a pre-draw cyclically loaded specimen. The fatigue response is used to identify the basic damaging mechanism of fatigue on the level of craze fibrils.

Table 3-3 : Quick reference of tests performed with tensile specimens.
Test results of all tests using tensile specimens are discussed in section 6.1 "Tensile and creep tests of bulk material".

3.5 Observations using the Scanning Electron Microscope (SEM)

The strength of scanning electron microscopy is the high magnification, possible while a high depth of field is retained.(i.e. a rough surface can be focused entirely over a considerable area). This makes the SEM ideal to study fracture surfaces of polyethylene, in which remains of fibrils cause a microscopically rough structure. The SEM used is a JEOL JSM-6400F. The polyethylene specimens must be sputtered with gold. Usually SEM images were obtained with an acceleration voltage of 5 kV. Two distinct SEM observations were used to support the understanding of failure at crack tip level:

1) Fractography, i.e. observation of fracture surfaces. The fracture surface gives information based on the situation *after* craze breakdown. Only fracture surfaces of CCT-type specimens (fatigue testing) and SENT-type specimens (PENT testing) were observed.
2) Side view of loaded crazes at the crack tip. A side view of a loaded but still unbroken craze provides further details about the origin and progress of craze breakdown.

Experimental procedures used in studying the fracture surfaces are straightforward. Small sections from fracture surfaces were sampled, degreased and sputtered with gold. During these preparations care was taken not to touch the fracture surface. It was found that even a light touching smears out the delicate fibril structure of the fracture surface. Results of the fractographic observations are discussed in section 6.2.1 "Fracture surfaces".
Experimental procedures necessary to obtain a side view of a craze are more complex and will be now be considered.

Side view of crazes

In [18, 19] an elegant method is presented for obtaining a side view of the craze structure, while an impression of the strain distribution over the craze length can also be estimated.
First a pre-notched PENT test specimen is loaded with a constant load until a craze is initiated (80°C). During the craze initiation the Crack Opening Displacement (COD) is recorded in the usual manner of the PENT test procedure, with clipgauges. Subsequently, *after unloading*, a thin slice of material is sampled from the centre of the specimen around the crack tip area (see figure 3-12). The crack tip slice is sampled by cutting it out slowly with a razor blade using the same technique as used in pre-notching. Irregularities on the edge of the razor blade produce a parallel array of fine scratches on the side of the slice. The array of fine scratches is used later as a reference grid to measure displacements (i.e. strains).
The slice is placed in a miniature tension rig where the notch is opened to its original COD value, as was present just before unloading. The slice, in the opened condition, is sputtered with gold for observation by the SEM. The tension rig with mounted slice is placed in the vacuum chamber of the SEM for observation. A clear view of the notch tip and the craze is obtained. The individual steps leading to the side view image are illustrated in figure 3-13.
Initially the scratches induced by cutting are equidistant. When the notch of the sample is opened the craze will be loaded and distances between scratches at the craze boundaries will increase. At the boundaries of the notch (i.e. free surface), the scratch pattern remains unchanged (i.e. unloaded) and can serve as a reference from which to calculate strains at the loaded craze boundaries. In this way the distribution of strain over the length of the craze can

be evaluated. Moreover, stresses can be inferred from a uniaxial stress-strain curve obtained in a normal tensile test at ambient temperature (20°C).

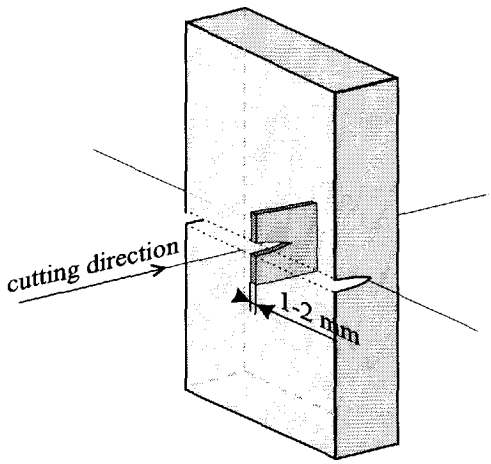

Figure 3-12 : sampling a slice of material around the crack tip of a PENT test specimen.

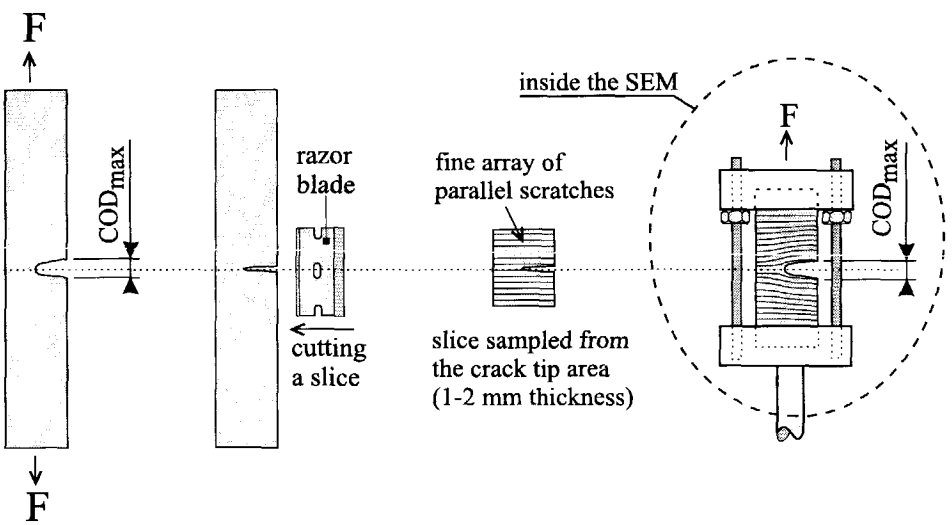

PENT test at 80°C. Max. COD at end of test.

SENT specimen as used in the PENT test. (see also figure 3-6)

Specimen is unloaded and cooled down.

A thin slice is sampled from the middle with a razor blade (see also figure 3-12).

Cutting the slice produced an array of fine parallel scratches on the surface.

The slice is placed in a miniature tension rig and elongated until the original COD_{max} is reached. In this condition the slice (and tension rig) is sputtered with gold and placed in the SEM. Deformation shows as widening of the scratches.

Figure 3-13 : Individual steps leading to a SEM side view image of the crack tip area.

The procedure used in order to determine the strain and stress distribution over a craze must be treated with some reservations.

- The craze and corresponding COD value were generated at a temperature of 80°C. However, the notch of the sliced sample is opened at a temperature of 20°C. It is assumed that identical COD values at 80°C and 20°C will also reflect corresponding strain values at craze level. However, the inferred stress levels at 20°C do not represent actual stress levels in the craze at 80°C. The significance of the stress levels determined is the relative distribution over the craze length.
- The strains measured do not show irreversible creep strains developed during actual loading of the PENT test specimen.
- The actual craze during a PENT test is loaded under plane strain conditions while the thin sliced sample does not satisfy plane strain conditions.

Measurements of strain and stress distributions at the craze boundaries were carried out for all materials **O**, **T** and **F**. An attempt was also made to evaluate the development of the craze by obtaining side views at increasing loading times (materials **O**, **T** and **F**).
The effect of fatigue at craze level was assessed by observation of craze formed under fatigue loading (material **O** only).
All results concerning crack tip geometry are discussed in section 6.2.2.

4. Crack length measurement using digital image processing techniques

In this section the suitability of digital image processing for application in measuring crack lengths during a fatigue test is evaluated. Attention is focused on the crack length measurement technique without detailed discussion of the fracture mechanical backgrounds of crack growth observed.

Most modern fatigue experiments are performed with servo-hydraulic test machines which are computer-controlled and have the potential of automated long-term testing. To make full use of these features it is necessary to have an accurate crack length measuring system which automatically performs the measurements.
It is also necessary that during the test itself the crack length measured is transmitted to the control computer of the servo-hydraulic fatigue machine. In this way the proceeding of the fatigue test can be programmed as a function of the crack length, for example the test can be terminated when the final crack length is reached or the fatigue loads can be adjusted during the test depending on the actual crack length (ΔK control possibility). The results of the crack length measurement, together with the number of load cycles elapsed (i.e. N-a data), should be stored on disk for later data analysis i.e. calculation of da/dN.

The image processing method is based on a video signal of the crack which is analysed by image processing techniques. With this technique the crack length is measured every 20 seconds during a fatigue test. The accuracy of one single measurement is about 0.05 mm, but this can be increased by averaging a large number of measurements. The automated data collection and subsequent data processing is discussed in relation to the recommendations given in ASTM E647-93, a standard test method for measurement of fatigue crack growth rates [44]

Starting up a new crack length measuring technique required much effort in order to obtain experience and evaluate the accuracy of the new technique. The new technique is not only useful in the context of this thesis but can also be of benefit in the general field of fracture mechanics, whenever measuring of crack lengths in polymers or other materials is required. In view of this, the flexibility of the image processing technique was verified by also testing polycarbonate in addition to polyethylene. Polycarbonate was chosen because this material has distinct optical and fatigue fracture properties as compared with polyethylene.

4.1 Automated crack length measurement in fatigue tests: an overview

Research into fatigue cracks in metals has been carried out over a longer period and more extensively than is the case for polymers. One of the commonly used methods of fatigue crack length measurement in metals is what is known as the potential drop method. This method is based on the increasing electrical resistance of a specimen in the presence of a growing crack. The electrical resistance of the specimen is derived from the potential drop when a current is sent through the specimen. Unfortunately, since polymers are not conductive, this method cannot be used.

A related option for polymers is the "indirect potential drop method", in which thin conductive foils are bonded to the surface of the specimen. The crack in the specimen is assumed to grow simultaneously in the foil. The crack in the foil is again measured with the potential drop method by sending a current through the foil. Foils with auxiliaries (bond, DC amplifier) are also commercially available [46]. The suitability of the bondable foils has been tested for polyethylene and polycarbonate and is reported in [47]. The results for polycarbonate are acceptable, but use of the foils for polyethylene is not possible owing to the poor bonding properties of polyethylene.

Another crack length method for polymers might be the "compliance" technique, which uses the increasing compliance of the specimen as the fatigue crack grows. However, this technique is complicated, due to the viscoelastic behaviour of most polymers.

A new technique for crack length measurement is discussed here, based on image processing. Image processing is the manipulation of a picture digitally stored in the memory of a personal computer.

4.2 Crack length measurement using digital image processing

The main components of the image processing system used are a video VCR camera and a personal computer. The personal computer must be equipped with a "frame grabber" extension board and software for image processing. The whole system is, however, commercially available [48].
The camera is directed to the crack in the specimen. The camera signal is connected to the "frame grabber" extension board, where it is transformed into a digital image of 768 horizontal pixels by 512 vertical pixels (pixel = picture element). Each pixel is assigned a grey value in the range of 0 (black) to 255 (white).
The total collection of pixel grey values is stored in the "frame grabber" and is a digital representation of the original analogue video signal. The digital representation of the video signal is referred to as the "image". The frame grabber is basically a memory extension board for a PC customised for storage and fast exchange of the image data (mainly pixel grey values). Several types of "frame grabber" extension boards are available from various manufacturers.
The software performs the actual image processing. Image processing can be considered as the manipulation of an image by means of mathematical operations on the pixel information stored in the "frame grabber". Image processing is widely used in the field of fractographic research, but more general software programs are also available. For the use of the software it is not necessary to be familiar with the theoretical background of image processing. It is sufficient to understand the functional descriptions of the image operations available (i.e. software commands). The essence, however, is to select the appropriate set and sequence of image operations from the total collection offered by the software.

The software program used was originally developed in the Physics Department of the Delft University of Technology. It consists of a variety of commands that each change the image in a specific way. For example, the command "invert" will produce the negative image by first inverting the grey value of each pixel followed by adding the value 256. Similarly there are commands to recognise distinct parts of the image that have a clearly different grey value compared with their surroundings. The dimensions of these parts can then also be determined using the commands available.
The camera position and the illumination of the crack in the specimen are chosen in such a way that the crack can be clearly distinguished from the uncracked material. It is obvious that different types of material will each have their own specific method for making the best video recording of the crack.
The image processing procedures are applied to the video picture obtained. The crack length measurement involves a characteristic sequence of image operations that has been proved to produce a reliable measurement of the crack length. The image operations and their sequence are selected by trial and error. Although details may differ for specific materials, it is possible to give a general set-up for the image processing operations:

- *Digitising.*
  A video signal from the crack in the specimen is digitised to an image of 768 x 512 pixels. The digitising command is triggered at the moment of maximum load to improve the reproducibility of the measurements.

- *Filtering*
  First small irregularities (dust particles, small scratches on the specimen surface) in the image are removed by a filter command. In this way only the significant information remains in the image.

- *Recognition of the crack*
  The crack is selected as an object. This is done by a command that selects all pixels within a specified range of grey values. The chosen range of grey values is characteristic for the crack in the image. The selected collection of pixels is labelled as one object (i.e. the crack!).

- *Measuring the crack length*
  Once an object (i.e. the crack) is labelled, there are several commands to measure characteristic dimensions of the object, such as vertical or horizontal dimension and area. The dimensions are returned as a number of pixels and can be converted to actual sizes with the scale of the image. The scale of the image is defined as the actual size in mm that is represented by one pixel. The scale can be varied by zooming in on or away from the specimen.

- *Output of crack length value*
  The crack length measured is transmitted to the control computer of the servo-hydraulic test machine by means of an analogue DC voltage proportional to the crack length measured. The DC voltage output is chosen specifically to achieve compatibility with the "potential drop" crack length measurement used in fatigue testing of metals. In this way the servo-hydraulic fatigue machine can easily be used for both metals and polymers.

- *Digital-Analogue Conversion*
  The Digital-Analogue Conversion (DAC) is carried out by a DAC extension board in the personal computer. The DAC extension board can be addressed using a software command in the image processing program. The control computer of the test machine stores the crack length measured, together with the corresponding number of load cycles elapsed, on a hard disk.

One crack length measurement has now been completed and the whole procedure is automatically repeated in a loop. One cycle of the measurement loop takes about 15 seconds.

4.3 Experimental

In section 3.2, experimental procedures are discussed as used in the actual fatigue test programme for this thesis. However, the initial fatigue tests were focused on the image processing technique and differ in some ways from the experiments described in section 3.2:

- the polyethylene specimens are not yet side-grooved.
- only one crack tip is monitored in the polyethylene specimens[1].
- the frequency of the cyclic loading is 10 Hz.

The polycarbonate material tested was a commercially available sheet material with a thickness of 6 mm. Consequently the polycarbonate CCT specimens have a thickness of 6 mm.

The image processing computer is a personal computer with a 386SX processor, a clock frequency of 20 MHz and an internal memory of 2 MB. The "frame grabber" extension board and image processing software used are commercially available.

The practical use of image processing is illustrated on the basis of the performance of two types of fatigue tests commonly used in the practice of fatigue testing. For both polyethylene and polycarbonate a *CA* fatigue test and a constant ΔK fatigue test were performed. Table 4-1 summarises the test parameters.

Test	Material	type of control	frequency	load ratio R
PE-K	polyethylene	constant ΔK	10 Hz	0.1
PE-F	polyethylene	*CA*	10 Hz	0.1
PC-K	polycarbonate	constant ΔK	10 Hz	0.1
PC-F	polycarbonate	*CA*	10 Hz	0.1

Table : 4-1: Initial fatigue tests used for evaluation of the crack length measurements.

4.4 Recording techniques for cracks in polycarbonate and polyethylene

The flexibility of the image processing method is verified by the selection of two polymers with distinct optical and fatigue fracture characteristics. Polycarbonate is transparent by nature and the fatigue crack is sharp without much crack opening. Polyethylene is not transparent and white by nature. Creep effects in polyethylene result in a considerable amount of crack opening, even at minimum load.
The tests were performed with unpigmented polycarbonate (i.e. transparent) and unpigmented polyethylene (i.e. white). However, the recording technique is also considered for cracks in black pigmented polyethylene.

[1] The actual fatigue test programme for Polyethylene, as described in chapter 3, monitored the whole crack (i.e. both crack tips). During the actual test programme it was found that asymmetrical crack growth occasionally occurs. This is no problem if the whole crack is monitored.

Polycarbonate set-up

The transparency of polycarbonate is used by placing the camera below the plane of the crack and directing the camera towards the crack. The tilt angle of the camera is about 45 degrees. A small fluorescent strip serves as a homogeneous light source and is placed behind the specimen with a crack. Owing to the refraction of light at the crack surface, the crack can be clearly distinguished from the transparent uncracked material. The crack is visible as a dark object in white surroundings of transparent polycarbonate. The set-up is illustrated in figure 4-1 and the image obtained can be seen in figure 4-2. polycarbonate is sensitive to asymmetrical crack growth. This means that the two crack tips in the CCT specimen may have different crack lengths. To avoid unacceptable development of asymmetry during a test, both crack tips were observed in polycarbonate. The asymmetry is detected as a difference between the centre position of a reference sticker and the centre position of the crack object obtained (see figure 4-2). Exceeding a pre-set limit of asymmetry results in the test being stopped. In this way uncontrolled crack growth during a test is avoided.

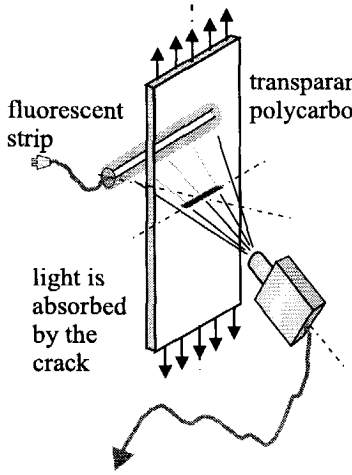

Figure 4-1: Video set-up for measurement of a fatigue crack in polycarbonate.

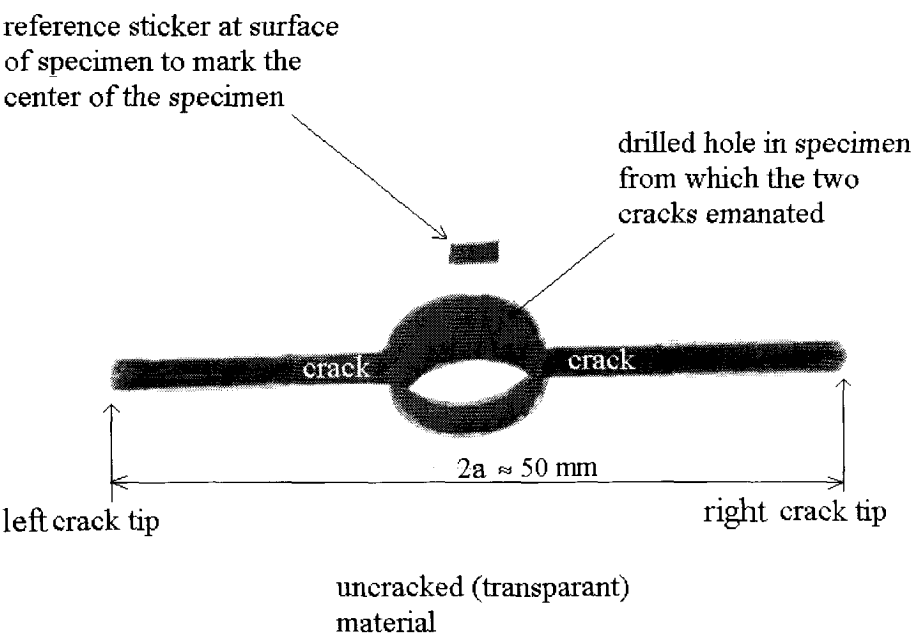

Figure 4-2 : The image obtained of a crack in a polycarbonate CCT specimen.

Polyethylene set-up

For the non-transparent polyethylene various set-ups can be used. One set-up uses the fact that the crack in polyethylene shows a clear opening due to creep effects. When the camera is placed in the plane of the crack and a light source is placed behind the opened crack, the crack will be visible as an illuminated object surrounded by the dark, uncracked material. This polyethylene set-up is illustrated in figure 4-3a and the image obtained is given in figure 4-4a . The round white object in figure 4-4a is a hole drilled in the specimen, which serves as a reference mark for the crack tip position. The pixel coordinates of both the reference mark and the crack tip are measured. The horizontal difference in position of the crack tip compared with the fixed position of the reference mark is used to calculate the crack length. The fatigue results discussed for polyethylene tests PE-K and PE-F are obtained with this set-up.

Another set-up for polyethylene is similar to the polycarbonate set-up. The camera is again placed below the plane of the crack and is directed towards the crack. However, the light source is now placed on the same side of the specimen as the camera. The light source is positioned in such a way that it reflects directly at the uncracked surface into the camera, while the crack cannot reflect the light. The crack will appear as a dark, unreflected object in light surroundings of uncracked, reflected material. The set-up and image obtained are given in figures 4-3b and figure 4-4b respectively. The set-up using surface reflection is evaluated using a dark, polished specimen surface of black pigmented polyethylene (material **T**).

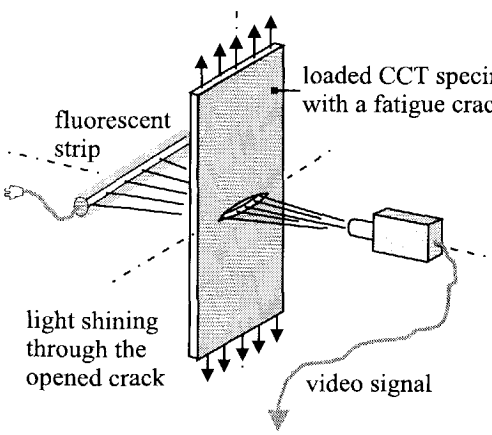

Figure 4-3a :
Video set-up for measurement of a fatigue crack in polyethylene.

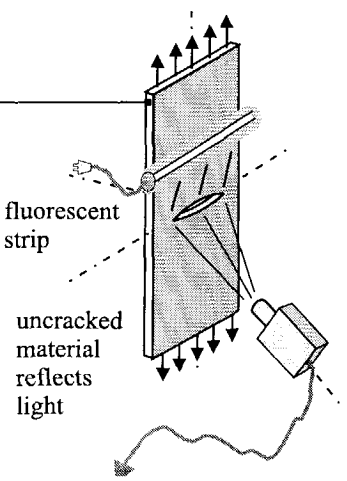

Figure 4-3b :
Alternative video set-up for measurement of a fatigue crack in polyethylene.

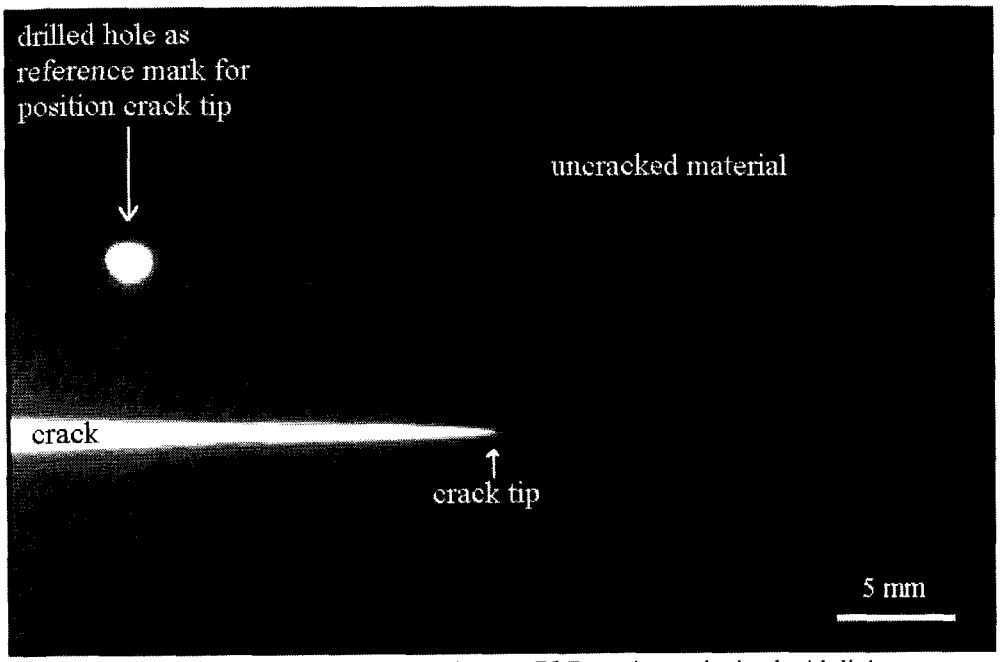

Figure 4-4a : Image of a crack in a polyethylene CCT specimen obtained with light shining through the opened crack.

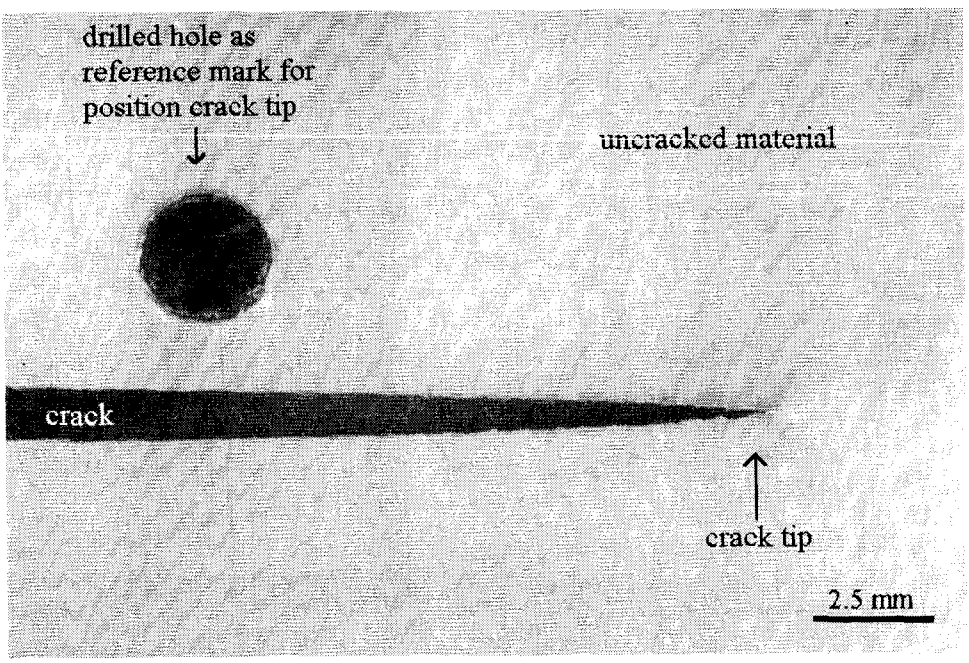

Figure 4-4b : Image of a crack in a polyethylene CCT specimen obtained with light reflecting at the polished specimen surface.

Figures 4-2, 4-4a and 4-4b are the raw images to which the image processing still has to be applied. Figure 4-5 is an enlargement of the crack tip in figure 4-4a and reveals the square pixel structure of an image. Each pixel can have a grey value between the limits 0 (black) and 255 (white). Figure 4-6 gives the situation of figure 4-5 after the image processing procedure is completed. All pixels with grey values in the range of 200[1]-255 are assigned a grey value of 255 (= white) while remaining grey values (0-199) are all set to 0 (=black). The image now contains only two grey values, 0 and 255. The crack is labelled as the complete white object in surroundings of black uncracked material. The length of the labelled crack is measured from figure 4-6.
The crack tip opening (CTOD) in figure 4-6 is larger than the CTOD in figure 4-5. This is not the case in reality but the result of a vertical filtering procedure of the image. The high grey values (i.e. the crack) are stretched somewhat in a vertical direction, resembling a more opened crack. The vertical filtering procedure was found to give less scatter in the measured crack length values. The vertical filtering procedure does not effect the crack length defined in a horizontal direction.

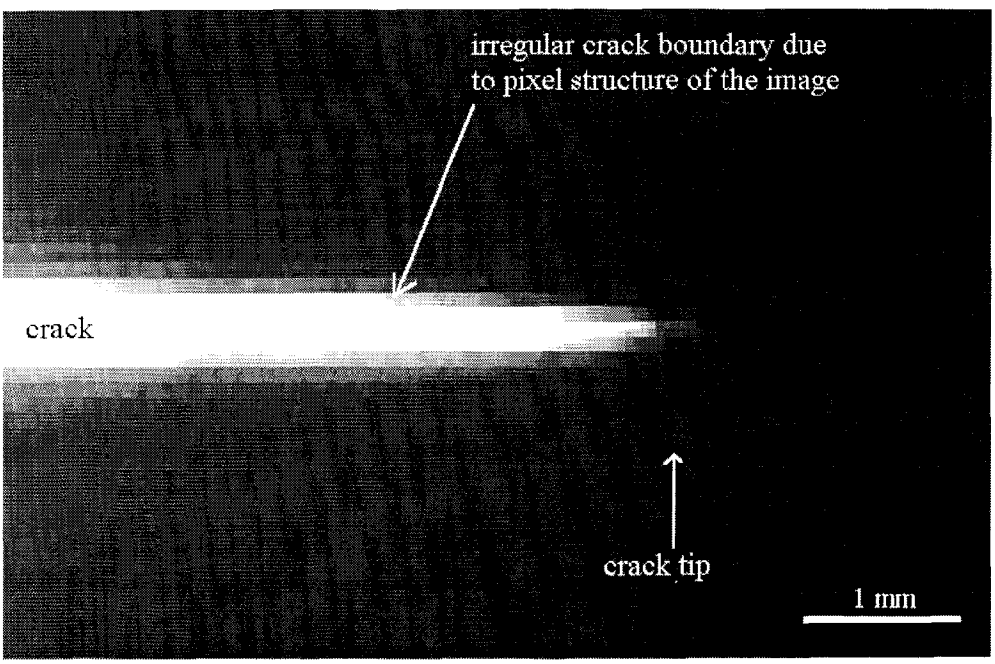

Figure 4-5 : Detailed view of the polyethylene crack tip of figure 4-4a .

[1] The onset of the grey value that can be considered to be a crack. A value of approximately 200 was used for tests using light shining through the opened crack in Polyethylene.

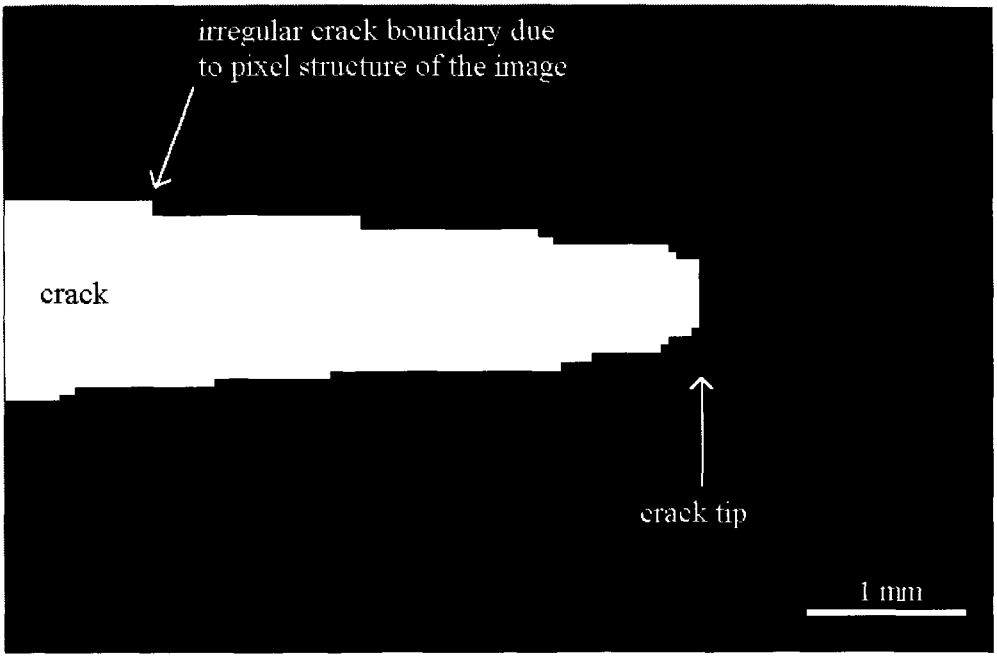

Figure 4-6 : The image obtained after application of the image processing procedures to the image of figure 4-5.

4.5 Aspects concerning precision of the image processing measuring technique

Resolution

The crack length can only be measured in discrete steps, owing to the digital pixel structure of the image. In the polyethylene tests a horizontal field of about 35 mm on the specimen surface was observed. Initially, during the evaluation of the crack length measuring technique, only one crack tip in the polyethylene CCT specimen was observed, since asymmetrical crack growth initially did not seem to appear in polyethylene. Observing one crack tip can reveal the discontinuous character of crack growth in polyethylene and measurements are not obscured by the averaging of the crack growth of two crack tips.

The field of 35 mm observed is distributed over 768 horizontal pixels, which results in a resolution of $35/768 \approx 0.05$ mm/pixel. Thus in this case the crack length is measured in discrete steps of 0.05 mm. The resolution can be increased by zooming in on the specimen. This is not always convenient, however, for example when a crack growth range of 30 mm is expected and the test can be performed automatically during a weekend to save time in the test programme.

For polycarbonate both crack tips in the CCT specimen were observed in order to monitor the asymmetry in crack lengths, as illustrated in figure 4-2. The total horizontal dimension of the crack object obtained in this way is the sum of the left and right crack length. The average is taken as the representative crack length. To measure crack lengths of about 35 mm in polycarbonate it is necessary to observe a horizontal field of about 70 mm. The resolution in this case is 70 mm over 768 pixels, which is approximately 0.1 mm. Since the crack length results from averaging the position of both crack tips, the resolution becomes $(0.1)/(2) = 0.05$ mm. The resolution of the measurement in polycarbonate therefore matches the resolution in the case of polyethylene.

In figures 4-7 and 4-8 the sets of N-a data are given for a crack length range of 15 to 16 mm, as measured in a polyethylene test (PE-K) and a polycarbonate test (PC-K) respectively.

In both figures 4-7 and 4-8 the resolution of 0.05 mm in the crack length measurement is apparent from the layered structure of the crack length data.

In both polyethylene and polycarbonate a crack length measurement is completed every 18 seconds. Since the tests were performed at a 10 Hz fatigue frequency, this is equivalent to one measurement in 180 load cycles or 55 measurements in 10^4 cycles. The number of 55 measurements per 10^4 load cycles can be verified in figures 4-7 and 4-8.

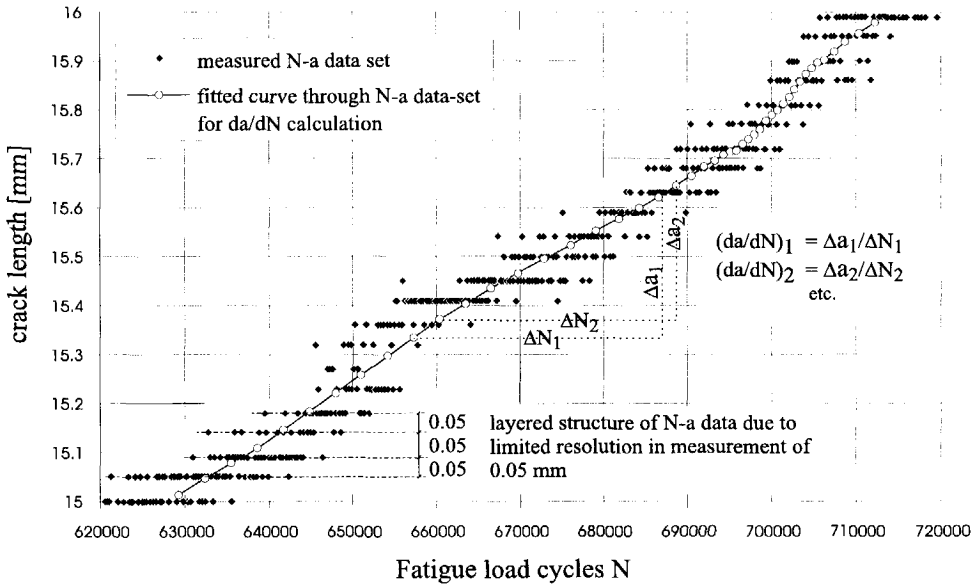

Figure 4-7 : Detailed view of measured N-a data set during a fatigue test in polyethylene.

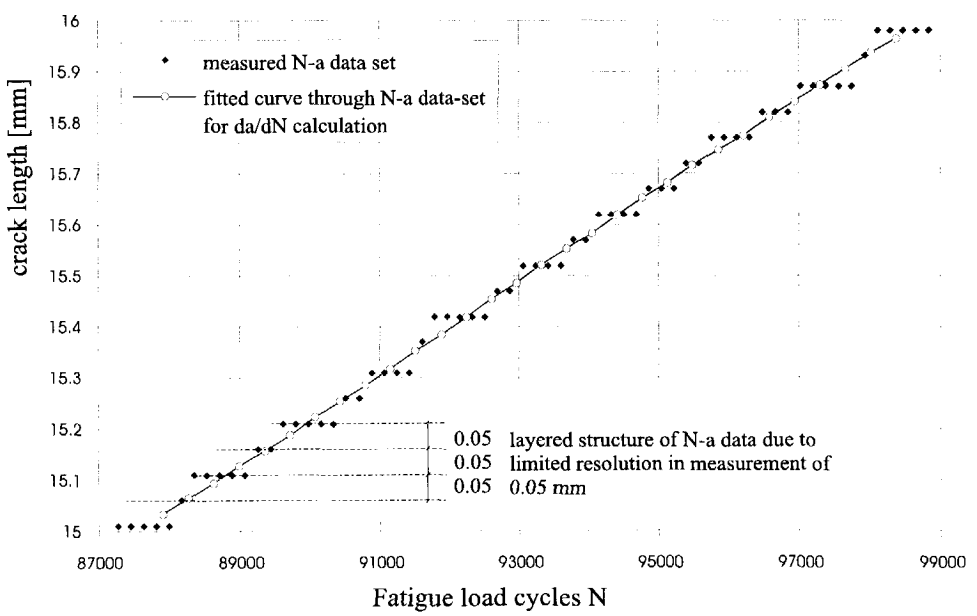

Figure 4-8 : Detailed view of measured N-a data set during a fatigue test in polycarbonate.

Reproducibility of measurements

The total error of a measurement is the difference between the measured value x and the true unknown value x_{true}. The total error is the sum of a constant systematic error and a random error. The random error can be seen as scatter in replicate measurements and represents the reproducibility of the measurement technique. The reproducibility of the crack length measurement in the polyethylene test is relatively low. In figure 4-7 it can be observed that in a range of successive measurements the crack length varies over 0.15 mm

In theory, by performing unlimited measurements (i.e. $N \rightarrow \infty$) the random error is outbalanced in the average value. This theoretical average value can be named $\bar{x}_{N=\infty}$ and is free of random error. The difference between x_{true} and $\bar{x}_{N\rightarrow\infty}$ is the remaining systematic error.

In ASTM E647-93 [44] the measurement precision is defined as the standard deviation σ on the mean value x_N of crack length determined for a set of N replicate measurements. For the polyethylene and polycarbonate tests the standard deviation (i.e. precision) of the crack length measurements is determined with data from the beginning of a *CA* fatigue test, where the crack growth rate is very low. In this way the standard deviation is determined over a large range of data with the same actual crack length. For both polyethylene and polycarbonate the precision was found to be approximately 0.04 mm.

Using surplus measurements to increase the measurement precision

The surplus of data points in the tests can be used to increase the accuracy of the crack length measurement. Once the precision of the measurement technique is determined with N replicate measurements, it can be used to evaluate the accuracy of one individual measurement performed during the test. From the definition of the standard deviation σ, for a normal distribution, it follows that one individual measurement x has a probability of 68% of being within the interval of :

$(\bar{x}_{N\rightarrow\infty} - \sigma\,;\ \bar{x}_{N\rightarrow\infty} + \sigma)$ i.e. $(\bar{x}_{N\rightarrow\infty} - 0.04;\ \bar{x}_{N\rightarrow\infty} + 0.04)$ [49].

If in a data set of 100 replicate measurements, 5 successive measurements are averaged to one value (i.e. reduction factor $R_f = 5$), the original data set is reduced to 20 averaged data points. The reduced data will expose less scatter compared with the original data. The standard deviation of the 20 average data points will be a factor of $\sqrt{5}$ better than the standard deviation of the original 100 data points. In general, averaging over R_f data points leads to a $\sqrt{R_f}$ better standard deviation of the averaged data set compared with the standard deviation of the original data [49].

In automated tests, when the measured crack length values are stored on computer hard disk, it requires no extra effort to measure and store a large number of data points during the test. The surplus of data points obtained is used to average successive measurements, resulting in greater precision of the reduced data set. More than 50 measurements over 1 mm crack extension is considered as surplus and will be reduced. In this way 100 measurements per mm crack extension will be reduced to 50 reduced data points ($R_f = 2$), while likewise 300 measurements per mm are reduced to 50 data points with $R_f = 6$. By scanning the original data file the reduction is executed in steps of 1 mm crack length. In each step the reduction is

adjusted to obtain about 50 reduced points per mm crack length, i.e. 0.02 mm crack growth per reduced data point. A value of 0.02 mm represents a small amount of crack growth in relation to the precision of the measurement technique ($\sigma = 0.04$ mm). Therefore the reduction procedure only effects the scatter of the measuring technique without smoothing fluctuations in actual physical crack growth. The reduced N-a file will have evenly distributed data points over the whole range of crack length measured, independent of variations in crack growth speed during the test. No reduction is applied below 50 measurements per mm crack extension.

In test PE-K 20 raw data points are reduced to 1 average value i.e. $R_f = 20$. The standard deviation of the reduced points in test PE-K is therefore $0.04/\sqrt{20} \approx 0.01$mm. Therefore, by using the surplus of measurements for test PE-K, the precision is improved fourfold.
Owing to the increased crack growth rate in test PC-K compared with the polyethylene test PE-K, there was less time available for the crack length measurements, resulting in fewer data points. Here the reduction is performed over only 2 points ($R_f = 2$). The standard deviation of the reduced points in test PC-K is therefore $0.04/\sqrt{2} \approx 0.03$ mm.

4.6 Calculation of crack growth rates; conformity with ASTM E647-93

After the reduction procedure the reduced N-a data may still exhibit scatter which cannot be related to actual crack growth phenomena (i.e. presence of negative crack growth!). In other words, the scatter in measurements can be improved but not completely eliminated. If more reduction is applied the scatter is reduced accordingly. However, in such a case the reduction is applied to a set of data points which contains actual physical crack growth. The reduction would therefore also include a portion of crack growth smoothing. To distinguish clearly between reduction in scatter of the measurement technique and smoothing of crack growth 50 reduced data points per mm crack extension were maintained. To the reduced data file a supplementary smoothing procedure is carried out by averaging data points {0 to N_s}; {1 to (N_s +1)}; {2 to (N_s +2)}, {3 to (N_s +3)} etc. Thus the smoothing procedure is averaging over N_s = 25 data points (i.e. 0.5 mm) without reducing the number of data points. This procedure is known as the method of moving average. Finally the reduced and smoothed data set is used to calculate da/dN as the secant of the curve, i.e. $\Delta a/\Delta N$ with $\Delta a \approx 0.5$mm. The results can be seen in figures 4-9 and 4-10.
Figures 4-7 and 4-8 show a part of the original raw data sets of test PE-K (polyethylene) and test PC-K (polycarbonate). The reduced and smoothed data sets are also given while the secant method for calculation of da/dN is illustrated in figure 4-7.
The image processing data collection, with data reduction, smoothing and da/dN calculation resulted in the curves given in Figures 4-9 and 4-10. The markers in figure 4-9 correspond to da/dN calculated in accordance with ASTM E647-93, which will be discussed in the following.

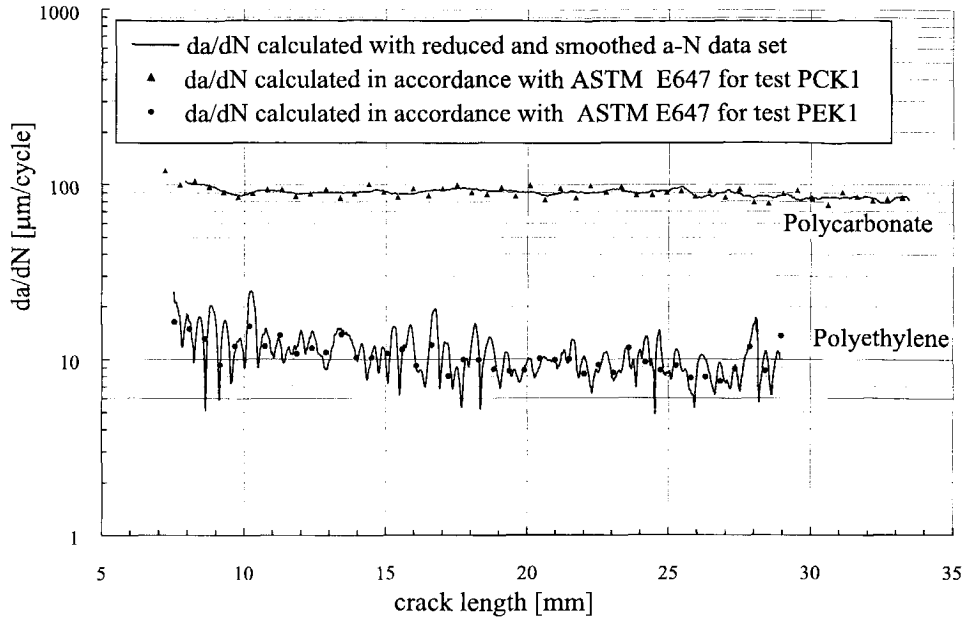

Figure 4-9 : Response of *da/dN* for polyethylene and polycarbonate under constant ΔK conditions of 1.0 and 0.8 MPa$\sqrt{m}$ respectively.

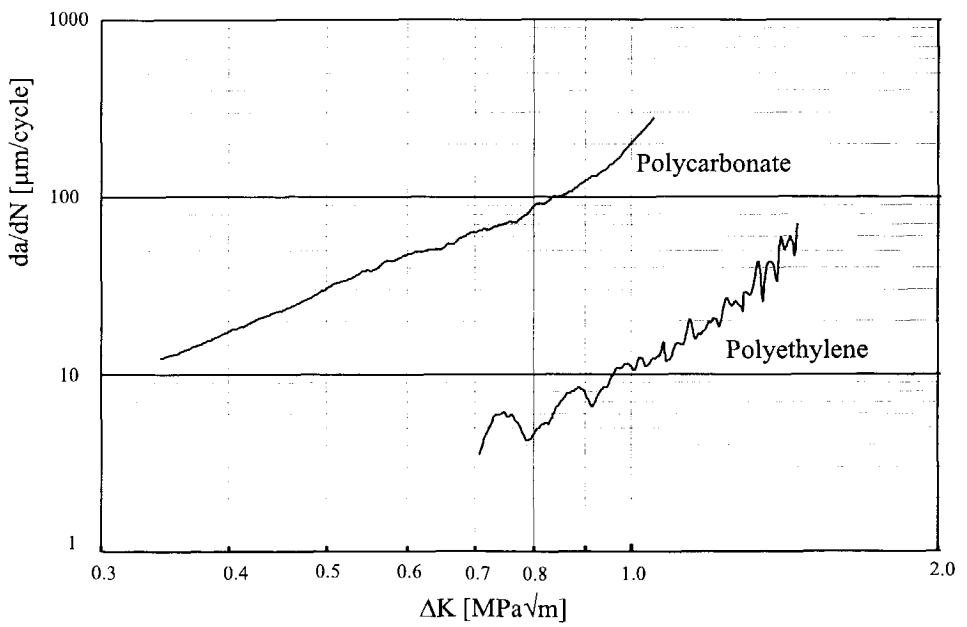

Figure 4-10 : Crack growth rate of polyethylene and polycarbonate as a function of ΔK.

Section 8.8.1 of ASTM E647-93 [44] gives recommendations concerning the crack length measurement interval (Δa_{meas}), while two techniques for calculation of da/dN are provided in appendix X1 of ASTM E647-93. Only the recommended "secant method" for calculation of da/dN will be discussed, since this method is used for calculating the crack growth rates of figures 4-9 and 4-10.
The "secant method" defines da/dN as the slope of the straight line connecting two adjacent data points on the a-N curve i.e. $da/dN = (a_{i+1}-a_i)/(N_{i+1}-N_i) = \Delta a_{meas}/\Delta N$.
Δa_{meas} is designated as the crack length interval between two adjacent data points of the **raw** data.

In discussing the recommendations of ASTM E647-93 two aspects should be clearly distinguished:

1) Raw data : the **original** N-a data set as measured during the test itself.
2) Reduced data: the raw data set reduced by averaging techniques.

ASTM E647-93 considers the recommended da/dN calculation to be based on the **raw** data. Consequently the measurement interval of the crack length (Δa_{meas}) directly characterises the crack length interval over which da/dN is averaged in the recommended "secant method". Accordingly the scatter in da/dN is directly affected by the value of Δa_{meas}. A low value of Δa_{meas} in relation to the measurement precision results in much scatter of da/dN. A large value of Δa_{meas} , however, reduces the number of data points and smoothes out variations in da/dN.
Based on the interdependence between measurement interval (Δa_{meas}) and the resulting da/dN curve, an optimal value of Δa_{meas} is indicated in ASTM E647-93 to be in the range of 0.25 to 2 mm (for a CCT specimen with W=100 mm). However, ASTM E647-93 indicates that the minimum measurement interval must be at least ten times the measurement precision, i.e. at least 0.4 mm for the polyethylene and polycarbonate tests.

The chosen data collection interval and the subsequent calculation of da/dN in the fatigue tests performed are not completely in accordance with the recommendations of ASTM E647-93. To verify if the da/dN curves obtained are similar to results according to the ASTM E647-93 standard the calculation of da/dN was duplicated with a simulated data file processed from the original raw data file. From the original raw data file, data points with crack length intervals of 0.5 mm are selected, as if only these points were measured during the fatigue test. The simulated crack length interval of 0.5 mm was chosen in accordance with the ASTM E647-93 recommendation for the measurement interval to be at least 10 times the measurement precision i.e. at least 10*0.04 mm = 0.4 mm. As a result the simulated data file is in accordance with ASTM E647-93.

Using the simulated data files of tests PC-K and PE-K, calculation of da/dN is performed by means of the "secant method" in accordance with ASTM E647-93 and the results are indicated in figure 4-9 by marked data points.

Compared with the strictly applied ASTM E647-93 recommendations, the image processing data collection and processing give da/dN results of the same order of magnitude. However, the surplus of data points with the automated data collection results in more detailed crack growth rate information.
With regard to data collection and processing, tests PE-F and PC-F correspond to the PE-K and PC-K tests discussed.

In measuring crack length, apart from a random error a systematic error may be present.
In the image processing technique the systematic error is verified by measuring the initial and final crack length values with a ruler. The measurements with the ruler also serve as a reference by which to verify the image processing measurements. The systematic error is found to be restricted to approximately 0.2 mm. It is assumed that the systematic error at intermediate crack lengths does not exceed the systematic errors measured at the initial and final crack lengths. The effect of a systematic error with respect to da/dN is limited, since a constant systematic error has no effect on the gradient of the a-N curve. A systematic error in crack length, however, causes a wrong assessment of applied stress intensity at the crack tip.
According to ASTM E647-93 a maximum difference between crack lengths on the front and back of the specimens of 25% of the specimen thickness B is permitted. In all tests this was verified at the beginning and end of the total crack growth range. For the polycarbonate tests the difference between the two crack lengths referenced from the centre-line was monitored during the test and found to be within 2.5% of the specimen width W, while for polyethylene this was only performed at the beginning and end of the test.
In the polyethylene tests the minimum crack length (mostly on the front or back surface of the specimen, due to crack tunnelling) determines the amount of light shining through the crack, i.e. the crack length measured. However, in the polycarbonate tests the maximum crack length value inside the specimen is measured, since the crack tip tunnelling is visible through the transparent material. Overall, in both polyethylene and polycarbonate, crack tunnelling causes a different crack length measurement, compared with the average through thickness value. This systematic error was found to be approximately 0.5 mm.

4.7 Comparison of the image processing technique with the direct potential drop method in metals

The direct potential drop method is widely used for measuring crack lengths in metals during fatigue fracture or static load fracture tests. In [50] fatigue tests in aluminium 2024 were performed by means of crack length measurements using a commercially available potential drop device [51]. The precision of these measurements is within 0.03 mm for replicate measurements. Thus, in fatigue testing, the precision of the direct potential drop method in aluminium is somewhat better than that of the image processing technique used for polyethylene and polycarbonate.

Within the context of the thesis the image processing technique is not applied to measure cracks in metals. Therefore a direct comparison between the image processing technique and the well established method of potential drop cannot be made here. In [52] however the suitability of image processing for measuring cracks in metals is evaluated for statically loaded CT specimens at elevated temperatures. In [52] the measurements were found to be obstructed by crack branching and a high degree of plasticity at the crack tip, which is inherent with crack growth under static loading conditions. In fatigue crack growth of metals, crack branching and crack tip plasticity are limited and image processing techniques may well be possible.

4.8 Initial fatigue test results for polyethylene and polycarbonate

The practical use of image processing is illustrated by using the measurement data in order to characterise the crack growth behaviour of both materials. The results concerning crack growth behaviour are discussed briefly here.

Polyethylene

The crack growth rates of the constant ΔK and *CA* fatigues test in polyethylene (tests PE-K and PE-F respectively) are given in figures 4-9 and 4-10.

In figure 4-9 (test PE-K) it can be seen that da/dN has a fluctuating character. The fluctuations observed in da/dN can be related to crack growth bands on the fracture surface. In figure 4-11 57 bands are counted on the fracture surface, which agrees well with the 54 fluctuations in da/dN as detected in figure 4-9.
Apart from the fluctuations, the average value of da/dN in test PE-K is almost constant over the total crack length range of 7 to 29 mm. This implies that although polyethylene is a very ductile material, the stress intensity concept can be considered a good crack growth parameter.
The first 8 bands in test PE-K, occurring from 7 to 11 mm crack length, are distinctly larger than the following bands, which are of more uniform dimensions. The reason for this phenomenon could be related to a creep effect, which is generally more pronounced during the beginning of a loading period. The different band sizes can also be seen as large fluctuations at the start of the da/dN curve in figure 4-9.
The 57 crack growth bands are formed over a period of $2.2 \cdot 10^6$ cycles, which means that each band is formed during 38000 cycles. Owing to the large number of cycles per band, these bands are known as "retarded" crack growth bands. Each band is thought to be formed during a process of chronological development, weakening and partial break-down of a craze at the crack tip. This process is also known as "retarded" crack growth and occurs with many polymers. [32,53]
The assumed "retarded" crack growth mechanism implies a relation between dimensions of the band and the actual craze length. The average band dimension in figure 4-11 is 0.4 mm. (57 bands over 22 mm crack length). The theoretical craze length L_c, according to the Dugdale model, is given by:

$$L_c = \frac{\pi}{8}\left(\frac{K}{\sigma_y}\right)^2$$

With the maximum stress intensity in test PE-K, of $K_{max} = \Delta K/(1\text{-}R) = 1/0.9 = 1.11$ MPa$\sqrt{\text{m}}$ and the yield stress $\sigma_y \approx 25$ MPa, this results in a theoretical craze length L_c of 0.77 mm. Therefore the band dimension is of the same order as the theoretical craze length calculated.
The fatigue crack growth rate, *da/dN*, of test PE-F is given in figure 4-10 as a function of the range of stress intensity ΔK. As usual the scales are double logarithmic. With ΔK ranging from 0.7 to 1.4 MPa$\sqrt{\text{m}}$, the resulting crack growth rate ranges from $2 \cdot 10^{-6}$ mm/cycle to $60 \cdot 10^{-6}$ mm/cycle. The visibility of fluctuations in *da/dN* is limited because of the logarithmic scales. The crack growth behaviour can be described by the Paris law:

$da/dN = C\,(\Delta K)^m$

With *da/dN* expressed in 10^{-6} mm/cycle and ΔK expressed in MPa$\sqrt{m}$ the Paris law material parameters are determined to be $C = 11$ and $n = 3.7$.
The band dimensions in test PE-F gradually increase in the crack growth direction, due to the increasing ΔK value for longer cracks in a constant load test.
At a crack length of 15 mm the value of ΔK in the constant load test PE-F corresponds with the ΔK =1.0 MPa$\sqrt{m}$ condition of test PE-K. These equivalent ΔK conditions are also reflected by the corresponding band size and crack growth rate of test PE-K, when compared with test PE-F at the specific crack length of 15 mm.

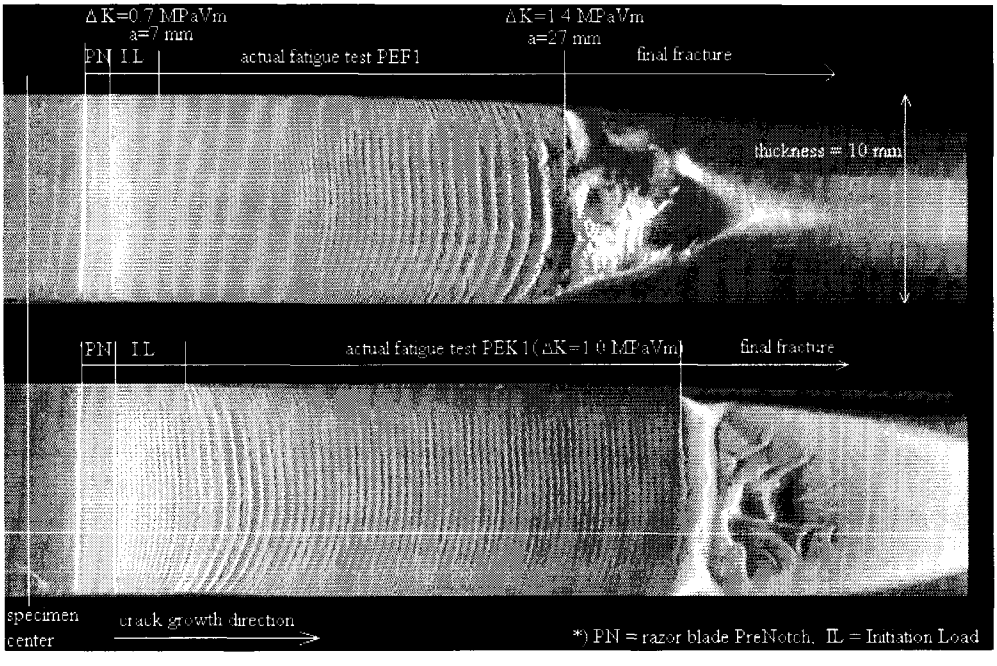

Figure 4-11: Fracture surfaces of fatigue-loaded polyethylene (constant ΔK and *CA* testing respectively).

Polycarbonate

The crack growth rates of the constant ΔK and *CA* fatigue tests in polycarbonate (PC-K and PC-F respectively) are also given in figures 4-9 and 4-10. The crack growth rates are of the same order of magnitude as reported in [53] for polycarbonate.
The average value of the crack growth rate da/dN in test PC-K is almost constant over the total range of the crack length of 7 to 34 mm(figure 4-9). Thus, as in polyethylene, ΔK can be considered a good fatigue fracture parameter for polycarbonate.

The crack growth rate as a function of ΔK for the constant load test PC-F is given in figure 4-10. With ΔK ranging from 0.35 to 1.1 MPa$\sqrt{m}$, the resulting crack growth rate ranges from $10 \cdot 10^{-6}$ mm/cycle to $300 \cdot 10^{-6}$ mm/cycle. As with polyethylene, the crack growth behaviour can be described by the Paris law. The parameters for polycarbonate are C=160 and n=2.5.
At a crack length of 24 mm, where ΔK = 0.8 MPa$\sqrt{m}$, the crack growth rate *da/dN* is $90 \cdot 10^{-6}$ mm/cycle. This is in accordance with the crack growth rate of test PC-K, in which ΔK = 0.8 MPa$\sqrt{m}$ during the whole test.

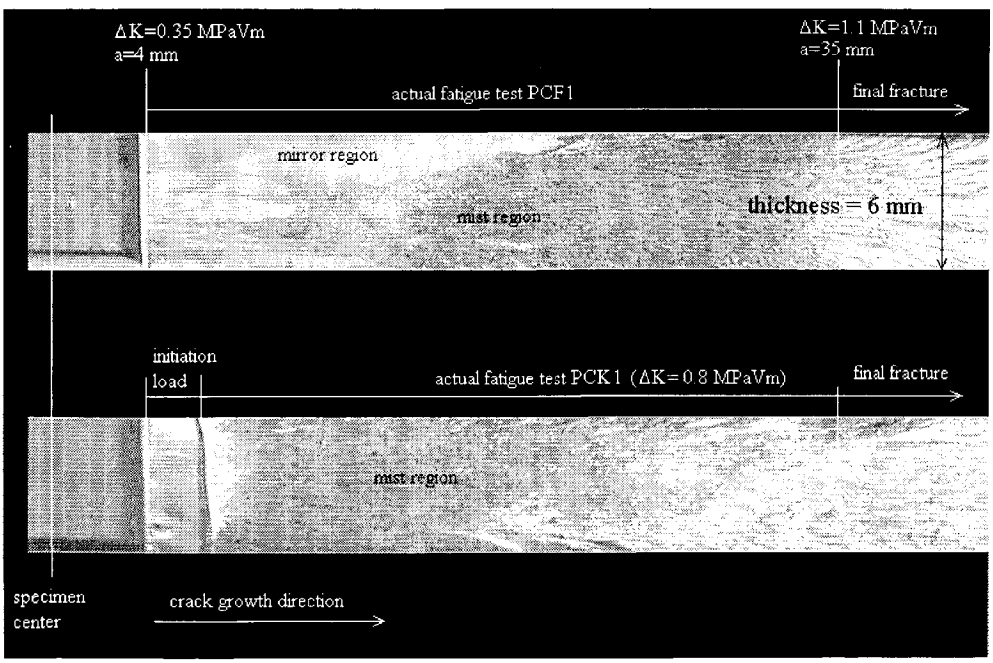

Figure 4-12: Fracture surfaces of fatigue-loaded polycarbonate (constant ΔK and *CA* testing respectively).

The fatigue fracture surface of polycarbonate, as for many other amorphous thermoplastics, can have two distinctive types of appearance. [32,53].
At high fatigue loads the fracture surface has a rough structure macroscopically, which is related to the presence of multiple crazes at the crack tip. The crack grows through the various

non-planar crazes, which causes a rough fracture surface. The rough appearance is referred to as "mist region". At low fatigue loads the fracture surface has a smooth structure macroscopically, which is related to the presence of only one single craze at the crack tip. In such a case, the crack always grows through the same craze, which causes a very smooth fracture surface. The smooth appearance is referred to as "mirror region".
The fracture surfaces of tests PC-F and PC-K are given in figure 4-12. The entire fracture surface of test PC-K is rough (mist region). According to [32,53] this means that at the fatigue load of $\Delta K = 0.8$ MPa$\sqrt{\text{m}}$ (R=0.1) the crack tip is preceded by a multiple craze zone.
The fracture surface of test PC-F shows a mirror region at a low crack length, while at a higher crack length the mirror region is replaced by a mist region. The transition from mirror to mist region is related to the increasing ΔK value during the crack growth in a constant load test.

4.9 Conclusions concerning crack length measurement with image processing

- Image processing is found to be useful for measuring crack lengths automatically during fatigue tests in polyethylene and polycarbonate. The standard deviation in the mean value of replicate crack length measurements is about 0.04 mm for both polyethylene and polycarbonate.
  By averaging the surplus of measurement data the accuracy is increased to 0.012 mm and 0.025 mm for polyethylene and polycarbonate respectively.

- In polyethylene fatigue crack growth is observed at fatigue loads in the range of $\Delta K = 0.7$-1.4 MPa$\sqrt{\text{m}}$ ($R = 0.1$, frequency 10 Hz.) with corresponding crack growth rates of (2-60)$\cdot 10^{-6}$ mm/cycle.
  The fracture surface shows crack growth bands of macroscopic dimensions. Each band is thought to be formed during a process of chronological development, weakening and partial breakdown of a craze at the crack tip. Since each band is formed over many thousands of load cycles, the fatigue mechanism is referred to as "retarded fatigue crack growth" [32,53].

- In polycarbonate fatigue crack growth is observed at fatigue loads in the range of $\Delta K = 0.35$-1.1 MPa$\sqrt{\text{m}}$ ($R = 0.1$, frequency 10 Hz.) with corresponding crack growth rates of (10-300)$\cdot 10^{-6}$ mm/cycle.
  The fracture surface can have two distinctive types of appearance, a smooth "mirror region" at low fatigue loads and a rough "mist region" at high fatigue loads. The mirror and mist regions are related to the presence at the crack tip of one single craze (at low loads) or multiple crazes (at high loads) [32,53].

5. Crack growth results

5.1 PENT test results

Creep crack growth results of PENT test series

PENT test results for materials **O** and **T** are shown in figure 5-1. (test temperature 80 °C). Clearly material **O** has the shortest failure times. At corresponding stress levels, the failure time of material **O** is approximately one hundred times shorter compared with material **T**. The COD signals recorded indicate that the relative contribution of craze initiation to the total failure time is similar for both materials. Therefore, the differences in total failure times of materials **O** and **T** also represent a difference in creep crack *growth* behaviour.
The transition from ductile to brittle failure in figure 5-1 shows as a typical zigzag behaviour, as also reported in [11] as a blunting-related phenomenon. The PENT test protocol [5] recommends testing at a stress level of 2.4 MPa (at 80°C) to obtain brittle failure in a short testing time. Figure 5-1 confirms the optimum value of 2.4 MPa in this respect for the materials tested.

Unlike materials **O** and **T**, material **F** does not display brittle failure at the optimum stress level of 2.4 MPa, even at prolonged testing times exceeding 10^4 hours. In chapter 6 the high resistance of material **F** with regard to creep crack growth is shown to be related to pronounced blunting at the crack tip.

The appearance of fractures showed that all failures above a stress level of 4 MPa are entirely ductile, while stress levels below 3 MPa satisfy brittle behaviour related to creep crack growth. At intermediate stress levels, between 3 and 4 MPa, the transition between brittle and ductile failure causes some variation in test results. The ductile and brittle regions in figure 5-1 are fitted by straight lines. The different slopes of the lines in ductile and brittle failure typically identify the different failure modes (see also section 2.3.1: *hydrostatic pressured pipe tests*).

Reproducibility of the PENT test

The PENT test is a relatively new test procedure and experimental know-how was initially not available within the laboratory. In order to obtain experience, a set of 29 replicate tests were performed, using material **O** at standard conditions (σ = 2.4 MPa, 80°C). Results of the replicate tests are shown in figure 5-2 , giving the initiation period and total failure time for each specimen loaded. The initiation period is obtained from the recorded COD signals and is taken as the period of time from the beginning of the test until the first step in the COD signal (see also figure 3-6). The time span between initiation until final fracture is referred to as "crack growth". In a PENT test the total failure time is conveniently used to characterise creep crack growth behaviour. An average failure time of 13.5 hours was measured with a standard deviation of 3.3 hours (= 24% of the average).

Recognition of the total failure time as a total of the initiation and the subsequent crack growth period reveals unusual aspects of the reproducibility. An average initiation time of 3.8

hours was measured with a standard deviation of 0.75 hours (i.e. 20% of its average value). Likewise, the average crack *growth* period was found to last 9.7 hours, with a standard deviation of 3.1 hours (i.e. 32% of its average value). Therefore, initiation seems to behave more predictably than crack growth, which contradicts established experience in the field of fracture mechanics.
What is designated here as "crack growth period" also includes the final stage of fracture. This final stage of fracture is likely to be responsible for the considerable scatter in total failure times.

The reproducibility of the PENT test has to be considered within the perspective of test results obtained in different materials. In testing different types of materials it is not uncommon to find test results differing by one or two decades. Taking this into consideration, the reproducibility of the PENT test is acceptable.

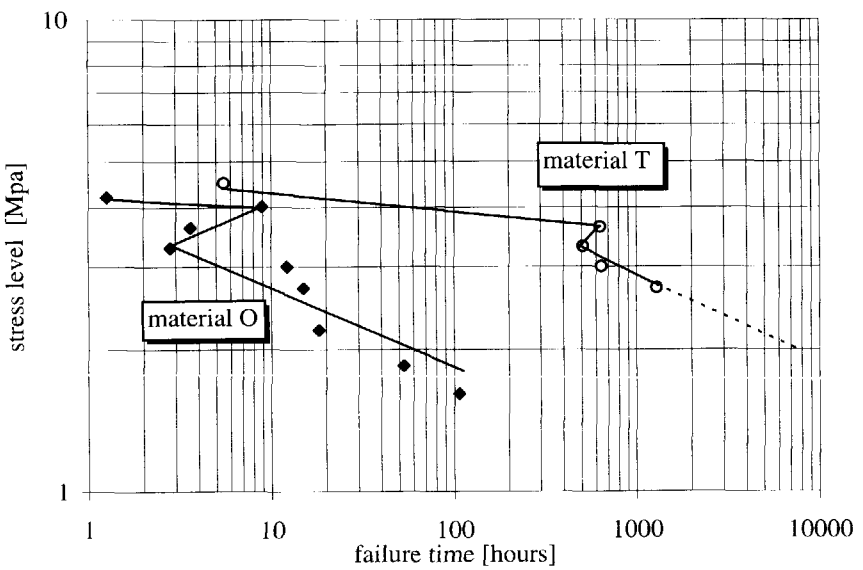

Figure 5-1 : PENT test results of materials **O** and **T** (80°C , various stress levels)

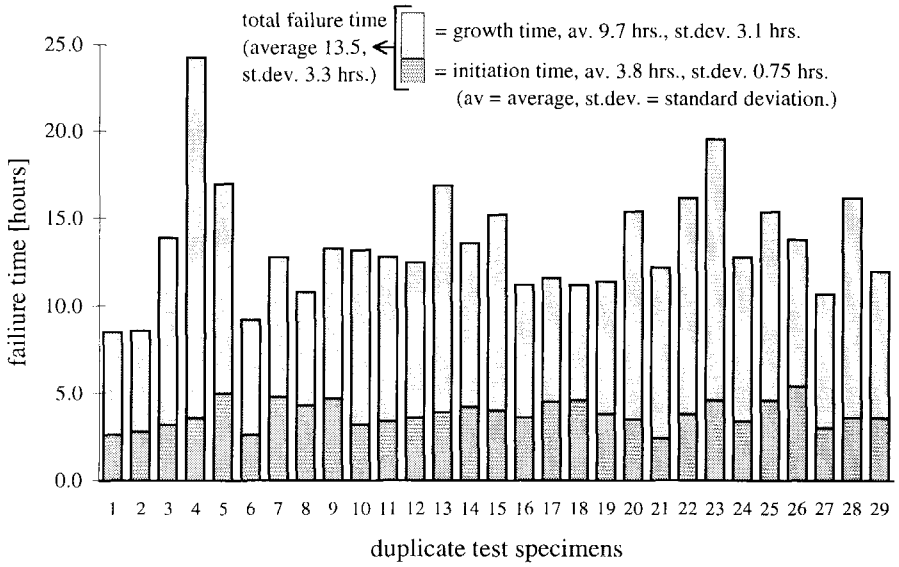

Figure 5-2 : Failure times of 29 replicate PENT tests performed (material **O**, σ = 2.4 MPa, 80°C).

Modelling creep crack growth with PENT test results

In the PENT test, creep crack growth is evaluated using the stress-lifetime approach with the results given in figure 5-1. In [1] a crack growth model is introduced which can be considered as an adjusted Paris law for creep crack growth:

$$da/dt = C_{ccg}\,(K)^b \qquad \{5\}$$

Where: C_{ccg} and b are constants and:

$$K = C_{pent}\sigma\sqrt{(\pi a)} \qquad \{6\}$$

$$C_{pent} = 1.12 - 0.231\left(\frac{a}{W}\right) + 10.55\left(\frac{a}{W}\right)^2 - 21.72\left(\frac{a}{W}\right)^3 + 30.39\left(\frac{a}{W}\right)^4$$

With the creep crack growth law given by equation {5} the PENT test results can be used to obtain the parameters C_{ccg} and b. In this way, the PENT test results (stress-lifetime data) lead to more detailed crack growth information, i.e.: $da/dt(K)$. The results of the crack growth model can be compared with the results of the extrapolation load series, in which direct measurement of da/dt under constant load conditions was incorporated (section 5.3).
With the model according to equation {5} the total failure time T_f can be calculated by integration over the total crack length range, from the start crack length, a_{st} , to the critical crack length, a_{cr} :

$$T_f = \int_{a_{st}}^{a_{cr}} \frac{da}{C_{ccg}\left(C_{pent}\sigma\sqrt{\pi a}\right)^b} \qquad \{7\}$$

The model according to equation {5} is used here to determine the values of parameters C_{ccg} and b in order to obtain knowledge of da/dt at a specific level of K. The solution of equation {7} with appropriate (but unknown) values of C_{ccg} and b produces the same calculated value of T_f as is obtained from a real PENT test. In this way the correct combination of C_{ccg} and b can be determined.

An analytical solution of equation {7} is not available and instead a numerical procedure is used. For the numerical procedure it is, however, necessary to obtain starting points for the values of C_{ccg} and b. The starting point for b is found taking into consideration that the K level during crack growth in a PENT test is proportional to the applied stress level, σ, while time to failure, T_f, is inversely proportional to the average value of da/dt. Therefore the solution of equation {7} is approximated as:

$$(1/T_f) = C'_{ccg}\,(\sigma)^b \qquad \{8\}$$

Using equation {8} and two PENT test failure times obtained, $T_{f,1}$ and $T_{f,2}$, at stress levels σ_1 and σ_2 respectively, a starting point for b is determined. It should be noted that the failure times, $T_{f,1}$ and $T_{f,2}$, were reduced by the initiation period, as observed from the *COD*-signals recorded during the PENT test. The initiation period is omitted, as it has no significance in relation to the crack *growth* model of equation {5}. In this way a value $b \approx 4$ is estimated for material **O** which agrees well with values known from the literature. With $b = 4$, values of C_{ccg} are scanned to find the specific value of C_{ccg} which produces an appropriate calculated value of T_f (i.e. the same value of T_f as observed in a real PENT test).

For the numerical calculation, the crack growth range is evenly distributed over 1000 crack length values, from $a_{i=1} = 3.5$ mm to $a_{i=1000} \approx 7$ mm, constituting crack length increments Δa of 0.0035mm. For each individual crack length the value of K is calculated using equation {6} with a corresponding creep crack growth rate $(da/dt)_i$ according to equation {5}. The value of da/dt for each individual crack length also gives the failure time $(\Delta t)_i$ for each crack length increment, i.e.: $(\Delta t)_i = \Delta a/(da/dt)_i$. The total time to failure, T_f, is found by summation of the individual contributions $(\Delta t)_i$:

For material **O**, with $b = 4$, a value of $C_{ccg} = 3.8\text{e-}8$ is found to give a similar calculated value of T_f as observed from PENT test results. With the values of C_{ccg} and b obtained, the value of da/dt can now be calculated for a specific K level. In this way for $K = 0.5$ MPa$\sqrt{\text{m}}$ a value of $da/dt = 24$ nm/s is found. This value agrees well with actual measured crack growth rates in the extrapolation load series ($da/dt \approx 20$ nm/s).

Since the value of $b = 4$ was only an estimate, the numerical procedures were additionally executed for values of $b = 3$ and $b = 5$. The results are given in table 5-3.

Different values of b are found also to be related to different values of C_{ccg}. However, at low levels of K each set of (b-C_{ccg}) produces da/dt values of the same order of magnitude. Hence the prediction of da/dt at K levels between 0.5 and 0.7 MPa$\sqrt{m}$ can be considered reliable.
In the upper regime of K, distinct predictions of da/dt are found using the different sets of (b-C_{ccg}) values, reflecting unreliable prediction in this case. The different values of da/dt at higher levels of K do not influence the outcome of the prediction at lower K levels (the high crack growth rates do not contribute greatly to the total failure time). For the same reason the choice of critical crack length, with corresponding high values of da/dt, is of minor importance with respect to the outcome of the calculations of b and C_{ccg}.

For material **T** the same method is used to find values of b and C_{ccg}. For b a starting value of $b = 5$ was found; calculations with $b = 3$ and $b = 4$ were also performed. The results are given in table 5-4. For material **T** a prediction of $da/dt \approx 2$ nm/s is found at a K level of 0.7 MPa$\sqrt{m}$. A direct comparison with results of the extrapolation series is not possible for material **T,** as actual creep crack growth is not found in the CCT specimens.

b (assumed)	C_{ccg} *) (calculated)	da/dt [nm/s] = C_{ccg} $(K)^b$ at various K-levels [MPa$\sqrt{m}$]		
		$K = 0.5$	$K = 0.7$	$K = 1.0$
3	$2.3 \cdot 10^{-7}$	29	79	230
4	$3.8 \cdot 10^{-7}$	24	91	380
5	$6.6 \cdot 10^{-7}$	21	111	660

*) The value of C_{ccg} is calculated, which produces a numerically calculated crack growth time of 9.7 hours in accordance with PENT test results at a stress level of $\sigma = 2.4$ MPa.

Table 5-3 : Prediction of $da/dt = C_{ccg}\,(K)^b$ for material **O**.

b (assumed)	C_{ccg} *) (calculated)	da/dt [nm/s] = C_{ccg} $(K)^b$ at several K-levels [MPa$\sqrt{m}$]		
		$K = 0.5$	$K = 0.7$	$K = 1.0$
3	$5.6 \cdot 10^{-9}$	0.70	1.92	5.6
4	$8.3 \cdot 10^{-9}$	0.52	1.98	8.2
5	$12.7 \cdot 10^{-9}$	0.40	2.13	12.7

*) The value of C_{ccg} is calculated, which produces a numerically calculated crack growth time of 280 hours in accordance with PENT test results at a stress level of $\sigma = 2.7$ MPa.

Table 5-4 : Prediction of $da/dt = C_{ccg}\,(K)^b$ for material **T**.

5.2 General fatigue crack growth behaviour

"General fatigue behaviour" mainly deals with the response of *da/dN* as a function of ΔK for materials **O**, **T** and **F** as measured in *CA* fatigue tests. For all materials (**O**, **T** and **F**) *CA* fatigue tests were performed at three load ratios (0.1, 0.3 and 0.5), two frequencies (0.4 and 4 Hz) and two test temperatures (20°C and 80°C). Unless specifically stated otherwise, all tests use a sinus waveform. The tests at different load ratios and frequencies were carried out in order to obtain a general idea of how creep mechanisms interact with fatigue crack growth. In sections 4.5 and 4.6 it is shown how crack growth rates are calculated from the *N-a* file measured.

Justification of the use of ΔK as a fatigue crack growth parameter

Figure 5-5 gives results of a test in which ΔK is kept constant at a value of 0.35 MPa$\sqrt{m}$ over a crack length range of 8 to 32 mm. The crack growth rate *da/dN* is at a constant level for all crack length values, demonstrating the validity of ΔK as a fatigue crack growth parameter.
The result of a constant ΔK test was discussed before in section 4.6 in the context of the evaluation of the crack length measurement with digital image processing.

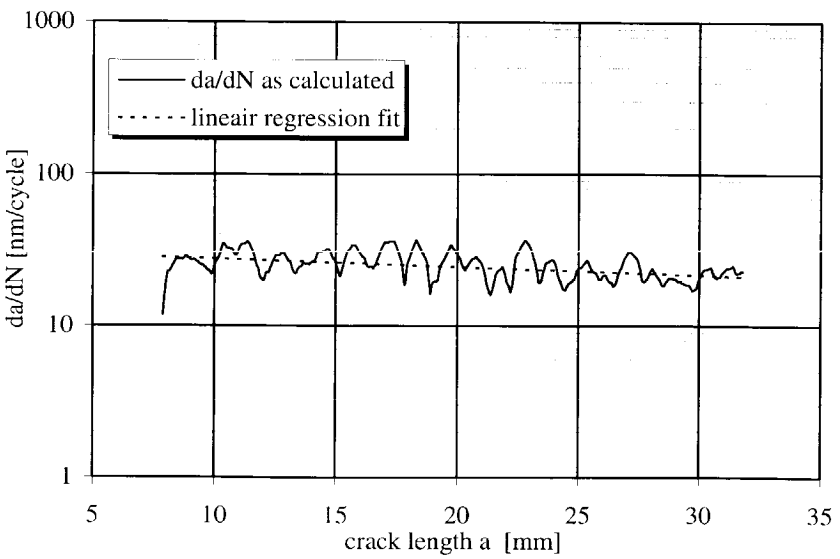

Figure 5-5: Response of *da/dN* for material **O** at a constant ΔK condition of 0.35 MPa$\sqrt{m}$ (sinus waveform of 4 Hz, temperature 80°C, load ratio R=0.1)

Reference fatigue behaviour of materials O, T and F (figure 5-6)

A fatigue load of 4 Hz, with sinus waveform and a load ratio of 0.1 is defined here as the *reference fatigue load*. The Paris fatigue behaviour of materials subjected to the reference fatigue load at a temperature of 20°C is designated as the "reference fatigue behaviour". The effects of secondary parameters such as temperature, load ratio and frequency are evaluated in comparison with the reference fatigue behaviour.

Figure 5-6 shows that, roughly speaking, materials **O**, **T** and **F** display similar reference fatigue behaviour. The reference response of da/dN as a function of ΔK can be represented by the Paris law with approximate parameter values of $m \approx 3.5$ and $C \approx 20$. (The dimension of C uses da/dN in nm/cycle and ΔK in MPa$\sqrt{\text{m}}$).

The ΔK range for reference fatigue crack growth ranges from 0.7 to 1.5-2 MPa$\sqrt{\text{m}}$, with corresponding crack growth rates of 2 to 200 nm/cycle.

The upper limits of ΔK in the curves of figure 5-6 approximately mark the transition from fatigue to final ductile fracture. However, the lower end of the curves do *not* represent fatigue threshold values. Very low ΔK values were simply not tested, in order to restrict the duration of tests to reasonable times.

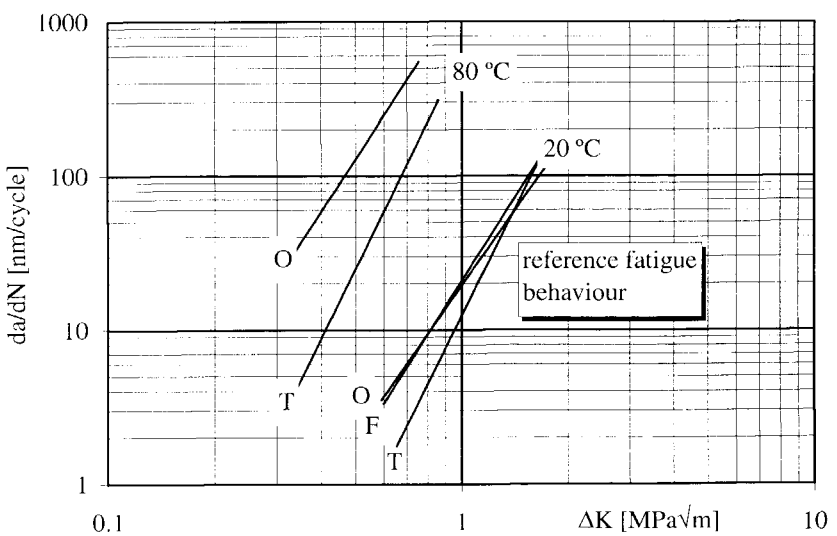

Figure 5-6 : Fatigue behaviour of materials **O**, **T** and **F** as a function of ΔK (sinus waveform of 4 Hz, load ratio R=0.1).

Effect of test temperature on da/dN for materials O, T and F

At an increased temperature of 80°C the fatigue crack growth rates of materials **O** and **T** are promoted. In contrast, fatigue crack growth of material **F** has stopped completely, even though a precrack initiated at 20°C was present.

The effect of temperature on *da/dN* (materials **O** and **T**) can be quantified as the multiple by which *da/dN* increases at the same level of ΔK (i.e. vertical shift in figure 5-6).
For materials **O** and **T** the vertical shift in *da/dN* is approximately a factor of 50 when the test temperature increases from 20°C to 80°C. The slopes *m* of the curves are not affected by the change in test temperature. Therefore, the ΔK sensitivity is the same at both temperatures, indicating similar crack growth mechanisms.
The fatigue crack growth stop of material **F** is consistent with the creep crack growth behaviour, for which crack arrest also occurs at a test temperature of 80°C. Apparently the additional damage of fatigue is not enough to initiate crack growth.

The vertical shift in *da/dN* of materials **O** and **T** at increased temperature does not extend to the upper fatigue regime, as at increased temperature the transition from fatigue to final ductile failure occurs at lower levels of ΔK (i.e. the upper fatigue regime displays a horizontal shift). As a consequence the maximal attainable values of *da/dN* are not greatly raised by an increased test temperature. Hence, in fatigue testing an increase in test temperature is not very effective as a means of reducing testing times. This is in contrast to the situation for creep crack growth testing, when increasing temperature can reduce testing times dramatically.

The observed promotion of *da/dN* with increased temperature is not all that obvious. As in all thermoplastics a temperature rise in polyethylene causes a shift to more ductile fracture behaviour. In general, ductile materials tend to show greater fatigue resistance. In [53] this trend is confirmed when different types of thermoplastics are compared.
However, ductility achieved by increased temperature is accompanied by a considerable drop in mechanical strength (yield strength, increased creep). In spite of the improved ductility, this apparently causes an overall increase in fatigue crack growth rates.

Effect of frequency on da/dN for materials O, T and F at test temperatures of 20°C and 80°C

Figures 5-7, 5-8 and 5-9 show fatigue behaviour of materials **O**, **T** and **F** respectively, tested at frequencies of 0.4 Hz and 4 Hz and temperatures of 20°C and 80°C.
At 20°C all materials **O**, **T** and **F** display a similar frequency effect, with an approximately doubled crack growth rate at a decade lower frequency of 0.4 Hz. Therefore, at room temperature the Frequency Sensitivity Factor is 2 for all materials.

Within the same type of material, the slopes m of the curves are not affected by the change in frequency, reflecting the same sensitivity with respect to ΔK. The consistent ΔK sensitivity is an indication of similar crack growth mechanisms at the frequencies applied.

The frequency effect is more pronounced at a test temperature of 80°C with FSF = 6 and 3 for materials **O** and **T** respectively (material **F** cannot be evaluated at 80°C).

The observed FSF values between 2 and 6 demonstrate a mixture of cyclic and creep mechanisms during crack growth under cyclic loading conditions. The increased values of FSF at higher temperatures represent increased creep contributions, induced by temperature.
At 80°C, fatigue crack growth in material **O** (FSF = 6) has more creep aspects than material **T** (FSF = 3).

Note:
As will be discussed later, frequencies of 4 Hz and 1 Hz were used in the context of the extrapolation load series (section 5.3, material **O**, square waveform, 80°C). Within this limited frequency range it was found that the crack growth rate per division of time (i.e. da/dt) is not changed, indicating a creep-dominated crack growth mechanism.

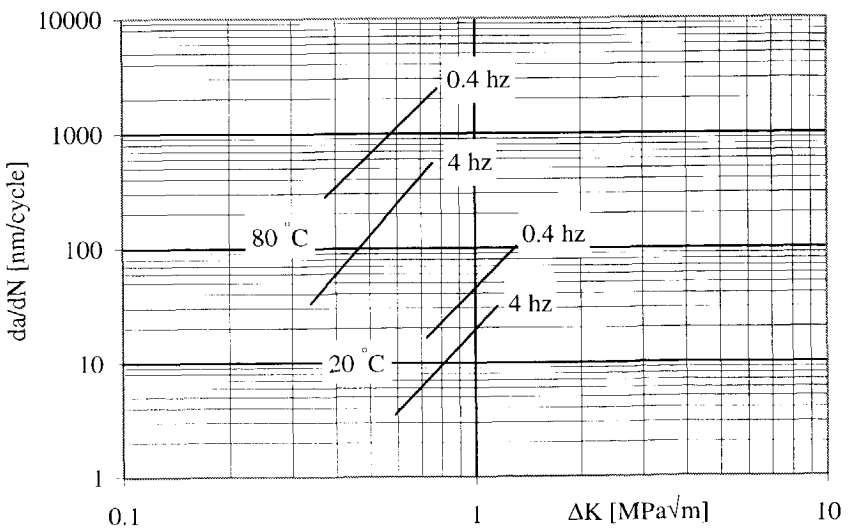

Figure 5-7: Effect of test frequency on fatigue behaviour of material **O** (sinus waveform, load ratio R = 0.1).

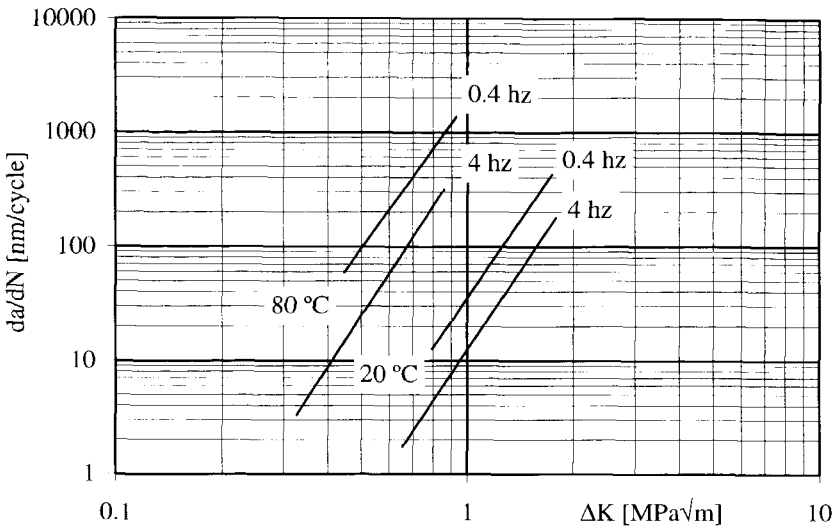

Figure 5-8: Effect of test frequency on fatigue behaviour of material **T** (sinus waveform, load ratio $R = 0.1$).

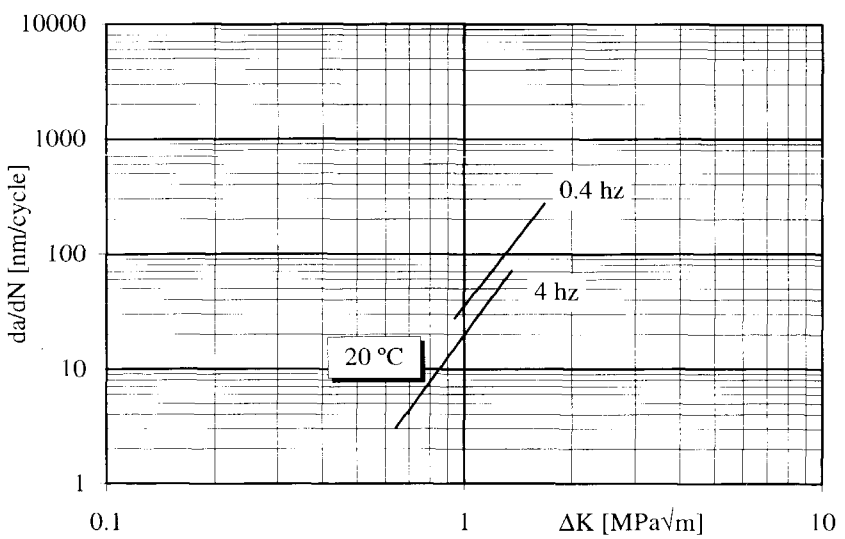

Figure 5-9: Effect of test frequency on fatigue behaviour of material **F** (sinus waveform, load ratio R = 0.1).

Effect of load ratio on da/dN for materials O, T and F at test temperatures of 20°C and 80°C

As a definition, an increase in da/dN at higher load ratios (R) but the same ΔK level is designated here as a *positive* load ratio effect. Analogously, a decrease of da/dN at higher load ratios and the same ΔK level is referred to as a *negative* load ratio effect. A positive load ratio effect is ascribed to promoted creep mechanisms while a negative load ratio effect indicates a dominating blunting mechanism (section 2.5)

Figures 5-10, 5-11, and 5-12 show fatigue behaviour of materials **O**, **T** and **F**, tested at load ratios of 0.1, 0.3 and 0.5 and temperatures of 20°C and 80°C respectively. The slopes m of the curves are clearly affected by the change in load ratio. Therefore the ΔK sensitivity of fatigue crack growth depends on load ratio, indicating a shift in crack growth mechanisms.

In testing at higher load ratios, the range of ΔK will be reduced. Obviously an increased load ratio yields higher K_{max} values at a given level of ΔK, whereas K_{max} controls the transition from fatigue to final failure. Therefore, testing at higher load ratios limits the range of ΔK.

From figures 5-10 to 5-12 it is apparent that the effect of load ratio on da/dN is not uniform for the materials tested. At 20°C materials **O** and **T** show a negative and positive load ratio effect respectively. However, at 80°C the situation is reversed and materials **O** and **T** now show a positive and negative load ratio effect respectively. Thus, in both materials **O** and **T** increasing test temperature inverts the effect of load ratio (from negative to positive for material **O** and vice versa for material **T**).
Material **F**, only tested at 20°C, displays a negative load ratio effect. At a load ratio of 0.5 crack arrest occurs, which is ascribed to dominant blunting.

So far the effects of load ratio have been considered in broad terms of "positive" or "negative", without considering different slopes of the curves at different load ratios. Different slopes constitute a varying effect of load ratio over the range of ΔK. For example, in the case of material **O** at 80°C, the effect of load ratio is clearly positive at low values of ΔK, while at high ΔK values the crack growth rates of R = 0.1 and R = 0.5 coincide. Apparently in this case the effect of blunting overrules creep contributions in the upper fatigue regime. Again, however, contradictory effects are also observed. In material **T** at 20°C in the low fatigue regime the curves of R = 0.1 and R = 0.5 coincide, while at high values of ΔK a clear positive effect of load ratio is observed. Hence, in this case creep contributions to da/dN apparently overrule blunting effects in the upper fatigue regime.

All things considered, the effect of load ratio on fatigue crack growth is to be considered a complicated issue. As discussed in section 2.5 the contradictory effects of creep (of fibrils) and blunting result in the overall net crack growth rate. Obviously the competitive mechanism of creep and blunting behave differently in materials **O** and **T** resulting in different effects of load ratio.

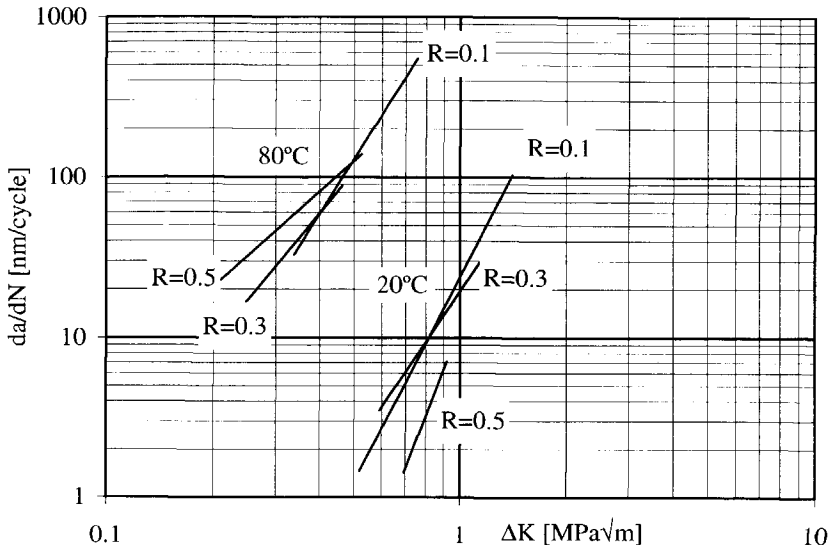

Figure 5-10 : Effect of load ratio on fatigue behaviour of material **O** (sinus waveform of 4 Hz).

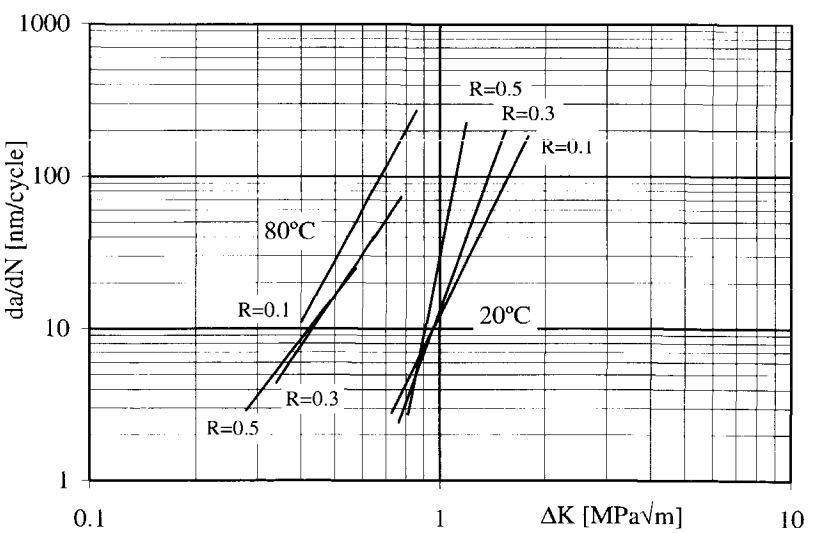

Figure 5-11 : Effect of load ratio on fatigue behaviour of material T (sinus waveform of 4 Hz).

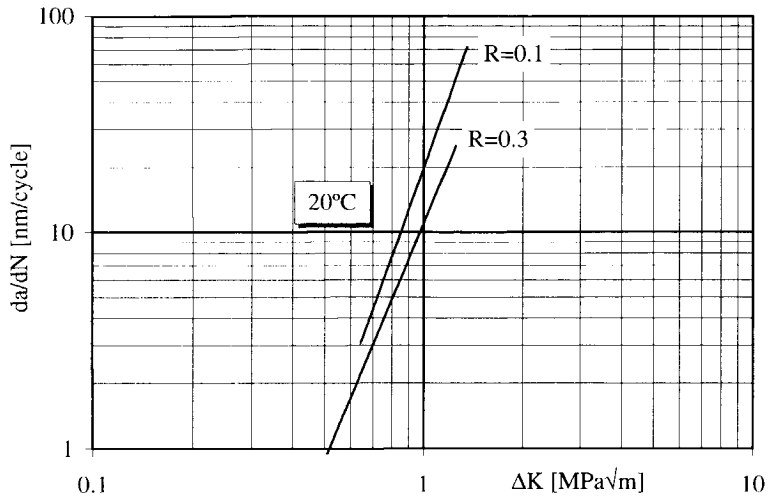

Figure 5-12 : Effect of load ratio on fatigue behaviour of material **F** (sinus waveform of 4 Hz).

Note:
Typically, in fatigue of metals, a positive load ratio effect is usually found which is ascribed to the phenomenon of crack closure. Figure 5-13 shows the crack opening during a fatigue test in polyethylene, triggered at maximum and minimum load level respectively. Although the visible crack length is reduced slightly at minimum load level, physical crack closure is thought to be unlikely, as the amount of crack opening is always substantial. Moreover, craze fibrils in compression will buckle and lack the ability to withstand compression forces. All things considered, crack closure is not thought to play a role in the effect of load ratio.

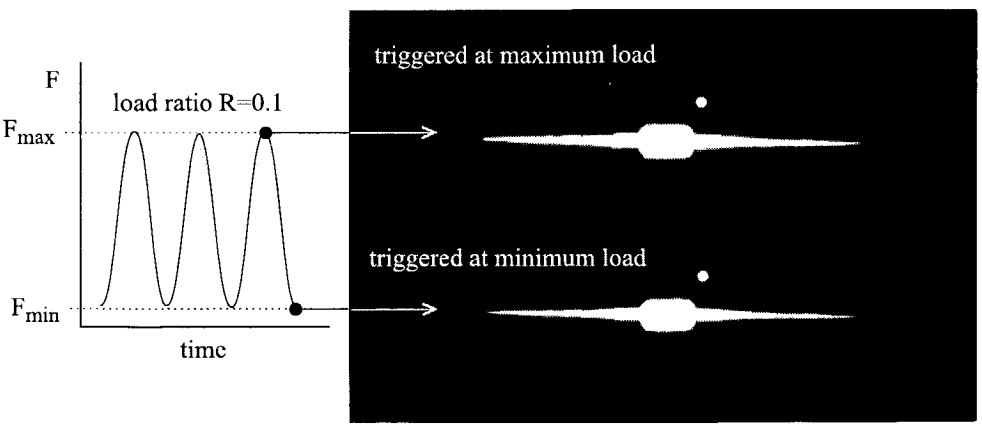

Figure 5-13 : Crack openings triggered at maximum and minimum load level respectively.

Local crack tip heating

Direct temperature measurements at the crack tip were not performed within the context of this thesis. The issue of local crack tip heating is considered theoretically.

Considering the composition of the crack tip as craze fibrils and adjacent bulk material, it can be argued that craze fibrils are loaded more intensely than adjacent bulk material. Moreover, heat transfer from individual fibrils to surrounding bulk material is limited and causes fibrils to be especially sensitive to hysteretic heating. Although hysteretic heating may occur in craze fibrils, this is difficult to confirm empirically by direct measurement of temperature at isolated fibril level.

When considering the net effect of *local* crack tip heating on crack growth, an indication can be obtained by the effect of an *ambient* temperature rise on crack growth. A clear increase in crack growth rate is found at rising ambient temperatures for materials **O** and **T**. A decrease in frequency and a corresponding decrease in hysteric energy input should therefore lead to a potentially lower temperature at crack tip level. Projecting the effect of ambient temperatures to local crack tip level, this implies a lower crack growth rate at lower frequencies. Indeed, on lowering the frequency a decade from 4 Hz to 0.4 Hz, many experiments showed a decrease in *da/dt*. However, some experiments in the frequency range of 4 Hz to 1 Hz resulted in the same value of *da/dt*, which rules out a temperature effect in this frequency range. As a conclusion local crack tip heating is thought to be at the most of minor importance at the frequencies tested.

5.3 Extrapolation load series

This section evaluates the behaviour of *da/dN* when fatigue loading is gradually changed to a constant load.

Figure 5-14 contains the results of the extrapolation load series for materials **O** and **T**. The level of K_{max} is chosen at 0.5 MPa$\sqrt{m}$ for material **O** and at 0.7 MPa$\sqrt{m}$ for material **T**. In this way the value of *da/dN* in the fatigue regime is similar for both materials and results are obtained within reasonable testing times. For material **O** the extrapolation load series is performed with specimen thicknesses of 10 mm and 19 mm (for the sake of clarity only the 10 mm thickness results are presented in figure 5-14).

In material **O** at increasing load ratios (i.e. decreasing ΔK) the crack growth rate decreases systematically from 70 nm/cycle in the fatigue region (R = 0.1) to a value of only 5-10 nm/cycle in the constant load condition (R = 1). Moreover the crack growth rate of the constant load condition is an extrapolation of the values in the fatigue region at rising load ratios. The creep crack growth rate shown, *da/dt*, is expressed with $dt = 0.25$s (i.e. the time of one 4 Hz fatigue load cycle). In this way *da/dN* and *da/dt* can be compared quantitatively in figure 5-14.

The crack growth rate da/dN is given on a logarithmic scale as a function of the load ratio on a linear scale. This representation was found to produce the clearest view on the relation between fatigue and slow crack growth, as in this way test results can be approximated by a straight line constituting an empirical relation $da/dN = C\,e^{-nR}$ in which C and n are fitting parameters. In the case of material **O** the values are $C \approx 117$ and $n \approx 3$, while *da/dN* is expressed in nm/cycle.
The crack growth response during the extrapolation load series of the 10 and 19 mm thick specimens is basically the same[1]. However, the results of the 10 mm specimens correlate somewhat better with the empirical model and the crack growth rates of the 19 mm thick specimens are about 30% higher compared with the 10 mm specimens. The effect of thickness can be ascribed to the influence of increased hydrostatic stress state in the thicker specimens, with corresponding attenuation of crack tip blunting. Once formed, the crazes themselves are not expected to be influenced much by thickness, as fibrils in the craze are in the uniaxial stress state.

Like material **O**, material **T** also displays a systematic decreasing trend in *da/dN* at increasing load ratios but the behaviour is confined to the fatigue regime (low values of load ratio). At load ratios exceeding $R = 0.5$ fatigue crack growth in CCT specimens no longer satisfies the systematic decreasing trend but is found to stop completely (crack arrest). Apparently a balance between fibril creep damage and blunting is established in which blunting becomes dominant and relieves the craze load under its threshold crack growth value. In section 2.5 the interrelation of crack growth rate and creep blunting was discussed with reference to a

[1] For the sake of clarity the results of the 19 mm specimens are not presented.

possible downward spiral of increasing blunting at decreasing crack growth rates. This mechanism is held responsible for the crack arrest observed in material **T** ($R > 0.5$, $K_{max} = 0.7$ MPa$\sqrt{m}$, extrapolation load series).

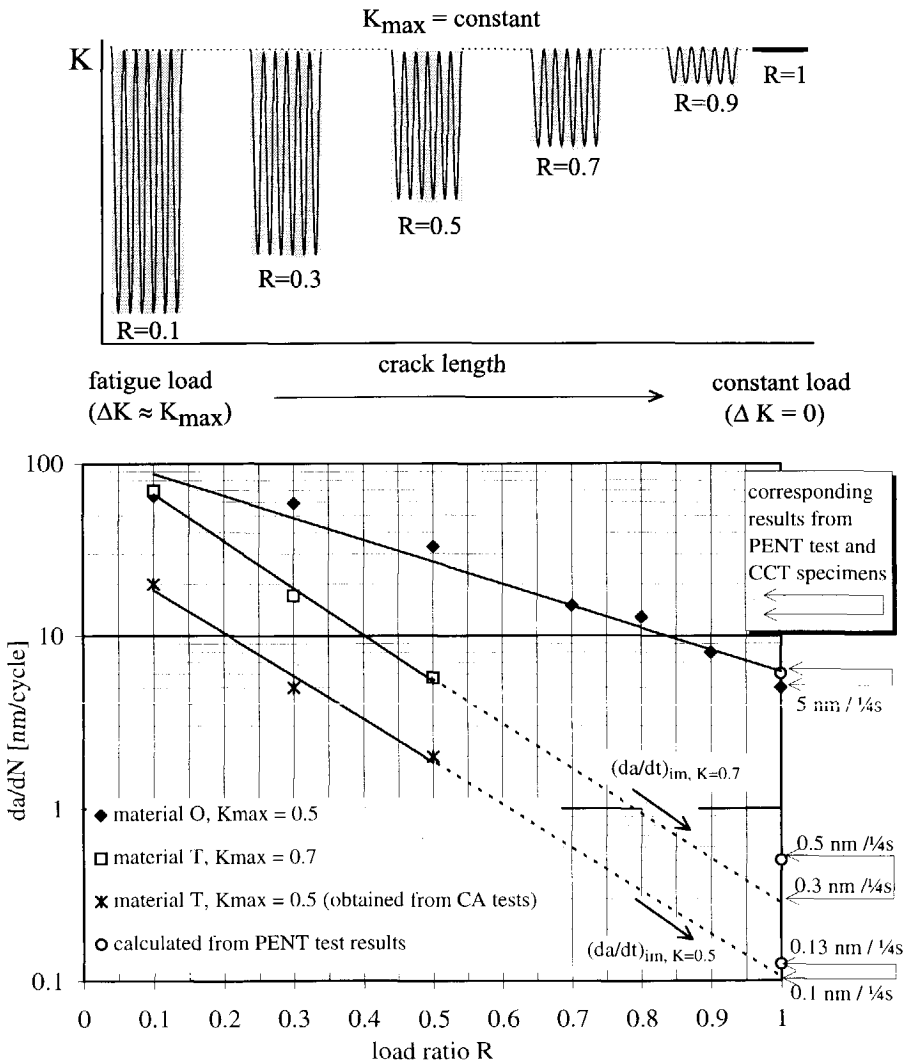

Figure 5-14 : Crack growth response during a transition from fatigue to a constant load situation (sine waveform of 4 Hz, 80°C).

However, in spite of the crack stop observed the trend of the curve at low load ratios is extrapolated to $R = 1$ to give an imaginary value of creep crack growth rate $(da/dt)_{im.}$. The extrapolation ignores the actual existence of a threshold load (in CCT specimens) and shows a theoretical prolongation of the balance in crack growth and blunting. The extrapolated and imaginary value of the creep crack growth rate, $(da/dt)_{im.}$, can be interpreted as a theoretical upper limit of the creep crack growth rate in CCT specimens.
In contrast to the situation with CCT specimens, creep crack growth is actually established during PENT tests of material **T** [1]. Moreover, in section 5.1 the stress-lifetime results were used to quantify the parameters of a creep crack growth model, producing knowledge of da/dt as function of K. The crack growth model predicts a value of $da/dt = 2$ nm/s at $K_{max} = 0.7$ MPa$\sqrt{m}$ which agrees well with the extrapolated value of $(da/dt)_{im.} = 0.3$ nm/0.25s (= 1.2 nm/s). Therefore, the results of the PENT test for material **T** give confidence in the extrapolation concept.

To limit the test duration, the extrapolation load series with material **T** were all performed at $K_{max} = 0.7$ MPa$\sqrt{m}$. A direct comparison with the extrapolation load series for material **O** ($K_{max} = 0.5$ MPa$\sqrt{m}$) is therefore not possible. However, results as obtained in the extrapolation load series can also be estimated from fatigue results shown in figure 5-11. In figure 5-11, fatigue loads of (ΔK=0.45, R=0.1), (ΔK=0.35, R=0.3) and (ΔK=0.25, R=0.5) represent K_{max} values of 0.5 MPa$\sqrt{m}$ at load ratios of 0.1, 0.3 and 0.5 respectively. The corresponding values of da/dN are shown in figure 5-14, from which an extrapolated creep crack growth rate of approximately $(da/dt)_{im.} = 0.1$nm/(0.25s) can be estimated.
Compared with material **O** this yields a factor of 50 decreased crack growth rate of material **T**. The ratio of 50 in creep crack growth between material **O** and **T** approaches the lifetime results of PENT tests.

For material **O** the extrapolation load series is repeated with a square wave fatigue load. According to the literature a square wave loading accelerates fatigue crack growth. The initial idea was to obtain increased values of da/dN in the fatigue regime (low R values), while of course the pure creep crack growth value ($R = 1$) remains unchanged. In this way, a somewhat different transition of fatigue to creep crack growth is forced during the extrapolation load series. However, for reasons which were not clear, da/dN for material **O** proved to be the same for cyclic and square-wave loading. Results given in figure 5-15 (square wave) are similar to the results of figure 5-14 (sine wave) and could be interpreted as a duplication load series.

However, another way of obtaining higher values of da/dN in the fatigue regime is by lowering the frequency. This effect was used in an extrapolation series with material **O** using a square waveform at a frequency of 1 Hz (figure 5-15). In this case, da/dN was actually increased by a factor of 4 for all load ratios tested. Moreover, the results (1 Hz, square wave)

[1] The exact reason why creep crack growth in material **T** occurs during PENT-tests but not in CCT specimens is not understood. Results obtained with material **O** indicate that difference in thickness is not likely to be responsible.

also satisfy a gradual transition from fatigue to creep crack growth, similar to the behaviour observed in figure 5-14 (4 Hz, sine wave). Of course, creep crack growth (*da/dt*, $R = 1$) is not affected by fatigue conditions. Therefore, it might be confusing to see different markers at $R=1$ for the 1 Hz and 4 Hz results. These values, however, represent the *same* creep crack growth value *da/dt* but are expressed as *(da/dt)/f* for the 1 Hz and 4 Hz test series, respectively. In this way, creep crack results can be compared quantitatively with the fatigue results.

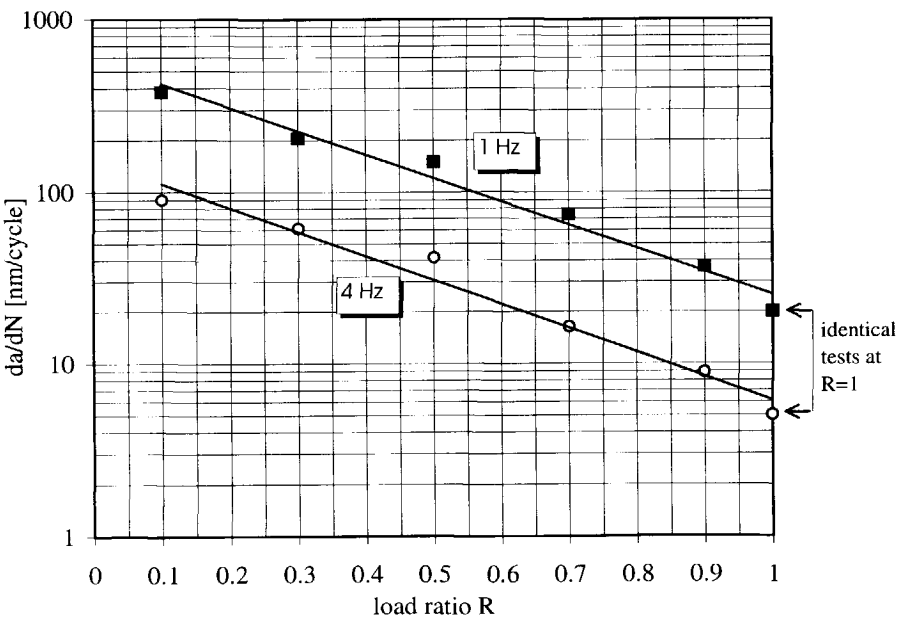

Figure 5-15 : Crack growth response of material **O** during the transition from fatigue to a constant load situation (square waveform, 80°C).

For material **T** an extrapolation load series with a square wave and frequency of 1 Hz was also conducted (figure 5-16) for a limited range of load ratios. The values of *da/dN* increase by a factor of 4-8 on decreasing the frequency from 4 Hz (sinus) to 1 Hz (square). The extrapolated and imaginary creep crack growth rates $(da/dt)_{im.}$ are 1 nm/s (4 Hz series)and 3nm/s (1 Hz series). In the ideal case both values of $(da/dt)_{im.}$ would be identical, indicating the validity of using fatigue to predict creep crack growth. Nevertheless, the predicted values of $(da/dt)_{im.}$ are of the same orders of magnitude and the difference could be ascribed to scatter in test results in combination with the limited number of data points available for the extrapolation procedure.

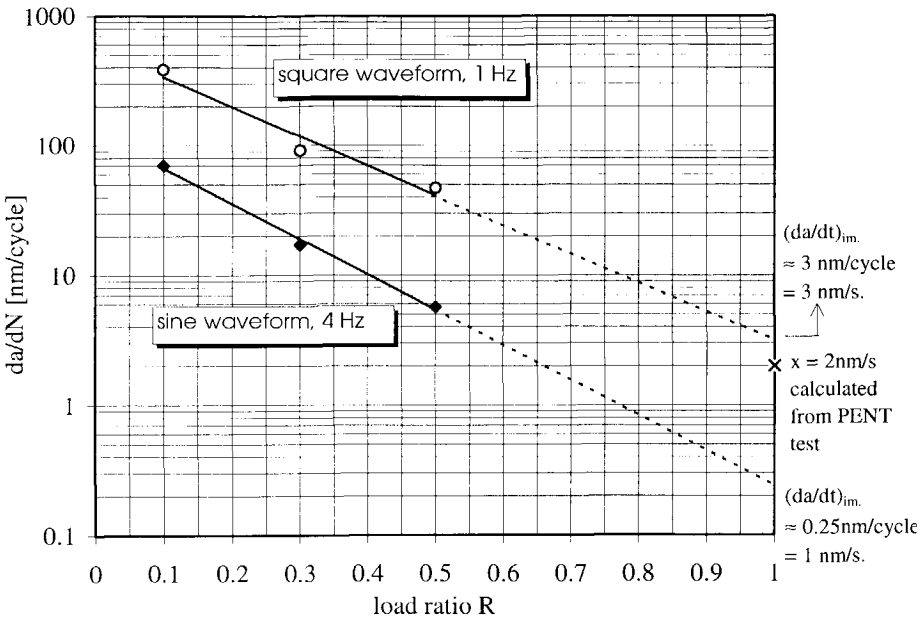

Figure 5-16 : Crack growth response of material **T** during the transition from fatigue to a constant load situation using different frequencies and waveforms (80°C).

The consistent crack growth behaviour during the extrapolation load series using different waveforms and frequencies suggests the general applicability of the principle.

5.4 Results of interrupted fatigue tests

Interrupted fatigue tests were performed in order to evaluate the role of creep-induced blunting during crack growth. In materials **O** and **T** constant ΔK tests were performed with K_{max} levels of 0.5 and 0.7 MPa$\sqrt{\text{m}}$ respectively ($R = 0.1$, 80°C, $f = 4$Hz), normally producing equivalent crack growth rates in both materials of 40-60 nm/cycle. At subsequent crack growth intervals of 4 mm the cyclic loading was stopped at a level corresponding to K_{max} of the cyclic loading. Each interruption was of a different duration, ranging from 5 minutes to 5 hours.

Figures 5-17 and 5-18 represent N-a curves of the interrupted fatigue tests in materials **O** and **T** respectively. After each interruption a plateau in the N-a curve occurs, representing a temporary crack arrest caused by creep-induced blunting. During the constant loading periods the crack length signal also increased by a discrete amount, ranging from 0.5 to 2 mm. This apparent crack growth occurs under constant load conditions but is too large to be interpreted as "creep crack growth". Most likely the increase in the crack length signal, within the constant load interruption, is caused by blunting. In addition, the image processing technique of measuring crack lengths probably responds somewhat differently to the suddenly changed (i.e. blunted) crack tip geometry. In figure 5-19 the image of the crack is given in the situation of stationary fatigue crack growth ($\Delta K = 0.45$ MPa$\sqrt{\text{m}}$). The image of the crack is also given at the moment when the load is kept at the value corresponding to K_{max} for 4800s. A pronounced crack tip opening and blunting is clearly visible, with a consequent increase in the crack length value measured.

In figure 5-20 the delay of crack growth is given as a function of the hold time periods applied, showing a consistent trend of increased delay times at increased hold-time periods. This clearly demonstrates the interaction of blunting crack growth, as introduced in section 2.5.

The retardation, after a temporary fixed load condition, is to a certain extent, comparable to the well-known overload response of fatigue in metals. The interrupted fatigue tests, discussed here for polyethylene, do not involve absolute overloading, i.e. K_{max} is not exceeded. However, the interaction of *average* load level and creep mechanisms implies that the designation overloading can in this case be applied to the "average load level".

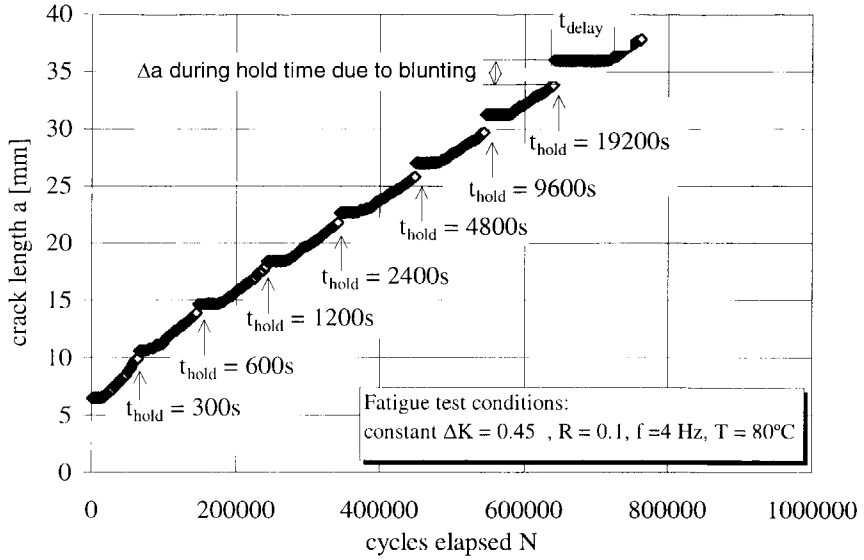

Figure 5-17 : Fatigue crack growth delay in material **O** after periods of constantly maintained load levels (at K_{max}) during a constant ΔK fatigue test.

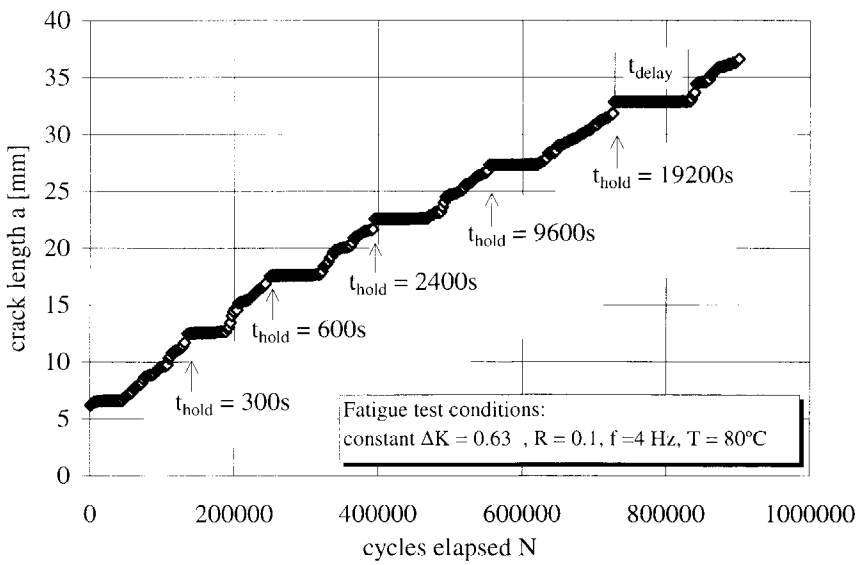

Figure 5-18 : Fatigue crack growth delay in material **T** after several periods of constantly maintained load levels (at K_{max}) during a constant ΔK fatigue test.

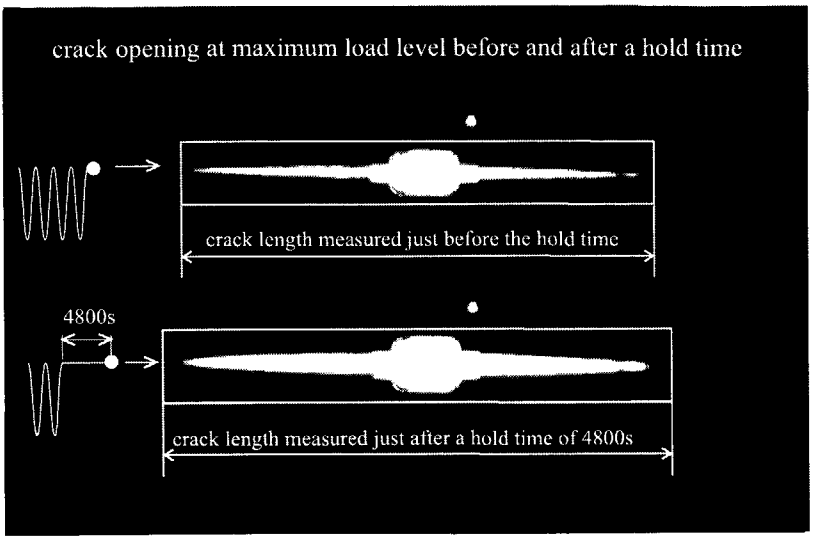

Figure 5-19 : Image of the crack during stationary fatigue crack growth and after a maintained load level corresponding to K_{max} for a time of 4800s (material **O** , fatigue test: ΔK = 0.45 MPa$\sqrt{m}$, R = 0.1, f =4 Hz, T = 80°C).

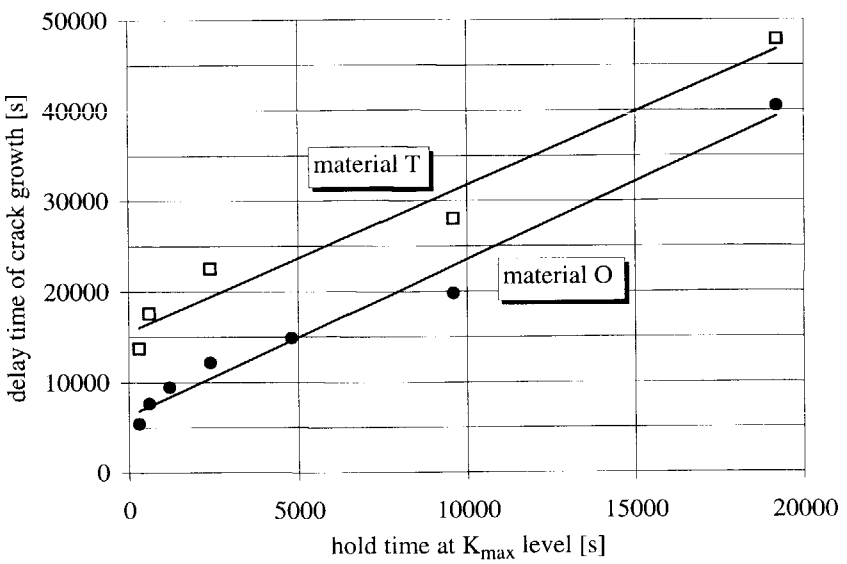

Figure 5-20 : Delay periods of crack growth as a function of hold times for materials **O** and **T** (see also figures 5-17 and 5-18).

5.5 Discussion: relation between fatigue and creep crack growth

The general fatigue behaviour in figure 5-6 (80°C, sinus 4 Hz) showed a factor of 3-5 increase in the value of *da/dN* when material **O** is compared with material **T**. The PENT tests produced a factor of 50-100 increased creep crack growth rate of material **O** compared with material **T** (figure 5-1).
Therefore general fatigue behaviour may reflect a trend in creep crack growth behaviour when materials are compared. However, accurate data for creep crack growth was not obtained.
When fatigue loading is extended to the more specific loading schedule of the extrapolation load series a better estimate of creep crack growth behaviour is obtained(figures 5-14, 5-15 and 5-16).

Paradoxical results concerning the role of creep damage during fatigue (material O)

In section 5.2 the effect of load ratio is discussed with respect to load-level induced creep contributions. Creep contributions are recognised as having contradictory aspects, namely creep-induced fibril damage (promoting crack growth) and blunting (attenuation of crack growth). In section 5.2 frequency effects are ascribed to pronounced time-induced creep damage per load cycle at the extended periodic times of lower frequencies.

In material **O** (figure 5-7) a considerable frequency effect is observed at 80°C during fatigue at test frequencies of 0.4 Hz and 4 Hz ($FSF = 6$). The effect of frequency is also found in the extrapolation load series results of figure 5-15, in which at 4 Hz and 1 Hz an identical value of *da/dt* is measured. An unchanged value of *da/dt* at different frequencies is generally considered to be a very strong indication that crack growth is dominated by creep mechanisms (independent of damage per load cycle).
In the extrapolation load series a pronounced creep contribution could be assumed at the higher load ratios, due to the corresponding high average load levels. From this point of view the ultimate creep contribution is to be expected in the constant load situation at $R = 1$. The creep crack growth rate, *da/dt*, in this situation ($R = 1$) is found to be only 5% of the crack growth rate in fatigue, *da/dN* at $R = 0.1$ (figures 5-14 and 5-15). Seen in this light, creep contributions cannot be substantial during fatigue.

Thus, frequency effects would appear to suggest that a major role is played by creep mechanisms during fatigue. However, extrapolation load series show the opposite effect, namely a minor role of creep during fatigue.

The conclusion must be that creep mechanisms during fatigue cannot be accounted for by a simple linear superposition of creep crack growth behaviour on the fatigue component. Creep damage during fatigue contributes to crack growth in interaction with the fatigue mechanism.

The answer to the paradox of creep contributions during the extrapolation load series can be found in the effect of cyclic damage on the degree of blunting. In section 6.1, cyclic loading of drawn polyethylene will be observed to cause failure at decreased levels of deformation. Therefore cyclic damage embrittles the fibrils of the craze, resulting in a diminished amount of craze-inherent blunting. In fatigue the crack will be sharp compared with the situation

under constant load conditions. In effect, the sharpness of the crack in fatigue can be regarded as the fundamental cause of high crack growth rates under fatigue conditions.
"Obstruction of blunting induced by fatigue" can be considered as the governing mechanism of fatigue crack growth.

Naturally, in a specific fatigue condition, mechanisms of creep-induced blunting also remain significant, as is clear from the frequency effect.

6. Micromechanisms at crack tip level

The test results discussed in this section are evaluated specifically in relation to crack growth behaviour. The main interest is to assess if crack growth behaviour can be related to more straightforward mechanical properties.

6.1 Tensile and creep tests of bulk material and material in the stretched condition

Tensile test results

In figures 6-1 and 6-2 the stress-strain curves of materials **O**, **T** and **F** are shown, using standard test specimens at test temperatures of 20°C and 80°C respectively. The tests do not extend to fracture of the specimens, due to the occurrence of large strains in combination with the practical limitation of extension range. The test results demonstrate similar mechanical behaviour for all materials with yield strengths of 21-25 MPa at 20°C and 6-7 MPa at 80°C.
In figures 6-3 and 6-4 the stress-strain curves of materials **O**, **T** and **F** are shown, using fibril test specimens at test temperatures[1] of 20°C and 80°C respectively. The yield strength values now vary from 22 to 28 MPa at 20°C and from 8 to 14 MPa at 80°C. It should be noted that the fibril specimen geometry is not standardised and therefore the "fibril" yield strengths obtained are not official. However, with fibril specimens, a complete test until fracture is obtained. After yielding and the subsequent drop in stress level the material is stretched, with corresponding strain hardening. The strain hardening region begins at a strain of about 100% and extends to fracture strains of 300% to 800%, depending on material and test temperature. The final stress at fracture can be as high as or even exceed the yield stress. It should be noted that stress and strain levels (i.e. σ and ε) mentioned here are "engineering" values. It is recognised that true strain is given by $ln(1+\varepsilon)$, while true stress is given by $\sigma(1+\varepsilon)$ if a constant volume is assumed during plastic deformation. To give a general idea, a fracture stress of $\sigma = 15$ MPa at a plastic strain of $\varepsilon = 800\%$ corresponds to a true stress level of 135 MPa at a true strain in the order of 200%. The use of true stresses could be useful in order to harmonise stress levels obtained at distinct strains. However, figures 6-3 and 6-4 show that most strains observed are of the same order of magnitude. Therefore, simply using of engineering values is maintained.

At the moment there is no general rule by which crack growth behaviour and tensile properties can be related in a consistent and quantitative manner. However, there is a qualitative trend of improved crack growth resistance in more ductile materials. This general trend is, not however, reflected in figure 6-4, where all materials display the same ductility (represented by strain at fracture) whereas their crack growth behaviour is very distinct. Therefore, a tensile test definitely cannot discriminate between the crack growth behaviour of materials **O**, **T** and **F**.

[1] At 20°C, the tensile tests with fibril specimens are performed at the very low speed of 0.1mm/min. At higher speeds fibril specimens were found to fracture too early at the end of the specimens (near the gripped area).

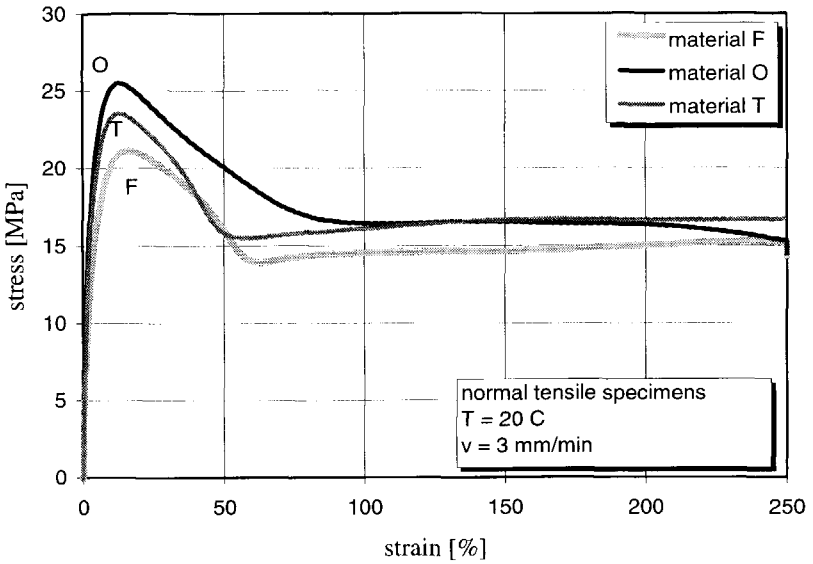

Figure 6-1: Stress-strain curves of materials **O**, **T** and **F**, using normal tensile specimens at 20°C.

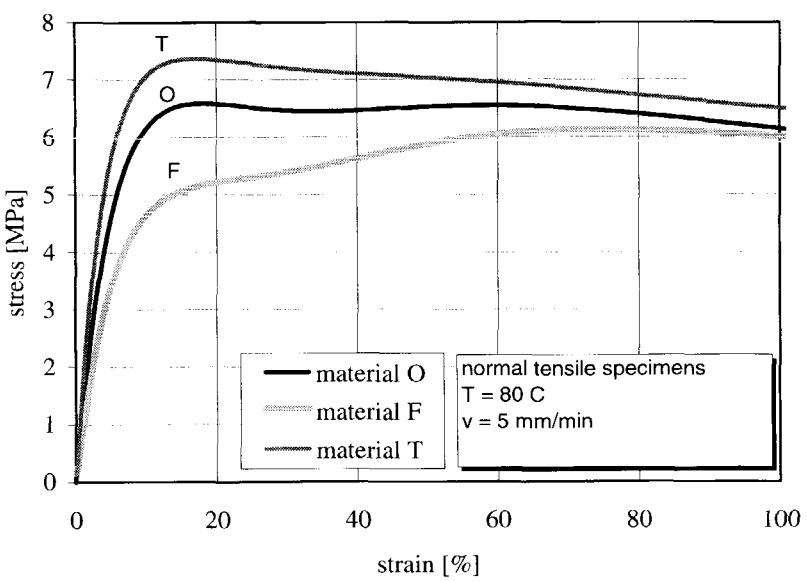

Figure 6-2: Stress-strain curves of materials **O**, **T** and **F**, using normal tensile specimens at 80°C.

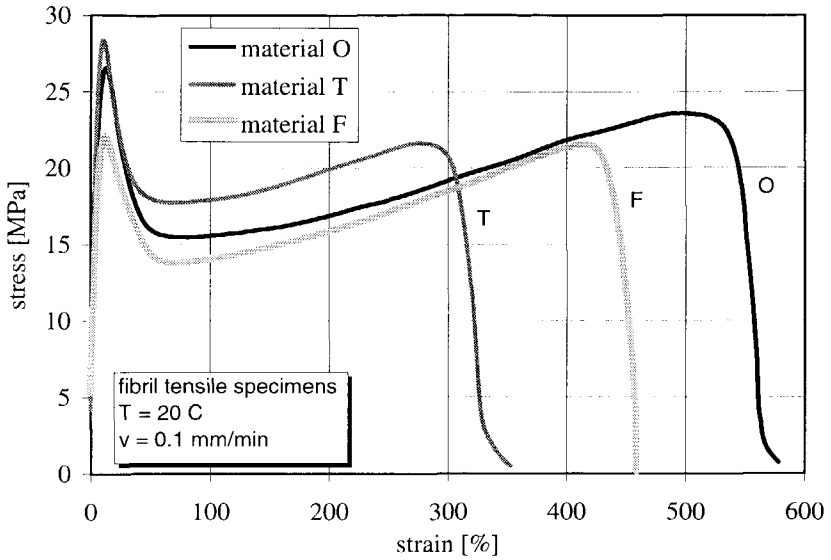

Figure 6-3: Stress-strain curves of materials **O**, **T** and **F**, using fibril tensile specimens at 20°C.

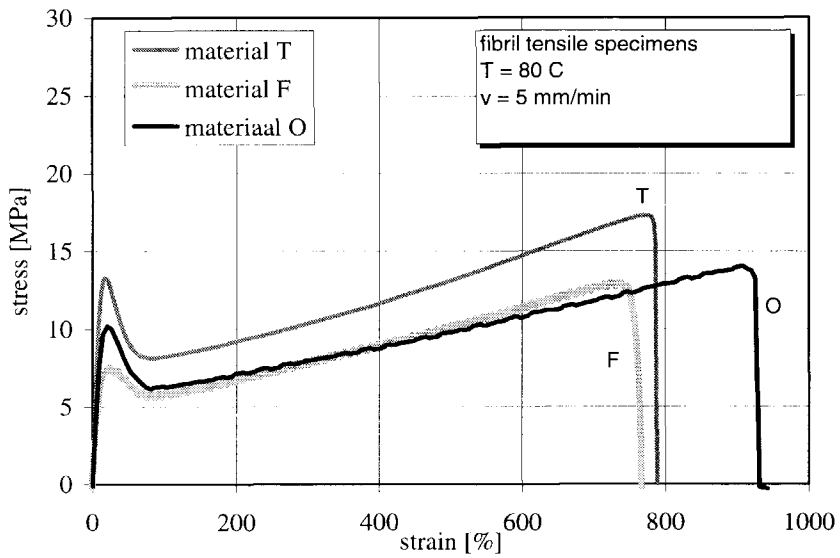

Figure 6-4: Stress-strain curves of materials **O**, **T** and **F**, using fibril tensile specimens at 80°C.

Creep results of bulk material using standard specimens

Figures 6-5 and 6-6 give creep results for materials **O**, **T** and **F**, using standard specimens, at stress levels of 2.5 MPa and 5 MPa respectively. A stress level of 5 MPa corresponds to 30-80% of the yield stress of bulk material (depending on the material). This relatively high creep stress level is chosen to reflect the creep characteristics of highly loaded bulk material at the crack tip area. The duration of the creep tests is long in order to cover the periods associated with long-term creep crack growth behaviour.
The creep results demonstrate non-linear creep behaviour. The final levels of creep deformations are found to increase by factors of 7, 4 and 1.6 for materials **O**, **T** and **F** respectively when the stress level is doubled from 2.5 MPa to 5 MPa.

The creep results should reflect the degree of blunting of bulk material around the crack tip. A high creep deformation and correspondingly high degree of blunting constitute a crack growth inhibitor. From crack tip observations, which will be discussed later in section 6.2.2, most bulk blunting is actually found to appear in material **F**. Comparing materials **F** and **T**, pronounced bulk blunting of material **F** is in accordance with creep results of figures 6-5 and 6-6.
Material **O** displays most creep deformation at the 5 MPa stress level. In contrast, however, bulk blunting of material **O** at real crack tips is found to be limited (as will be discussed in section 6.2.2). There are two arguments which may be given in explanation :

1) pronounced non-linear creep in material **O**:
Although the creep deformations in material **O** are pronounced at the high stress level, this is not the case at the low stress level. At the low stress level, creep in material **O** is situated in between the behaviour of materials **T** and **F**. Projected to the situation at a crack tip, this means that *pronounced* blunting in material **O** only extends to highly loaded bulk material in a close area around the craze.

2) Viscous behaviour of creep deformation in material **O** (only at σ=5 MPa).
Materials **T** and **F** show typical creep behaviour in which creep deformations are predominantly produced shortly after load application, with subsequent stabilisation of creep level at prolonged loading times. This type of creep response is characterised by the parallel damper-spring model (Voigt element), as was discussed in section 2.1.
Material **O** shows a more viscous creep response in which creep deformation continues to increase throughout the test. The viscous behaviour can be visualised by the serial damper spring model (Maxwell element), as discussed in section 2.1. Although the creep deformation in material **O** is pronounced at prolonged testing times, this is *not* yet the case within a confined load period (several hours). It is in the time domain of hours that creep crack growth in material **O** is manifested and consequently the viscous creep of material **O** has no significance in this respect.

The creep results of bulk material of materials **O**, **T** and **F** show that there is no simple relationship with crack growth behaviour. The ranking of materials **O**, **T** and **F** from poor to excellent creep crack growth resistance (figure 5-1) cannot be ascribed exclusively to creep behaviour of bulk material (figures 6-5 and 6-6).

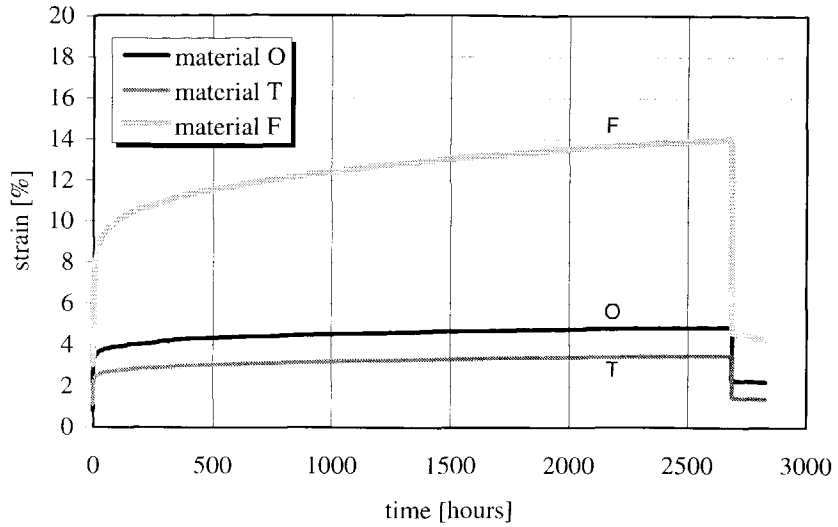

Figure 6-5: Creep response of materials **O**, **T** and **F**
(bulk material using standard specimens, 2.5 MPa, 80°C).

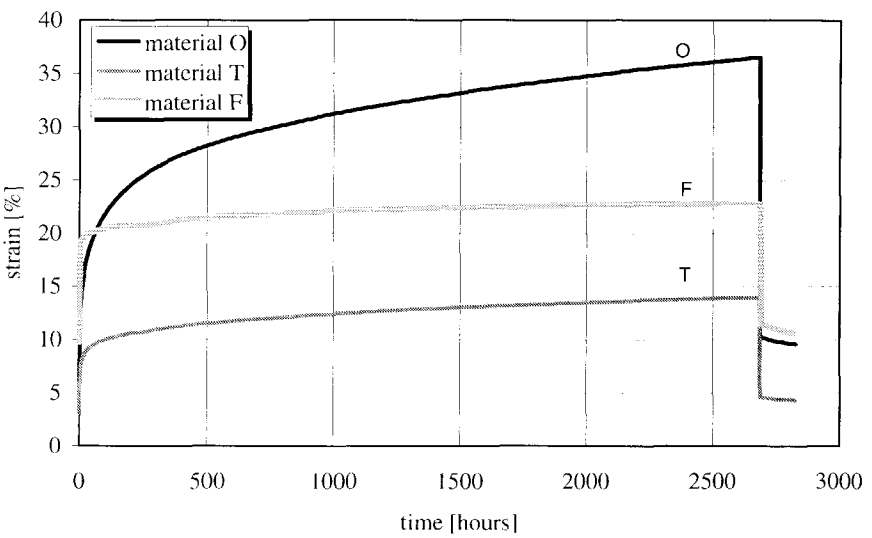

Figure 6-6: Creep response of materials **O**, **T** and **F**
(bulk material using standard specimens, 5 MPa, 80°C).

Creep failure results of stretched material using fibril specimens

In figure 6-7 the creep response of materials **O**, **T** and **F** in the *stretched* condition is given for a test temperature of 80°C and a creep load of 200 N (≈ 10 MPa). Clearly all materials finally fail, whereas material **O** shows a distinctively short failure time compared with materials **T** and **F**. The short creep failure time of material **O** confirms pronounced viscous creep behaviour this material, as was already observed in the creep response of *bulk* material (i.e. standard specimens). The short creep failure time of material **O** implies a short lifetime of fibrils in real crazes, with consequent promotion of creep crack growth. Indeed, material **O** is more sensitive to creep crack growth than materials **T** and **F**. However, creep failure times as tested with fibril specimens do not rank materials by the same amount as is observed in actual creep crack growth tests (i.e. PENT tests). Under creep crack growth conditions, the lifetime of material **O** is found to be only 1-2% of the values observed in material **T** (figure 5-1, PENT test results). Using fibril specimens, the creep failure time of material **O** covers about 30% of the value found for material **T**. Therefore, creep results of stretched material reflect creep crack growth behaviour in a *qualitative* manner only.

A creep failure test simulates failure of an isolated fibril and does not account for interactions with crack tip geometry (i.e. aspects of blunting). The most direct observation of crack tip blunting is discussed in detail in section 6.2.2. It is found that materials **O** and **T** display similar amounts of blunting, while material **F** shows a distinctly excessive amount of bulk blunting. Clearly, in the case of material **F,** the huge amount of bulk blunting is responsible for its excellent creep crack growth resistance. However, when comparing materials **O** and **T**, which have the same degree of blunting, interaction of blunting cannot account for the very distinct creep crack growth behaviour of the two materials.

In conclusion, the creep failure times of stretched material can be considered a qualitative indication of creep crack growth behaviour. An increasing creep failure time in addition to the possibility of bulk blunting results in increasing crack growth resistance.

Fatigue failure results of stretched material using fibril specimens

In figure 6-8 the creep response of material **O** is given, using fibril specimens tested under fatigue conditions (sinus, 0.3 Hz, 80°C) at several load ratios. The test procedure is discussed in section 3.4. During all tests the value of $F_{max} = 200$ N is maintained. The load ratio $R = 1$ represents the creep failure test as discussed earlier (figure 3-3).
The failure times, as shown in figure 6-8 appear *not* to relate systematically to the load ratios applied. The fatigue failure times ($R = 0.1$ to 0.7) all appear to be of the same order, about two hours, while the pure creep failure time is 10 hours. The results do not simply reflect differences in crack growth rates between fatigue crack growth and creep crack growth, as found in the extrapolation load series. Again, however, it can be argued that testing isolated fibril materials does not account for interactions with crack tip geometry.

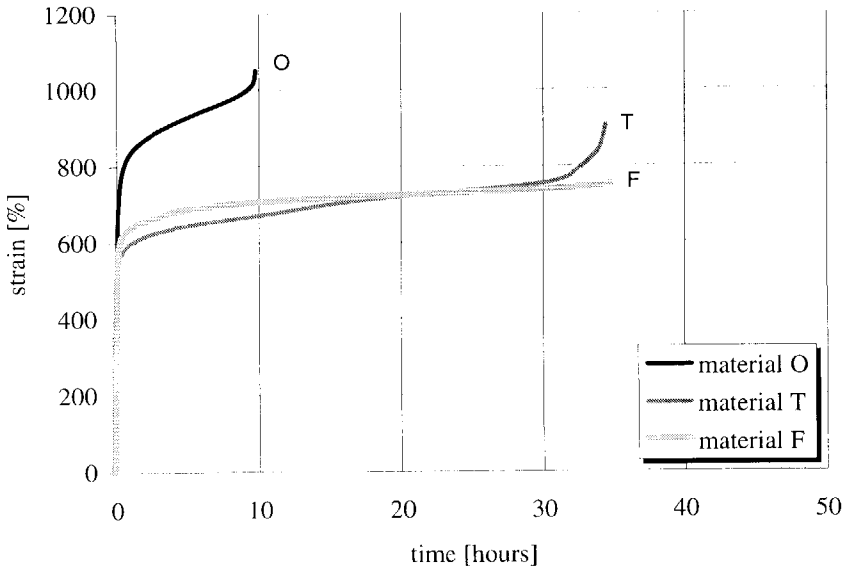

Figure 6-7: Creep response of drawn materials **O**, **T** and **F** (using fibril specimens, F = 200N, 80°C).

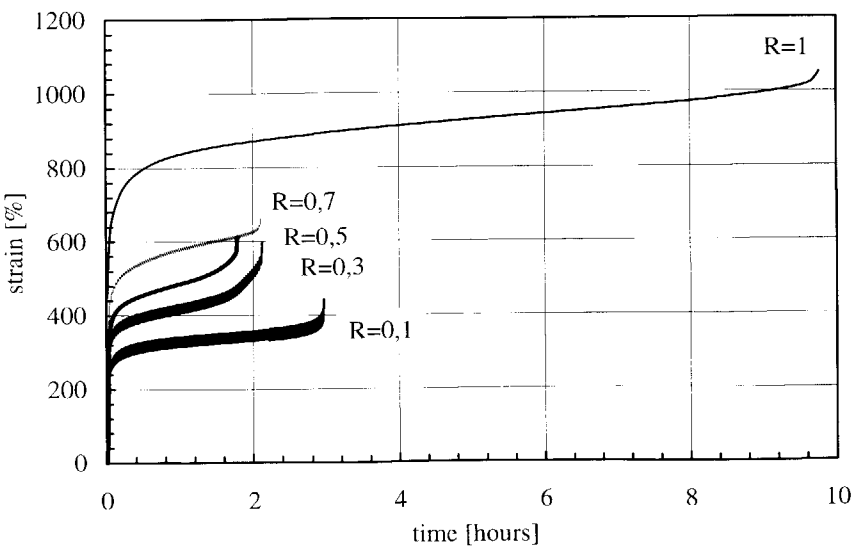

Figure 6-8 : Creep response of material **O** under cyclic loading conditions (using fibril specimens, F_{max} = 200N, various load ratios, 80°C.).

In this respect it is interesting to note that the strain at failure in figure 6-8 consistently drops at decreasing load ratios, along with decreasing load levels. Therefore fatigue loading causes cycle-induced damage, manifested as embrittlement (i.e. failure at lower strains). Applied to real crazes, lower strains of fibrils constitute less "craze-inherent blunting" and consequently more intense loading of fibrils. As a result, more brittle failure of fibrils constitutes an increase in crack growth rate.

In section 2.5, the effect of blunting on crack tip stress levels was discussed by comparison of two blunted crack tips (equation {4}). From the simulated fibril behaviour of figure 6-8 it is found that the fibril strain at failure, at a load ratio of $R = 1$ (i.e. constant load condition), is about a factor of 2.5 times the value of the fatigue condition at $R = 0.1$. In terms of blunting in real crazes this would relate to an increased stress intensity (according to equation {4}) by a factor of $\sqrt{2.5}$. Consequently the crack growth rate is increased by a factor of $(\sqrt{2.5})^{3.5} = 5$ according to the Paris fatigue law for material **O** (equation {2}). In reality, fatigue conditions ($R = 0.1$) were found to enhance crack growth by a factor of 15 compared with pure creep crack growth ($R = 1$, material **O**). Therefore the embrittlement of simulated fibrils and corresponding crack sharpness do not entirely explain the fatigue mechanism. In the next section, however, the appearance of fracture surfaces indicates a more pronounced difference in fibril lengths compared with results obtained from the simulated fibril tests. Moreover, in section 6.2.2, crack tip geometries produced under fatigue and constant load conditions are compared with the observation that under fatigue the *total* amount of blunting ($CTOD_{total}$) is reduced by a factor of 5. According to equation {4} the stress intensity is consequently increased by a factor of $\sqrt{5}$ and with the Paris fatigue model for material **O** this results in an increase in crack growth rate by the amount of $(\sqrt{5})^{3.5} \approx 17$. Therefore, the blunting as measured in real crazes justifies the ratio of crack growth rates under fatigue and constant load conditions, as observed in the extrapolation load series.

In conclusion, embrittlement of stretched material during fatigue can be considered an important cause of increased crack growth rate under fatigue conditions.

6.2 SEM observations of fracture surface and crack tip geometry

The appearance of fracture surfaces and side views of crazes (crack tip geometry) will now be discussed.

6.2.1 Fracture surfaces

Fracture surfaces of the extrapolation load series (CCT specimens)

Figures 6-9 and 6-10 show the fracture surfaces of specimens as tested in the extrapolation load series (figure 5-14) for materials **O** and **T** respectively. The fracture surfaces therefore mark the transition from fatigue to creep crack growth. For material **T** only load ratios up to $R = 0.5$ are available.

At rising load ratios the fracture surfaces exhibit a rougher appearance with a larger fibril structure. The increase in fibril dimensions as observed on the fracture surface is in agreement with results obtained in the simulated fibril tests (see previous section), in which strains also increased at rising load ratios. Moreover the change in fibril dimensions at the fracture surfaces seems to be more pronounced compared with results found in the simulated fibril tests. This supports the previously discussed relationship between fibril embrittlement, blunting and crack growth rate, based on the simulated fibril tests (section 6.1).

Fracture surfaces of PENT tests

Figure 6-11 gives an overview of the fracture surface of a PENT test specimen (material **O**, 80°C, $\sigma = 2.4$ MPa). During crack growth the stress intensity level has increased producing larger craze dimensions. As a result, the fracture surface has a rougher appearance at higher crack lengths.

Figures 6-12a), b), c) are obtained by tilting the specimens in the microscope, giving a three-dimensional impression of the fracture surfaces (material **O**, stress levels $\sigma = 2.7$, 3.6 and 4.2 MPa respectively). A clear view of discontinuous crack growth bands can be seen in the specimen of the low stress level ($\sigma = 2.7$ MPa). The transition from brittle to ductile failure is visible on the fracture surface as a change from a fibrillated structure to a smooth surface.

Figures 6-13a) and b) show the fracture surfaces of material **T**, tested at stress levels of 2.7 and 4.2 MPa respectively, with an appearance similar to that observed in material **O**.

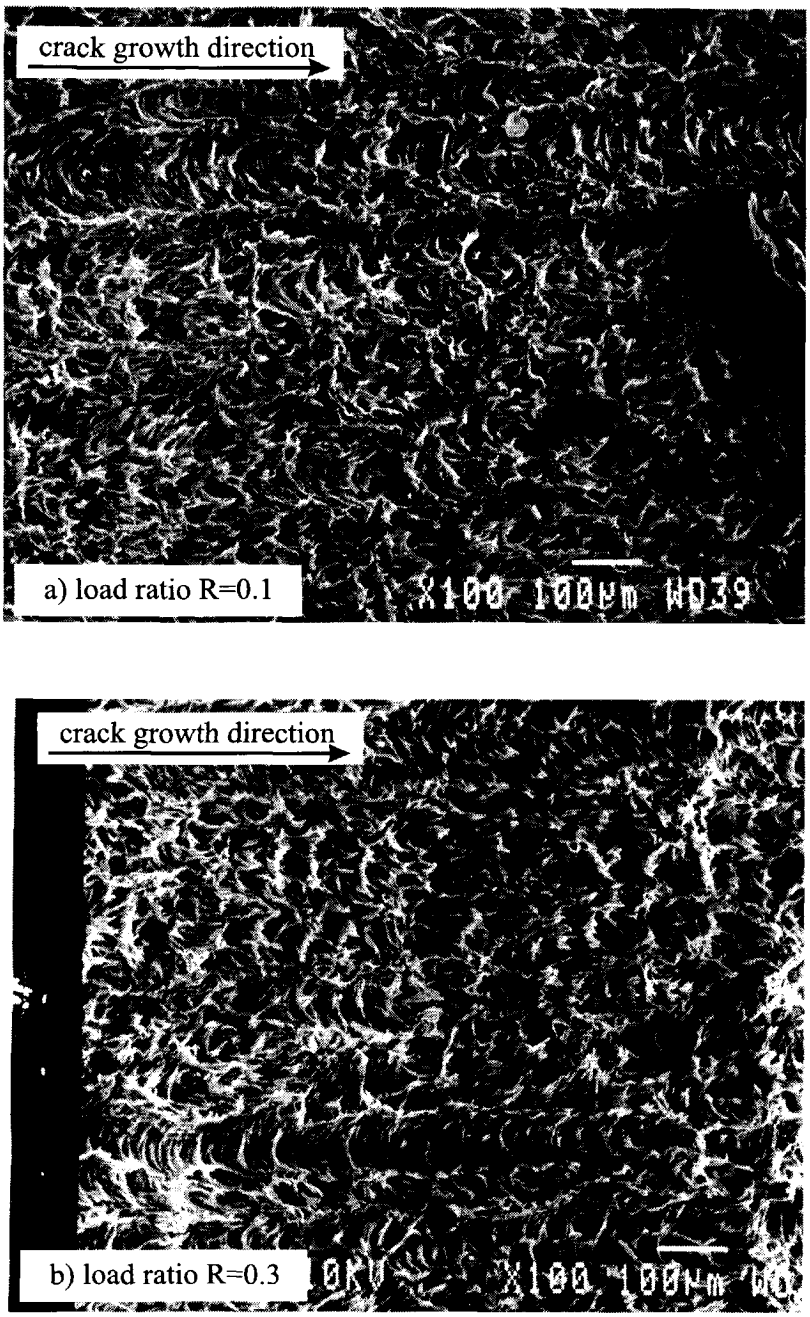

Figure 6-9: Fracture surfaces of extrapolation load series specimens of material **O**.

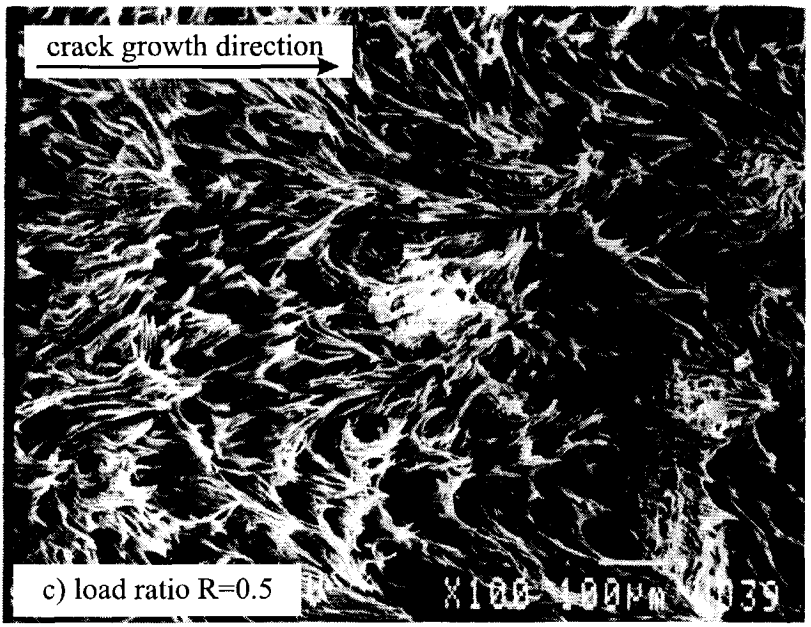

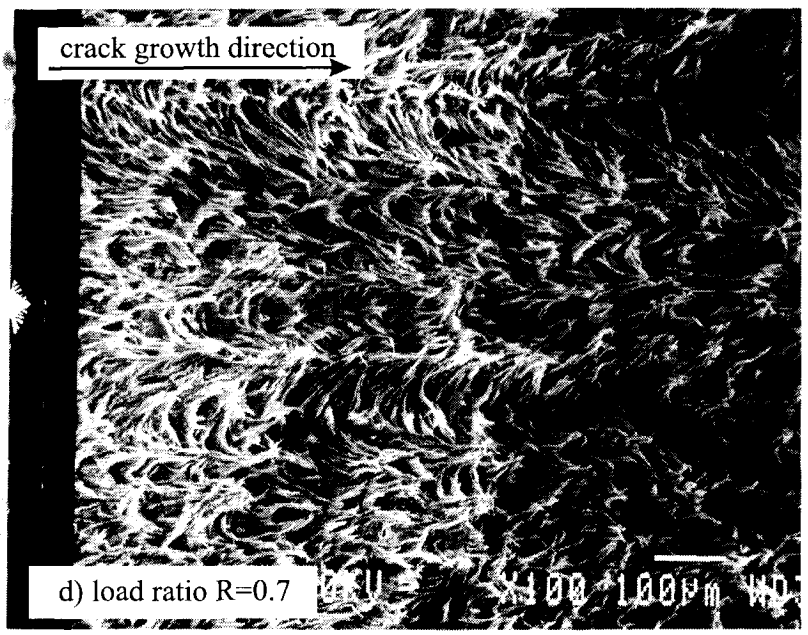

Figure 6-9: Fracture surfaces of extrapolation load series specimens of material **O** (continued).

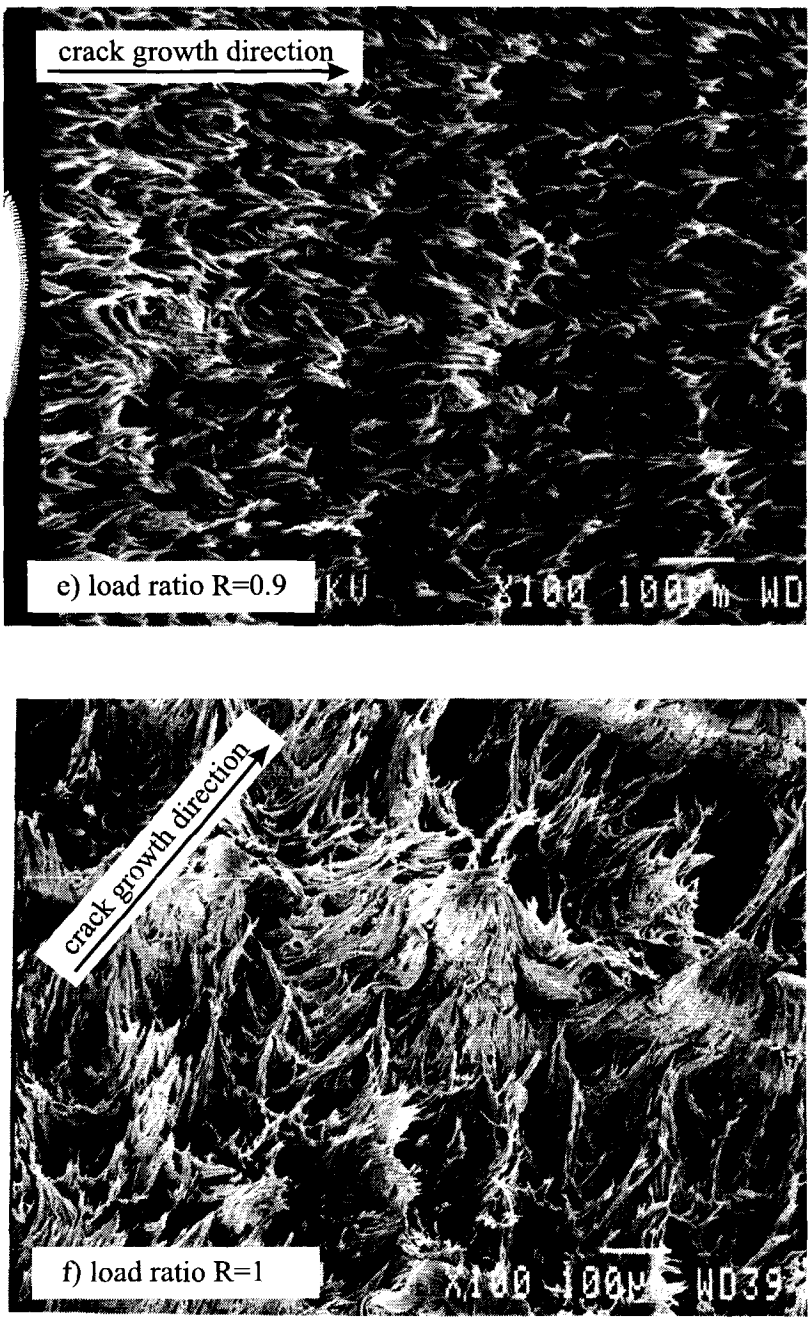

Figure 6-9: Fracture surfaces of extrapolation load series specimens of material **O** (continued).

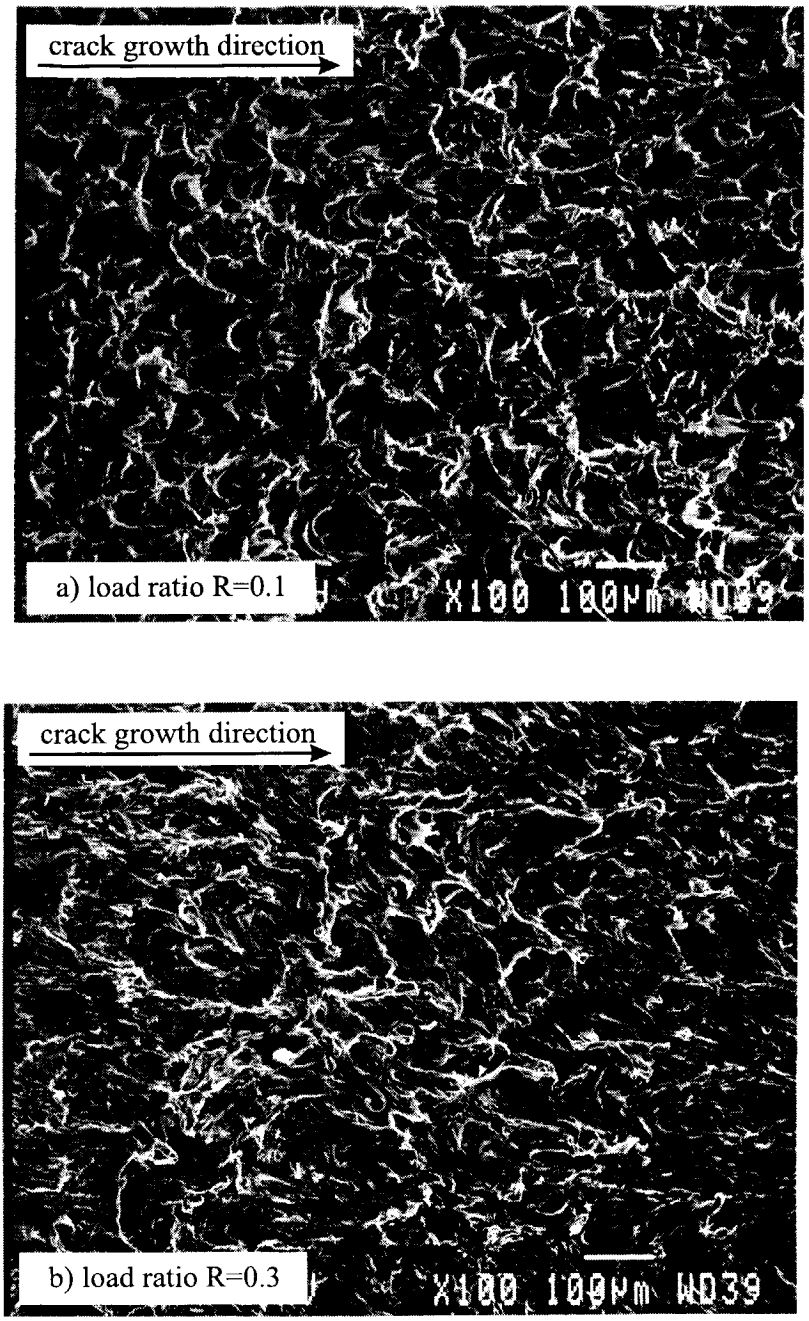

Figure 6-10: Fracture surfaces of extrapolation load series specimens of material **T**.

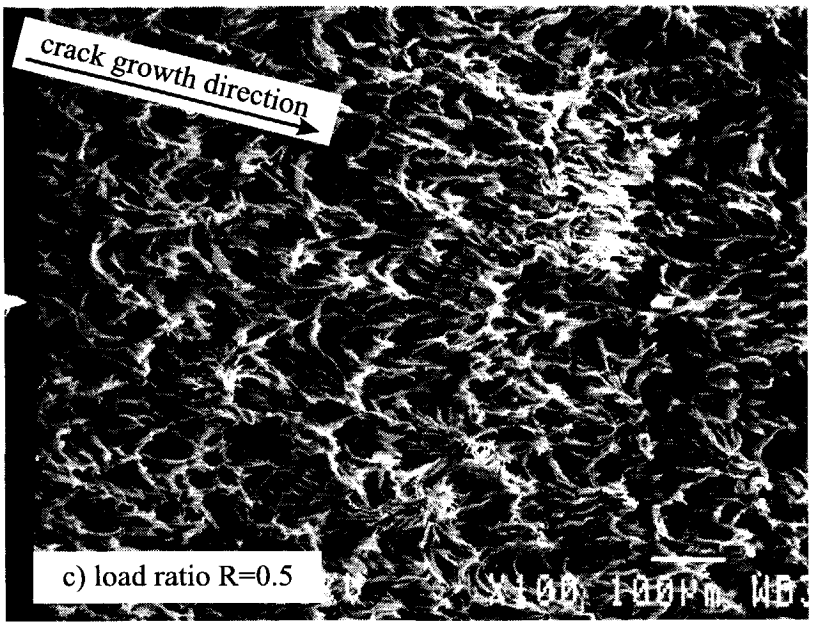

Figure 6-10: Fracture surfaces of extrapolation load series specimens of material **T** (continued).

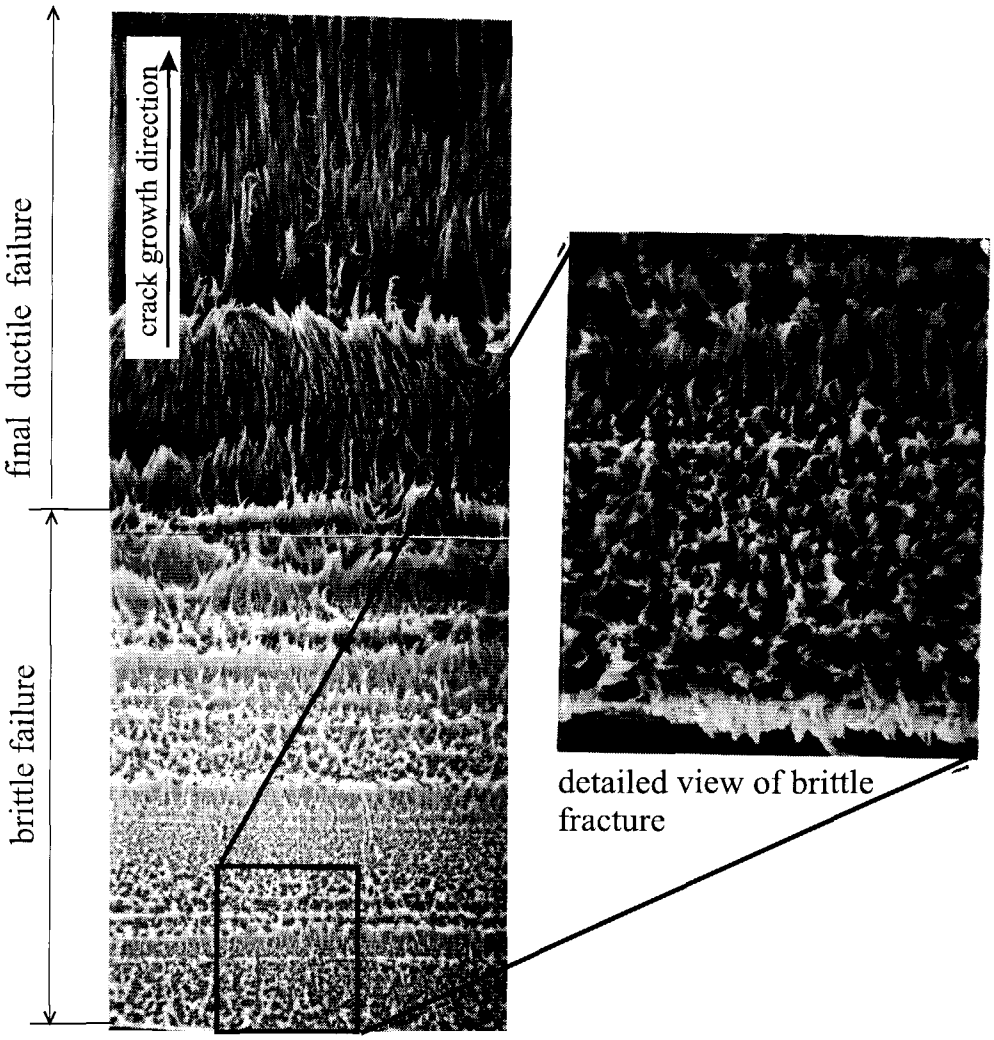

Figure 6-11: Overview of the fracture surface of a PENT test specimen (material **O**, σ = 2.4 MPa, 80°C).

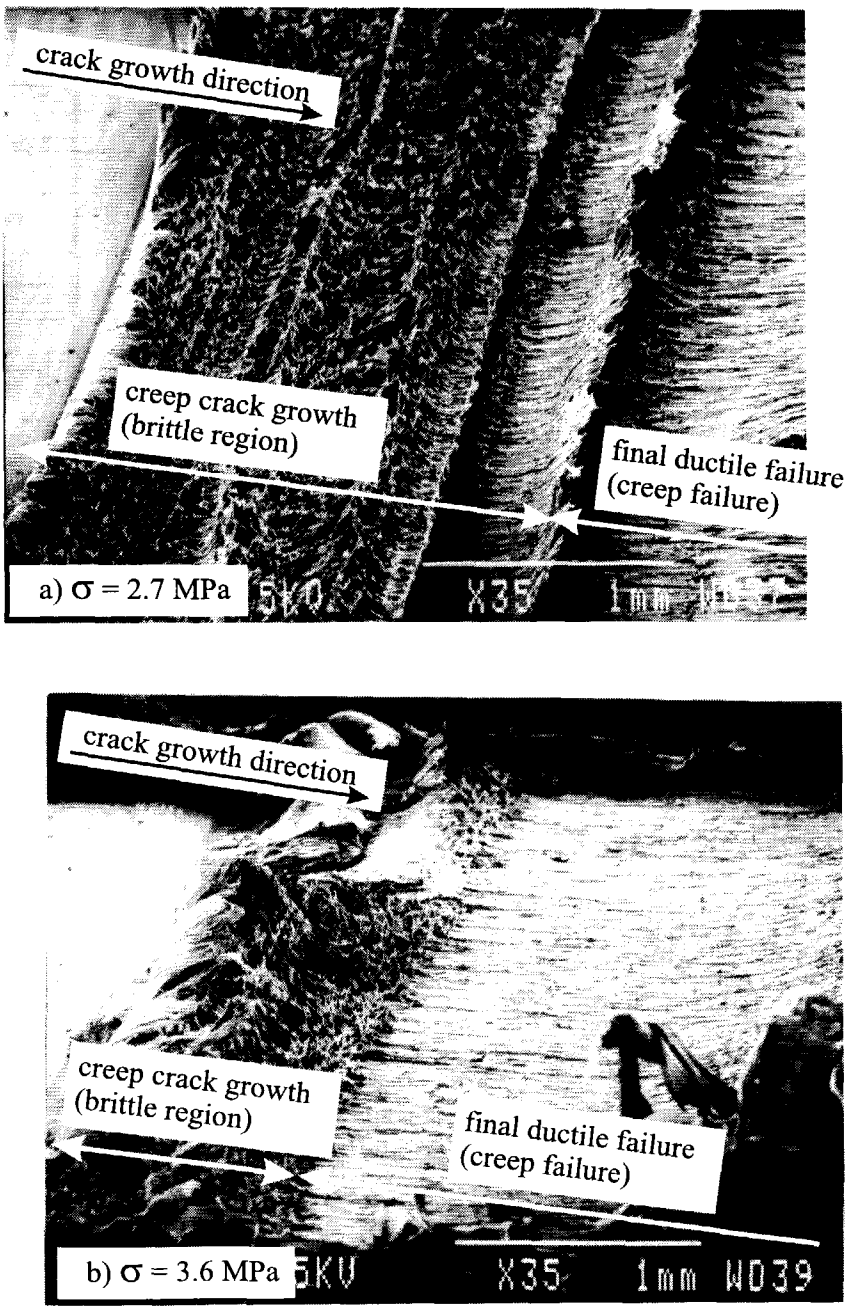

Figure 6-12: Tilted views of the fracture surface of PENT test specimens (material **O**, stress levels σ = 2.7 and 3.6 MPa respectively, 80 °C).

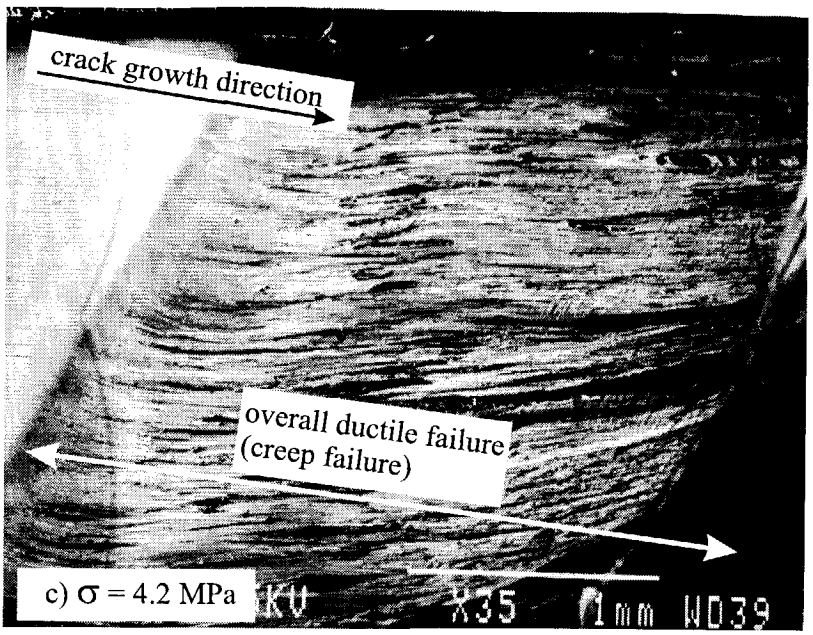

Figure 6-12: Tilted views of the fracture surface of PENT test specimens (continued) (material **O**, stress level $\sigma = 4.2$ MPa, 80°C).

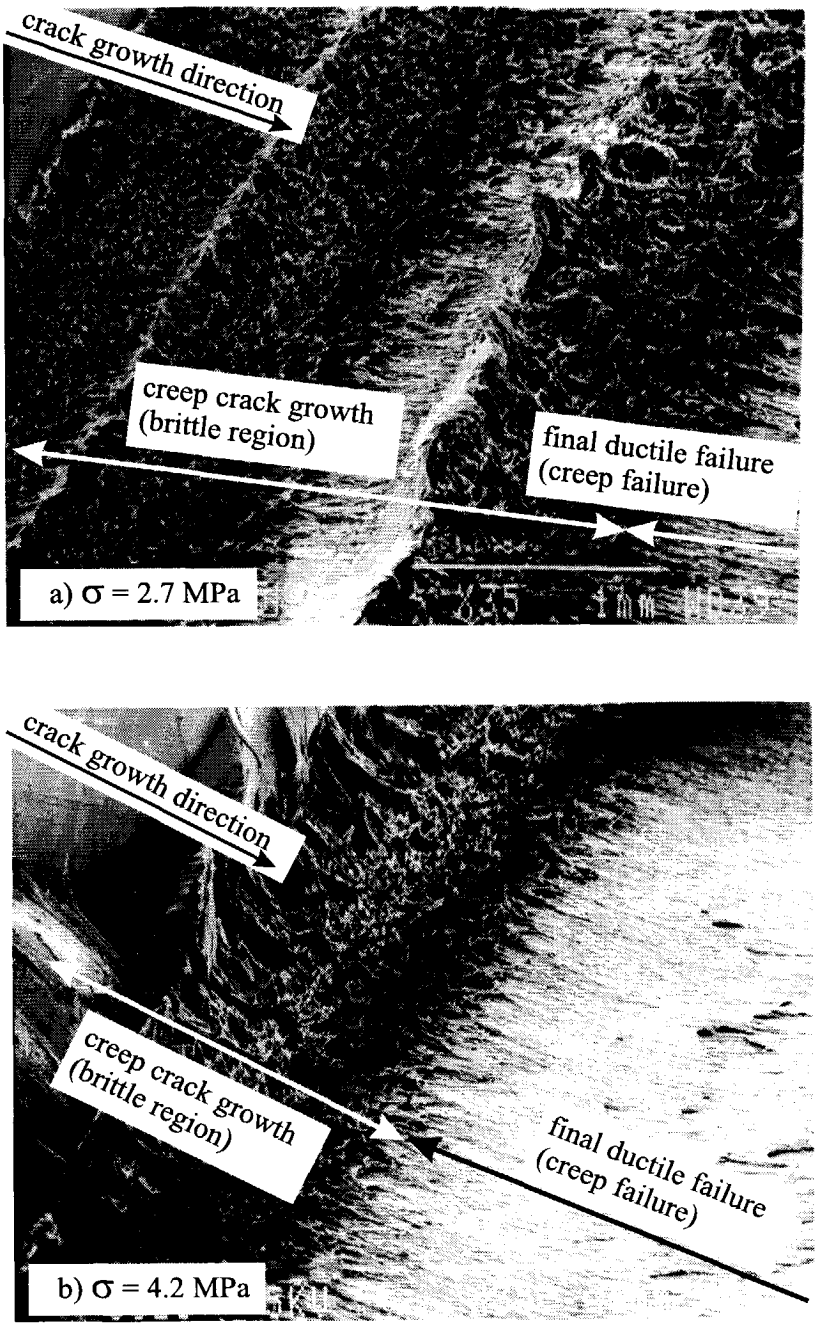

Figure 6-13: Tilted views of the fracture surface of PENT test specimens (material **T**, stress levels σ = 2.7 and 4.2 MPa respectively, 80°C).

6.2.2 Crack tip geometry

Blunting and craze length properties under constant load conditions (80°C)

Figures 6-14a, 6-15a and 6-16a give crack tip geometries at a *relatively* early stage of craze development for materials **O**, **T** and **F** respectively (PENT test, $\sigma = 2.4$ MPa). The crack tip geometries of materials **O** and **T** are very similar, both having a craze length of $L_c \approx 600\ \mu m$ and a total crack tip opening displacement ($CTOD_{total}$) of 150-200 μm. Therefore, the distinctive crack growth behaviour of materials **O** and **T** is not related to differences in crack tip geometry. In section 6.1 the short creep failure times of fibrillated material **O** is mentioned as a cause of the relatively high crack growth rate of material **O**.

Material **F** displays a very different crack tip geometry when compared with materials **O** and **T**. The large amount of bulk blunting ($CTOD_{bulk}$) is particularly obvious and can be held responsible for the high crack growth resistance of material **F**. It should be noted that for all materials **O**, **T** and **F** the craze-inherent amount of blunting ($CTOD_{craze}$) is about the same. This is in agreement with creep failure results of the simulated fibril tests (section 6.1) in which all materials displayed similar amounts of elongation (figure 6-7).

Figures 6-14b, 6-15b and 6-16b show crack tip geometries of materials **O**, **T** and **F** respectively, at extended loading times (PENT test, $\sigma = 2.4$ MPa). It should be recalled that the crack tips observed at different loading times were created with a razor blade, in *different* specimen samples. Thus the crack tips at different loading times are not physically the same and may differ somewhat in appearance, in addition to the isolated effect of loading time.
By comparing crack tip geometries at short and extended loading times the development of crack tip geometry during loading can be evaluated (see table 6-1). In all materials **O**, **T** and **F** both the craze length (L_c) and the craze contribution to blunting ($CTOD_{craze}$) remain almost unaffected by loading time. This observation can be related to results of creep experiments with simulated fibrils (figure 6-7), in which a plateau in creep deformation is observed during loading time. Therefore creep damage in fibrils, during loading, is not caused by macroscopic deformations.
With regard to bulk blunting, materials **O**, **T** and **F** behave differently. In material **O** (figures 6-5 and 6-6) the amount of bulk blunting is limited at short loading times and remains so for extended loading times. Obviously the fibrils of the craze fail before bulk blunting can take place. (The short creep failure time of material **O** is also manifested during the simulated fibril tests (figure 6-7, section 6.1).
Material **T** does not show any bulk blunting at short loading times (figure 6-15a), while at prolonged loading times some bulk blunting develops (figure 6-15b). The fibrils of material **T** withstand prolonged loading, enabling bulk blunting to occur (see also figure 6-7, section 6.1). However, the amount of bulk blunting produced does not relieve the craze enough to prevent ultimate failure of the actual craze. As mentioned before, even at short loading times a huge amount of bulk blunting is present at the crack tip of material **F**. Figure 6-16b shows the crack geometry after a very long loading time, at a stage when crack arrest can be assumed. The amount of bulk blunting has further increased, whereas dimensions of the actual craze (i.e.

$CTOD_{craze}$ and L_c) remained relatively unaffected. Obviously, the large amount of bulk blunting in material **F** relieves the loading of the actual craze, with crack arrest as a result.

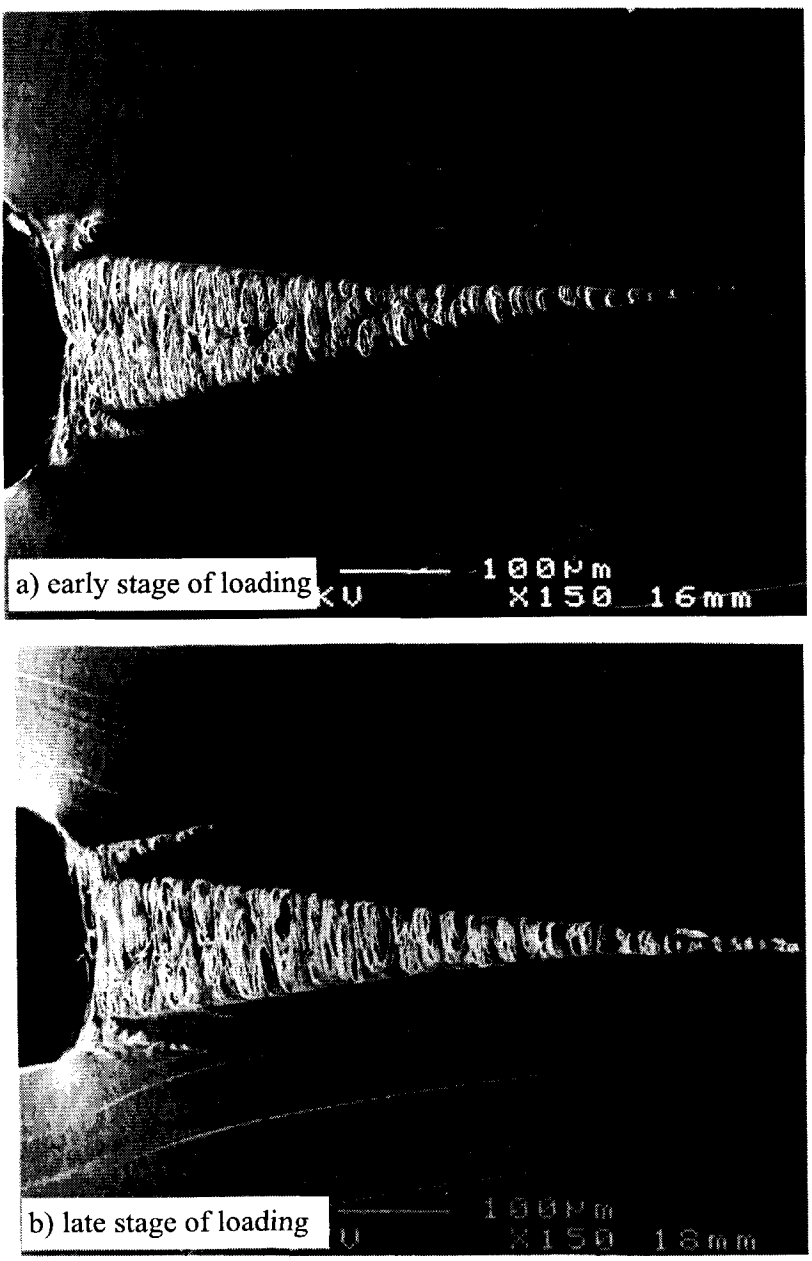

Figure 6-14 : Crack tip geometry of material **O** at a relatively early and relatively late stage of loading respectively.

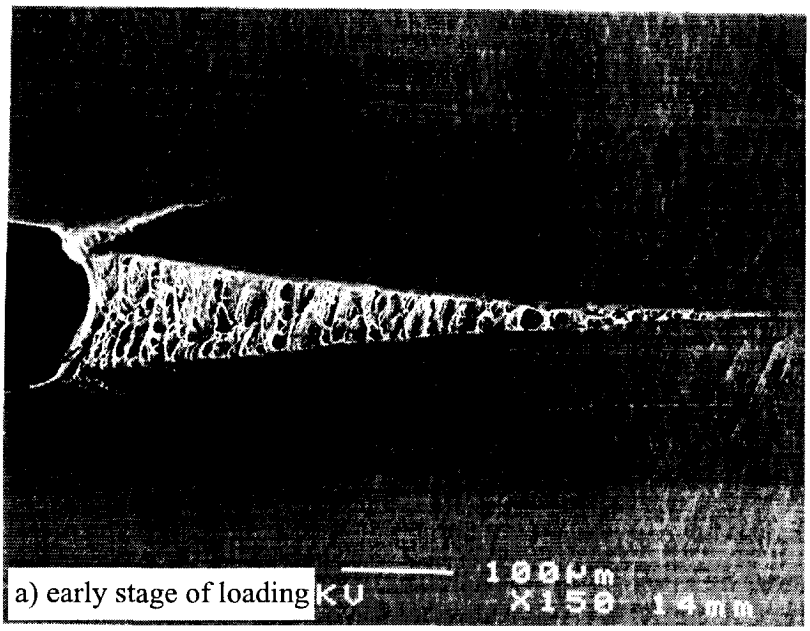

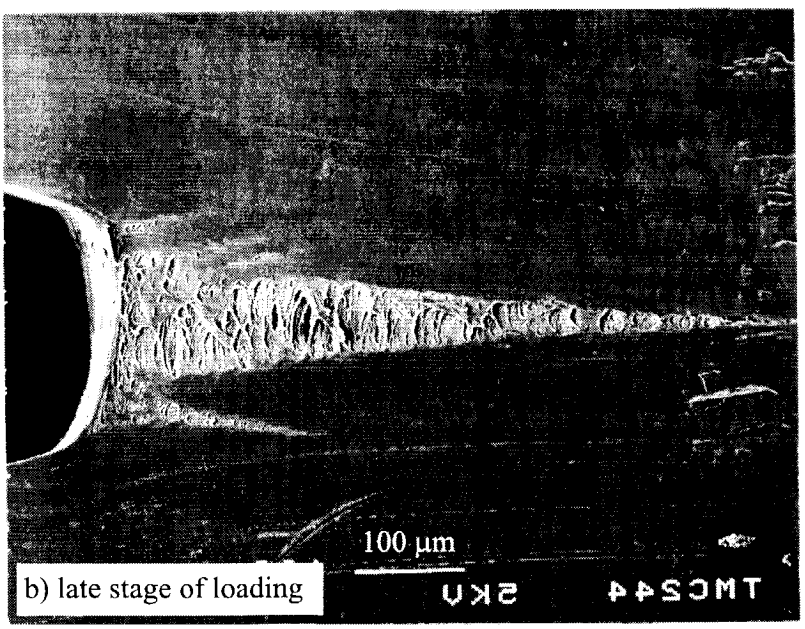

Figure 6-15 : Crack tip geometry of material **T** at a relatively early and relatively late stage of loading respectively.

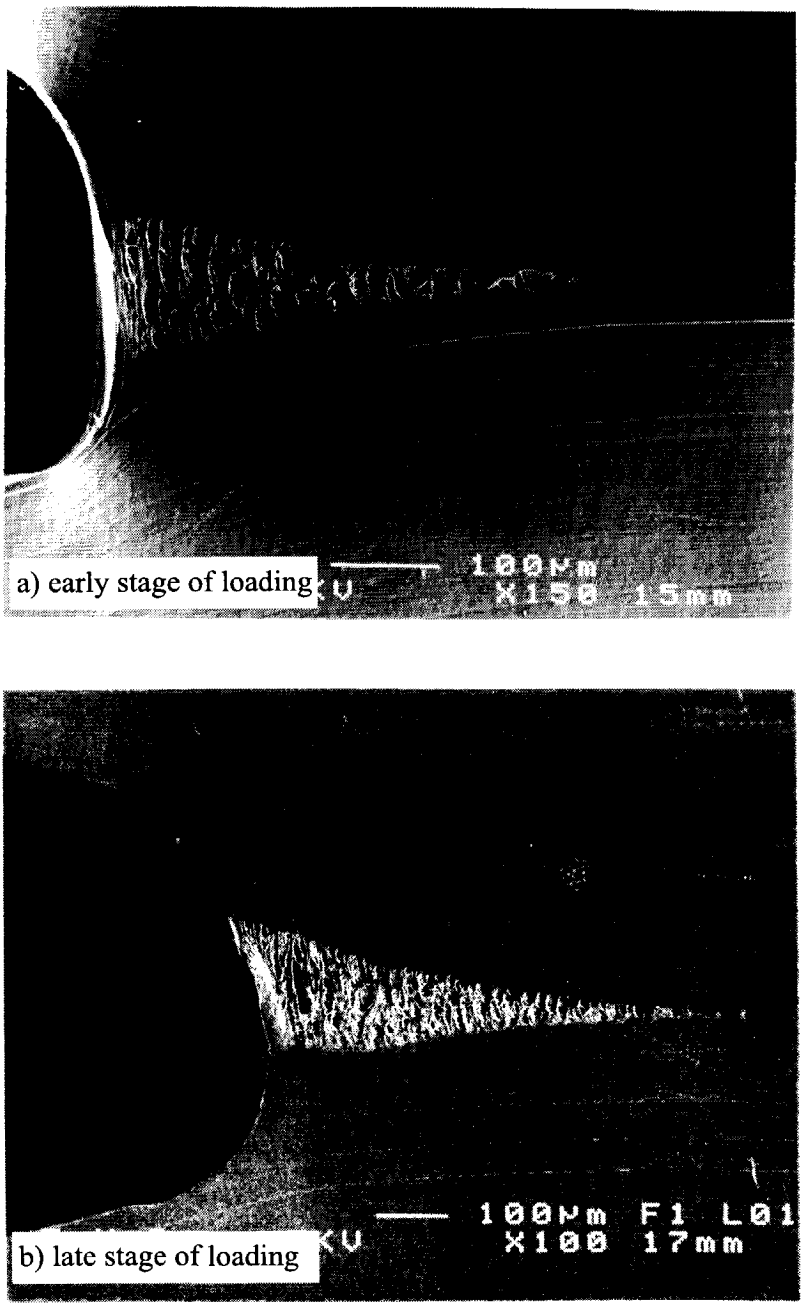

Figure 6-16 : Crack tip geometry of material **F** at a relatively early and relatively late stage of loading respectively.

Dugdale craze dimensions

The Dugdale model was originally developed to model the plastic zone size in metals, assuming ideal elastic-plastic deformation behaviour. The craze length L_c according to Dugdale becomes:

$$L_{c,Dugdale} = \frac{\pi}{8}\left(\frac{K}{\sigma_y}\right)^2 \qquad \{9\}$$

The definition of the yield stress σ_y, in the Dugdale model applied to crazes, is open to some discussion, since the crack tip is a two-phase system containing bulk material at the craze boundaries as well as highly drawn material within the actual craze.
The yield stress of bulk material, in combination with a hydrostatic stress component, governs the initiation of craze from the notch. In this respect, use of the yield stress of bulk material in equation {9} seems reasonable. On the other hand, growth of an existing craze depends on the mechanical response of fibrils and this implies that yield behaviour of drawn material should be used in equation {9}.
To avoid interpretation problems concerning the value of σ_y, in equation {9}, the Dugdale model is used to calculate a value of σ_y which satisfies the craze length $L_{c,meas.}$, as measured from the side view images. The calculated value of σ_y is referred to as inferred yield stress, $\sigma_{y,inf.}$

$$\sigma_{y,\text{inf.}} = K\sqrt{\frac{\pi}{8L_{c,meas.}}} \qquad \{9a\}$$

The calculated inferred yield stress can be compared with tensile properties of standard tensile specimens (σ_y of bulk material) and fibril tensile specimens (lower and upper drawing stress, see figure 6-4). Table 6-1 summarises the results. The data of table 6-1 indicates that the Dugdale model predicts realistic craze length values when the upper drawing stress is used for σ_y in equation {9}.
Although material **F** displays a huge amount of bulk blunting, this is not reflected in a smaller craze length when compared with the predicted Dugdale value. Here it can be argued that bulk blunting probably occurs after the craze has already been initiated.

Apart from the craze length the Crack Tip Opening Displacement (CTOD) in plane stress can also be calculated according to Dugdale's strip yield model. In [41] the expression is given as:

$$CTOD_{Dugdale} = \frac{K^2}{E\sigma_y} \qquad \{10\}$$

Analogously to the evaluation of the Dugdale craze length, the yield stress can be calculated from equation {10} if the CTOD is measured.
In addition to the parameters discussed earlier, equation {10} also contains the elastic modulus as a parameter. Enlargements of figures 6-2 and 6-4 were used to obtain the tangent at the origin of the stress strain curves, reflecting the elastic modulus. In this way elastic

moduli of 120 MPa, 175 MPa and 85 MPa were estimated for materials **O**, **T** and **F** respectively. Inferred yield stresses according to equation {10a} are incorporated in table 6-1. Inferred yield stresses based on CTOD measurements are found to be more related to the yield stress of bulk material than the upper drawing stress of drawn material. Therefore the CTOD calculation according to equation {10} gives reasonable results when the yield stress of bulk material is used.

In conclusion, the Dugdale model can give a reasonable impression of the crack tip geometry. *The upper drawing stress of drawn material is suitable for calculating the craze length, while the yield stress of bulk material is more appropriate for calculating the total amount of CTOD.*

Crack tip properties:	Mat. **O**		Mat. **T**		Mat. **F**	
Loading time [hrs]	1	3	100	800	200	9600
Figure reference	6-14a	6-14b	6-15a	6-15b	6-16a	6-16b
Stress intensity K [MPa$\sqrt{m}$]	0.5	0.5	0.5	0.5	0.5	0.5
Craze length measured [μm]	630	640	630	610	460	640
Inferred yield stress from craze length. [MPa]	**12.5**	**12.4**	**12.5**	**12.7**	**14.7**	**12.4**
Total CTOD measured [μm]	250	230	140	220	360	580
E-modulus at 80°C [MPa]	120	120	175	175	85	85
Inferred yield stress from CTOD [MPa]	**8.3**	**9.0**	**10.2**	**6.5**	**8.2**	**5.1**
Tensile properties: values as measured from figures 6-2 and 6-4.						
Yield stress bulk mat. [MPa]	**6.5**		**7.4**		**6.1**	
Lower drawing stress [MPa]	**6.2**		**8.1**		**5.6**	
Upper drawing stress [MPa]	**13.8**		**16.9**		**12.7**	

Table 6-1: Tensile properties as measured compared with yield stresses measured from craze length and CTOD values.

Blunting and craze length properties under fatigue conditions (80°C)

The study of crack tip geometry under fatigue conditions is limited to material **O**. Figure 6-17 shows the crack tip of a notched PENT test specimen loaded under fatigue conditions during a loading time of one hour ($\sigma_{max} = 2.4$ MPa $\leftrightarrow$ $K_{max} = 0.5$ MPa$\sqrt{\text{m}}$, $R = 0.1$, $f = 0.3$ Hz, $T = 80°C$). The crack tip geometry during fatigue (figure 6-17) can be compared directly with the constant load condition represented by figure 6-14b. Table 6-2 summarises the crack tip features of figure 6-14b (constant load) and figure 6-17 (fatigue).

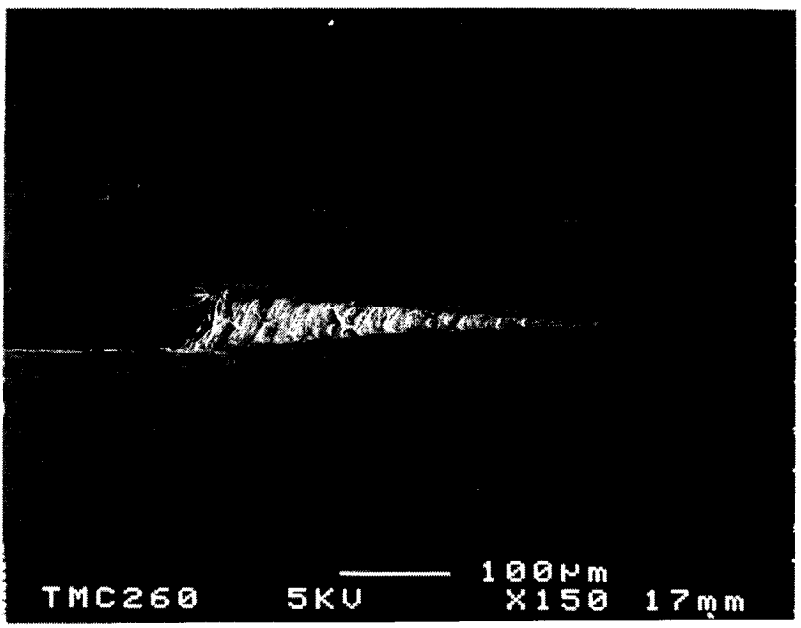

Figure 6-17: Crack tip geometry of material **O** during fatigue conditions.

	$L_{c,meas.}$ [µm]	$CTOD_{craze}$ [µm]	$CTOD_{bulk}$ [µm]	$CTOD_{total}$ [µm]
Constant load (figure 6-14b)	630	160	90	250
Fatigue (figure 6-17)	380	50	0	50
Ratio of dimensions under fatigue and constant load conditions.	60%	31%	0%	20%

Table 6-2: Crack tip geometry features under constant load and fatigue conditions.

Obviously the craze dimensions under fatigue conditions are reduced compared with the constant load condition, due to the lower average load level. In fatigue, the craze height ($CTOD_{craze}$) is reduced by a factor of 3. The simulated fibril tests (section 6.1) showed a similar result, when fracture strain under fatigue conditions was reduced by a factor of 2.5 compared with the strain values under constant load conditions. Moreover the total amount of blunting ($CTOD_{total}$) is reduced by a factor of 5, the influence of which on crack growth rate has already been discussed in section 6.1.

Stress and strain distributions in bulk material around the crack tip during constant load conditions

Figures 6-18 to 6-20 provide a qualitative impression of relative strain and stress distributions around crack tips of materials **O**, **T** and **F** (PENT tests at $\sigma = 2.4$ MPa and a temperature of 80°C). It should be recalled that the experimental technique involved craze initiation at a temperature of 80°C, cutting a slice from the unloaded specimen and finally loading the sliced sample at room temperature. The drawbacks of this procedure are given in section 3.5 (side view of crazes).
The strain distributions all show a peak at the crack tip with a subsequent reduction along the length of the craze. Obviously this response is due to the fact that at the crack tip the fibrils are drawn to their maximum extent with consequent high strain in adjacent bulk material. Materials **O** and **T** display peak strains at the crack tip of 20-25%, while in material **F** the value is limited to 14% due to the huge amount of blunting.

The strain values can be translated into stress levels using the stress-strain relation as measured in tensile tests with standard tensile specimens (figure 6-2). However the significance of this translation is limited, since the plateau in the stress-strain curve produces a uniform stress level for a wide range of strain levels. A uniform stress level along the craze length then becomes apparent, as is confirmed in figures 6-18, 6-19 and 6-20 for materials **O**, **T** and **F**, respectively. The stress levels determined in this way apply to bulk material at the craze boundaries and do not reflect stress levels of drawn material within the craze. The uniform stress level measured along the length of the craze is in agreement with the Dugdale model.

The stress and strain levels measured provide an impression of how stresses and strains are distributed along the length of the craze. The results cannot be related directly to crack growth behaviour.

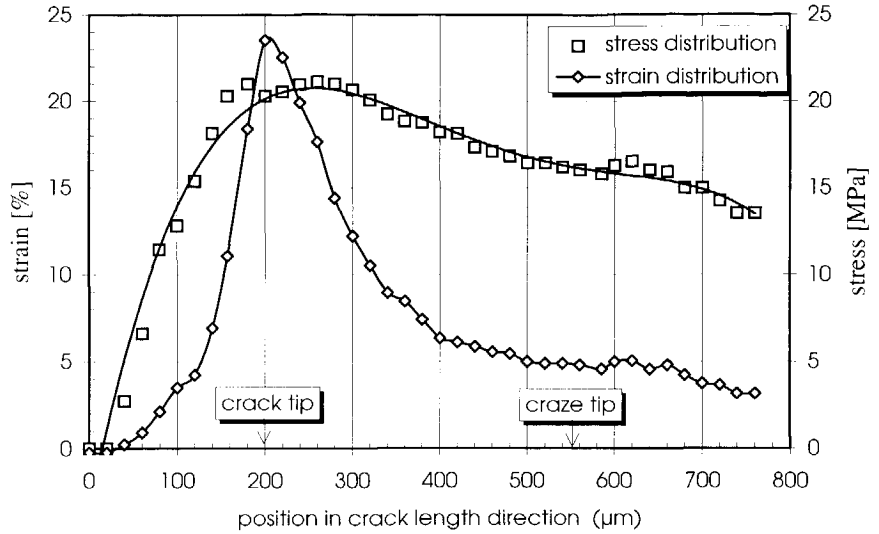

Figure 6-18 : Strain and stress distribution around a crack tip in material **O.**

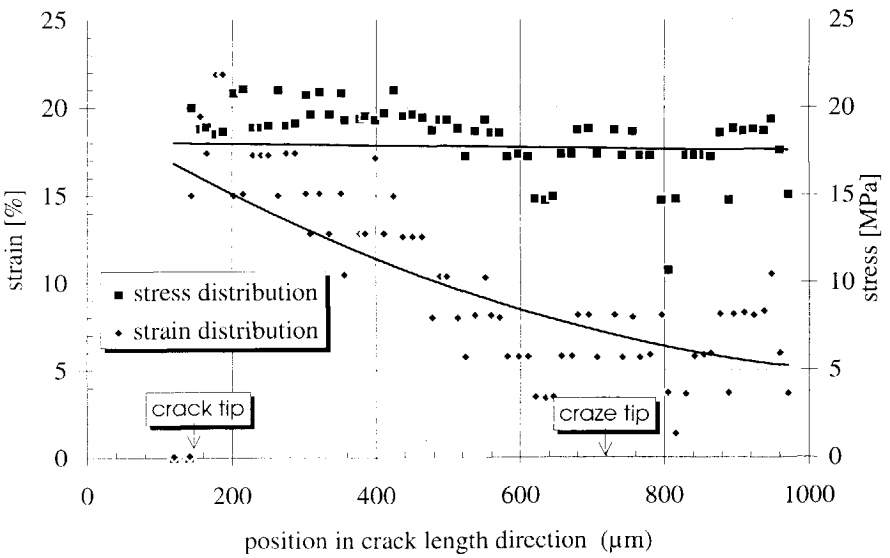

Figure 6-19 : Strain and stress distribution around a crack tip in material **T.**

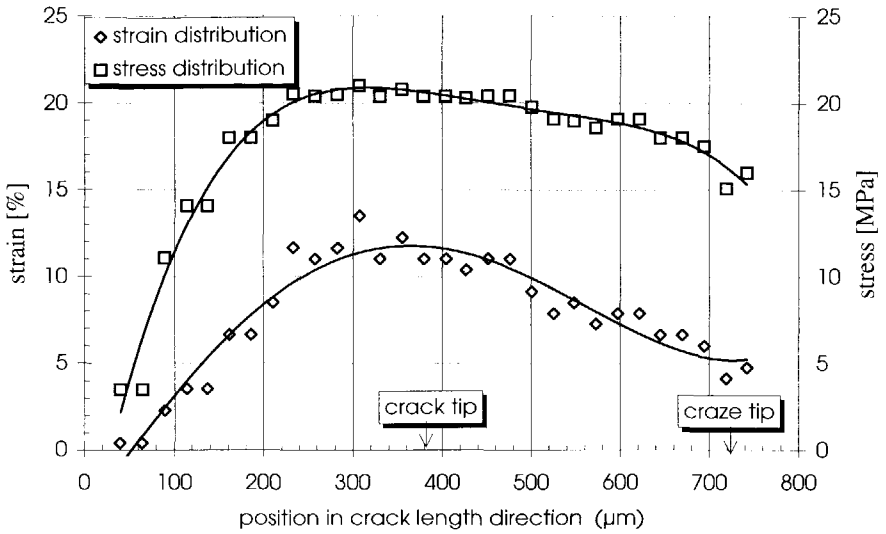

Figure 6-20 : Strain and stress distribution around a crack tip in material **F.**

7. Conclusions

This dissertation has focused on the crack growth behaviour of three polyethylene gas pipe materials. Originally the aim of the research was to develop of a reliable accelerated test method to predict long-term creep crack growth damage. During the process a more general study of the crack growth of polyethylene also evolved. From the results the following conclusions can be drawn.

1) Simple *CA* fatigue tests are not suitable for accurate prediction of creep crack growth behaviour. *CA* fatigue tests can be expected to give only a rough indication of the creep crack growth behaviour (qualitative ranking of materials).

2) A series of fatigue tests in which the fatigue load is gradually transformed into a constant load situation shows a consistent decrease in crack growth rate for two of three materials tested. The crack growth data of the fatigue regime can be used to extrapolate towards the situation of pure creep crack growth. In this respect fatigue can be used to predict long creep crack growth within a relatively short testing time.

3) Crack growth in polyethylene is a repeated, discontinuous process of development, weakening and final breakdown of the craze at the crack tip. The mechanism is referred to as "discontinuous" or "retarded" crack growth and is apparent from macroscopic crack growth bands on the fracture surface which can be related to crack growth steps measured.
   Discontinuous crack growth is a feature of both slow crack growth and fatigue crack growth.
   On a microscopic scale the fracture surfaces resulting from both creep crack growth and fatigue crack growth exhibit a similar appearance, a fibrillated structure, indicating similar crack growth mechanisms.

4) The crack tip is recognised as a two-phase system of highly drawn material within the craze and bulk material at the craze boundaries.

5) Blunting of the crack tip is found to play an important role in crack growth behaviour. The craze itself always provides a substantial amount of blunting, referred to as craze-inherent blunting. Craze-inherent blunting can be substantial, due to the unconstrained deformation potential of fibrils within the craze. Deformation of fibrils within the craze therefore constitutes damage but at the same time also causes the stress in the craze to be relieved by the blunting mechanism.

   In addition to craze-inherent blunting, deformation of bulk material around the craze leads to extra blunting (i.e. bulk blunting), which acts as a crack growth inhibitor.

   Thus creep of highly drawn material (i.e. the fibrils) is the essential cause of crack growth, while creep of bulk material can inhibit crack growth by providing an additional

amount of blunting. Therefore crack growth behaviour results from a combination of both bulk and drawn material.

6) During crack growth, part of the blunting is caused by creep deformations and depends on load level as well as time under loading (i.e. crack growth rate). Therefore blunting depends on the crack growth rate, while vice versa the crack growth rate is affected by blunting. The crack growth rate and the amount of blunting are interdependent and exist in balance with each other.

7) Fatigue crack growth in polyethylene is controlled by both cyclic and creep damage mechanisms but cannot be considered as a simple superposition of both mechanisms. Cyclic loading embrittles highly drawn material, effectively reducing the amount of blunting, with acceleration of crack growth as a result.

8) The creep failure of a highly drawn fibril specimen qualitatively indicates the creep crack growth behaviour. In this way the complicated issue of creep crack growth is reduced to a more simple level of testing.

9) Digital image processing is found to work very well for automatically measuring crack lengths during fatigue testing of both polyethylene and polycarbonate. With automated crack length measurement, tests are performed more efficiently, while crack growth can also be controlled by ΔK.

10) Qualitative impressions of stress and strain distributions around a crack tip in polyethylene are obtained. A fairly uniform stress level is found along the length of the craze in accordance with the assumption of ideally elastic-plastic mechanical behaviour. The geometry of the crack tip in polyethylene is modelled appropriately by the Dugdale strip yield model of a plastic zone.

References

1. R. Qian, X. Lu and N. Brown, investigating the existence of a threshold stress intenstity for slow crack growth in high-density polyethylene, Journal of Materials Science 24 (1989) ,2467-2472.
2. Y. Zhou, X. Lu and N. Brown, a fatigue test for controlling the quality of polyethylene copolymers, Polymer Engineering and Science, May 1991, Vol.31, no.10.
3. Y. Zhou and N. Brown, the mechanism of fatigue failure in a polyethylene copolymer, Journal of Polymer Science: Part B:Polymer Physics, Vol.30, 477-487 (1992).
4. A. Ward, X. Lu and N. Brown, accelerated test for evaluating slow crack growth of polyethylene copolymers in igepal and air, Department of Materials Science & Engineering, University of Pennsylvania, Philidelphia, PA 19104-6272.
5. N. Brown and X. Lu, PENT quality control test for polyethylene gas pipes and resins, Department of Materials Science & Engineering, University of Pennsylvania, Philidelphia, PA 19104-6272.
6. Y. Zhou and N. Brown, the fatigue behaviour of notched polyethylene as a function of R, Journal of Materials Science 24 (1989), 1458-1466.
7. N. Brown and X. Lu , the kinetics and microscopic processes of long-term fracture in polyethylene piping materials, annual report, Februari 1, 1990-Februari 1, 1991. Gas Research Institute, 8600 West Bryn Mawr Avenue, Chigago, IL 60631.
8. N. Brown and X. Lu, the fracture mechanics of slow crack growth in polyethylene, International Journal of fracture.
9. S. Bhattacharya and N. Brown, the initiation of crack growth in linear polyethylene, Journal of Materials Science 20 (1985) 2767-2775.
10. X. Lu and N. Brown, the relationship of the initiation stage to the rate of slow crack growth in linear polyethylene, Journal of Materials Science 21 (1986) 2423-2429.
11. X. Lu and N. Brown, the ductile-brittle transition in a polyethylene copolymer, Journal of Materials Science 25 (1990), 29-34.
12. X. Lu and N. Brown, a test for slow crack growth failure in polyethylene under a constant load, Polymer testing 11 (1992), 309-319.
13. X. Lu and N. Brown, the transition from ductile to slow crack growth failure in a copolymer of polyethylene, Journal of Materials Science 25 (1990), 411-416.
14. X. Lu and N. Brown, predicting failure from the initiation stage of slow crack growth in polyethylene, Journal of Materials Science 21 (1986), 4081-4088.
15. X. Lu, R. Qian and N. Brown, discontinuous crack growth in polyethylene under a constant load, Journal of Materials Science 26 (1991), 917-924.
16. X. Lu, X. Wang and N. Brown, slow fracture in a homopolymer and copolymer of polyethylene, Journal of Materials Science 23 (1988), 643-648.

17. Y. Huang and N. Brown, the effect of molecular weight on slow crack growth in linear polyethylene homopolymers, Journal of Materials Science 23 (1988), 3648-3655.

18. X. Wang and N. Brown, the stress and strain fields in the neighboorhood of a notch in polyethylene, Polymer, 1989, Vol. 30, August, 1456-1461.

19. X. Wang, N. Brown and L. Fager, the stress distribution on the boundary of crazes in polyethylene by the direct and semi-theoretical method, Polymer, 1989, Vol. 30, March, 453-460.

20. B. Wunderlich, Macromolecular Physics Volume I, Academic Press, New York 1973.

21. A. van der Vegt, polymeren, van keten tot kunststof (in Dutch), DUM 1991, Delft, the Netherlands. ISBN 90-6562-130-X.

22. J. Lai, non-linear time-dependent deformation behaviour of high-density polyethylene (thesis), DUM 1995, Delft, the Netherlands. ISBN 90-407-1136-4.

23. I. Ward, mechanical properties of solid polymers, John Wiley and Sons, 1985 second edition, ISBN 0-471-90011-7.

24. L. Struik, physical ageing of amorphous polymers and other materials, Elsevier, Amsterdam 1978, the Netherlands.

25. A. Lustiger, tie molecules in polyethylene, Final Report, Gas Research Institute, June 1985.

26. D. Barry and O. Delatycki, the effect of molecular structure and polymer morphology on the fracture resistance of high-density polyethylene, Polymer, 1992, Volume 33, Number 6.

27. S. Carr and B. Crist, structural basis for the mechanical properties of polyethylenes, Final Report, Gas Research Institute, Februari 1991.

28. D. Duvall, P. So and L. Broutman, effect of molecular weight on slow crack growth in high-density polyethylene, Antec 1992.

29. H. Kausch, Crazing in polymers, Vol.2, Springer-Verlag, 1989.

30. A. Atkins and Y. Mai, elastic and plastic fracture, John Whiley and Sons Limited, 1985, ISBN 0-85312-562-7.

31. M. Kasakevich, A. Moet and A. Chudnovsky, a crack layer approach to fatigue propagation in high-density polyethylene, Journal of Applied Polymer Science 39 (1990), 395-413.

32. A. Roulin-Moloney, fractography and failure mechanisms of polymers and composites, edited by Elsevier Applied Science 1989, ISBN 1-85166-296-0.

33. P. Reynolds and C. Lawrence, deformation and failure in polyethylene; correlation between mechanisms of creep and fatigue, Journal of Materials Science 26 (1991), 6197-6202.

34. P. Reynolds, stress-activated micro mechanistic deformation transitions in the failure of polyethylene, Journal of Materials Science Letters 11 (1992), 244-247.

35. J. Yeh and J. Runt, fatigue crack propagation in high density polyethylene, Journal of Polymer Science: Part B:Polymer Physics, Vol.29 (1991), 371-388.

36. H. Nishimura and I. Narisawa, fatigue behavior of medium density polyethylene pipes, Polymer Engineering and Science, March 1991, Vol.31, no. 6.

37. H. Nishimura, A. Nakashiba, M. Nakakura and K. Sasai, fatigue behavior of medium density polyethylene pipes for gas distribution, Polymer Engineering and Science, July 1993, Vol.33, No.14.

38. J. Strebel and A. Moet, accelerated fatigue fracture mechanism of medium density polyethylene pipe material, Journal of Materials Science 26 (1991), 5671-5680.

39. J. Runt and M. Jacq, effect of crystalline morphology on fatigue crack propagation in polyethylene, Journal of Materials Science 24 (1989) 1421-1428.

40. A. Riemslag, fatigue testing of high density polyethylene and polycarbonate with crack length measurement using image processing techniques, Journal of Testing and Evaluation, JTEVA, Vol 22, no.5, September 1994, 410-419.

41. H. Ewalds and R. Wanhill, fracture mechanics, DUM, 1986, Delft, the Netherlands, ISBN 90-6562-024-9.

42. A. Riemslag, fatigue crack growth in high-density polyethylene, Delft University of Technology, internal report, 1990.

43. R. Attermo and G. Östberg, Measurements of the temperature rise ahead of a fatigue crack, International Journal of Fracture Mechanics, 7 (1971), 122-124.

44. ASTM E647-93, standard test method for measurement of fatigue crack growth rates, annual book of ASTM standards, volume 03.01, ASTM 1916, Philadelphia, USA. ISBN 0-8031-1684-5.

45. M. Cawood, A. Chanell and G. Capaccio, fibre creep and long-term fracture resistance in polyethylene, Plastic Pipe Conference 1992, Eindhoven, the Netherlands.

46. Bondable KRAK-GAGES with a temporary strippable Teflon backing.TTI Division, Hartrun Corporation, St. Augustine, Florida 32084, USA.

47. A. Riemslag, the use of KRAK GAGES in measuring cracks in polyethylene and polycarbonate during a fatigue test, Internal report, Delft University of Technology, the Netherlands, 1990.

48. Difa Measurement Systems B.V, P.O. Box 3132, 4800 DC Breda, the Netherlands.

49. M. Spiegel, Schaum's outline series, Theory and Problems of Statistics, McGraw-Hill Book Company, 1972.

50. J. Zuidema, W. Shen and M. Janssen, retardation in fatigue crack growth in Al-2024 after blocks of underloading, Fatigue&Fracture of Engineering Materials&Structures, Vol.14, No. 10 (1991), 991-1005.

51. Howden, pulsed direct current crack length measurement, Howden machinery (Leamington Spa) LTD, United Kingdom.

52. B. Wittkowsky, N. Meyendorf, K. Schwalbe and B. Dogan, Rißlängenmessung mit digitaler Bildverarbeiting (in English: crack length measurement using digital image processing). Report in German with English abstract.GKSS-Forschungszentrum Geesthacht GMBH, Rapport no. GKSS 92/E/89, 1992.

53. R. Herzberg and J. Manson, fatigue of engineering plastics. Academic Press 1980, ISBN 0-12-343550-1.

Acknowledgements

I should like to express my sincere thanks to **Peter Wichers Schreur, Dick van der Grinten and Paul Peereboom** from **GASTEC** for their close co-operation and enthusiasm throughout the project. Their knowledge and experience were a great support.

The experiments were all performed at the **Laboratory of Materials Science (Delft University of Technology)** in the **Mechanical Behaviour of Materials** section.
I greatly appreciated the pleasant co-operation with the many people of the laboratory over recent years.

Within the Mechanical Behaviour of Materials section I would like to express my gratitude to **Prof. A. Bakker,** who supervised the research programme and gave me the opportunity to write this thesis.
Jan Zuidema always made time for me when I struggled with a work-related or other problem. His confidence in me supported me on many occasions.
I learned much from the almost daily discussions with **Michael Janssen** on the subject of fracture mechanics, computers and experimental techniques.
Thanks to the network co-ordinator **Alfons Krom,** the computer network efficiently managed my computer files.

My special thanks also to **Theo van Soest** for his assistance and advice during the experiments. Theo's positive approach in solving problems was most stimulating, especially during the period when our room was severely damaged by fire.
Many of the software programs used in the experiments were written by **Bart Wiersma.** They proved highly effective in reducing the efforts required for testing.

Many research students have directly or indirectly contributed to this work. My thanks to them all - **Harry ten Klooster, Jocco Dekker, Dirk-Jan Molenaar, Marieke Loos and Adriaan den Herder.**

Duco Smissaert and **Sjef de Bruijn** from the **Faculty of Industrial Design** gave me great support, even though this was beyond their call of duty.

I am very grateful to my late mother, for the love, care and education which she gave me.
I deeply appreciate the active interest taken in my work by my father, my sister Josine and my brother-in-law Pieter Kersscmakers. There were times when they helped me to keep things in perspective.

Ton Riemslag

About the author

The author was born on 10 June 1961 in Amsterdam, the Netherlands. He obtained his *Atheneum* diploma in 1979 and went on to study Mechanical Engineering at the *Hogere Technische School* in Amsterdam, receiving his diploma there in 1983. His final project involved implementing the mechanical dimensioning of gears in a computer program. The project was carried out at *FDO Technische Adviseurs B.V*, Amsterdam. In the period from 1983 to 1985 the author was employed by *FDO* as a mechanical engineer. His work was concerned with the calculation of the mechanical properties for most parts of a wind turbine. The wind turbine concerned was at that time the largest of its kind in the Netherlands, with a rotor diameter of forty-five metres.

In 1985 the author commenced his studies at the Delft University of Technology in the Faculty of Mechanical Engineering. In 1988 he joined the Mechanical Behaviour of Materials section in the Faculty of Chemical Technology and Material Science as a research student. His research on the subject of fatigue crack growth in polyethylene resulted in a Master's Degree in 1990. Fascinated by the research, the author was able to expand this work with the aim of writing a Ph.D. thesis. In the period from 1994 to 1996 he was also occupied with an educational project and developed multimedia instructions for laboratory exercises in materials engineering.

In January 1997 the author started working for Bodycote Materials Testing B.V., as a failure analyst and laboratory manager at the branch located in Emmen, the Netherlands.